Acta Geologica Polonica, Vol. 76 (2026), No. 2, e75
DOI: 10.24425/agp.2026.158189

Geochemical signatures of chert concretions and bedded cherts from the Kraków-Częstochowa Upland (Poland), the southeastern Franconian Alb, and the Bayerwald (Germany)

ALICJA KOCHMAN

AGH University of Krakow, Faculty of Geology, Geophysics and Environmental Protection, al. Mickiewicza 30; 30-059 Kraków, Poland; e-mail: kochman@agh.edu.pl

ABSTRACT:

Kochman, A. 2026. Geochemical signatures of chert concretions and bedded cherts from the Kraków-Częstochowa Upland (Poland), the southeastern Franconian Alb, and the Bayerwald (Germany). *Acta Geologica Polonica*, **76** (2), e75.

The Upper Jurassic bedded limestones developed within the microbial-sponge megafacies along the northern margin of the Tethys Ocean host, among other things, chert concretions and bedded cherts. This megafacies has been identified in a number of exposures located in the Kraków-Częstochowa Upland (Poland) as well as in the southeastern Franconian Alb and the Bayerwald (Germany), where it revealed mineralogical, petrographic and geochemical similarities. Hence, siliceous rocks formed by the replacement of primary calcium carbonate with silica also showed significant resemblance. The major chemical component of the analyzed siliceous rocks is SiO_2, accompanied by minor amounts of Al_2O_3, TiO_2, Fe_2O_3, and trace elements. The field observations combined with the results of geochemical analyses have indicated that the silica forming the chert concretions and the bedded cherts was primarily supplied by hydrothermal solutions rather than being supplied by the skeletons of siliceous sponges and radiolarians. The results of geochemical analyses document the formation of siliceous rocks during multistage diagenetic processes strongly influenced by hydrothermal solutions. The negative Ce anomalies observed in samples from all studied locations suggest oxic conditions during the silicification processes whereas the positive Eu anomalies indicate the local contribution of hydrothermal solutions under partially anoxic conditions. The differences in Eu anomalies found between particular locations are the result of the varying temperatures and intensity of hydrothermal solutions influx during the replacement processes, thus revealing the spatial variability of hydrothermal activity in the studied regions of the northern Tethys margin.

Key words: Chert concretions; Bedded cherts; Geochemical signatures; Rare Earth Elements (REE); Hydrothermal silicification; Kraków-Częstochowa Upland; Franconian Alb; Bayerwald.

INTRODUCTION

The Upper Jurassic siliceous deposits exposed over the vast area of the Kraków-Częstochowa Upland (KCU) are developed as chert concretions, bedded cherts and epigenetic siliceous rocks. However, their characterization and origin have been relatively rarely presented and discussed in publications, despite interest from geologists and from archaeologists. Considering the historical context, the products of the silicification of Upper Jurassic limestones from both the southern and the central parts of the KCU were described first by geologists (see e.g.: Staszic 1815; Zejszner 1841; Roemer 1870; Wiśniowski 1888;

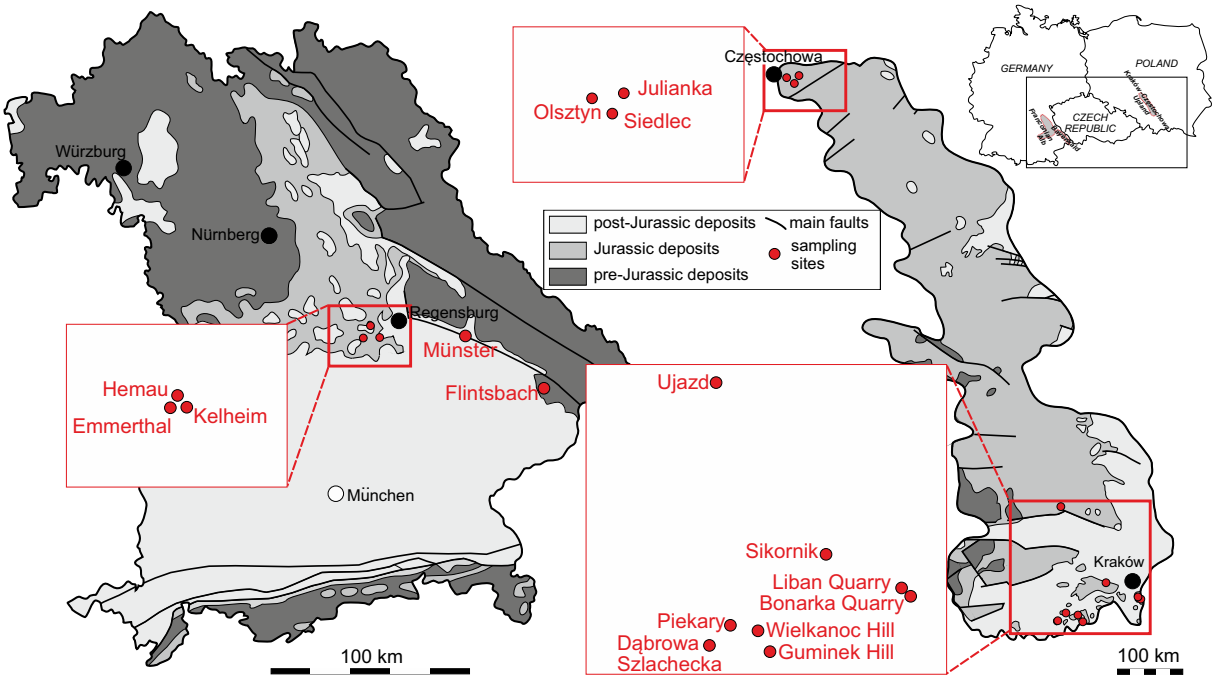

Text-fig. 1. Simplified geological maps of Bavaria (after Doben *et al.* 1996) and Poland (after Rühle *et al*. 1977); red circles mark sampling sites of chert concretions, bedded cherts and chert concretions hosted within gravity flow deposits.

Zaręczny 1894; Gaweł 1925; Sujkowski 1926, 1937; Kuźniar and Żelechowski 1927). Unfortunately, publications dealing directly with Jurassic cherts, including their genesis, development, petrography, geochemistry, weathering and fossils were limited in both number and extent (see e.g.: Wiśniowski 1888; Miernik 1911; Gaweł 1925).

Modern publications presenting geological studies on siliceous rocks from the KCU include: Dżułyński 1952; Bukowy 1956; Alexandrowicz 1960; Rajchel 1971; Pawlikowski *et al*. 1978; Matyszkiewicz 1987, 1989a, 1996; Michniak 1989; Świerczewska 1990, 1997; Sitarz *et al*. 2014; Matyszkiewicz *et al*. 2015a, 2015b, 2016; Kochman *et al*. 2020a, b; Matyszkiewicz and Kochman 2020; Kochman and Matyszkiewicz 2023, 2025.

Regardless of geological research, cherts have attracted the interest of archaeologists (see e.g.: Krukowski 1920; Schild 1971; Kaczanowska and Kozłowski 1976; Morawski 1976; Kaczanowska *et al*. 1979; Lech 1980, 1981; Ginter and Kozłowski 1990; Kopacz and Pelisiak 1992; Pelisiak 2003, 2006, 2008; Sulgostowska 2005; Janák and Přichystal 2007; Budziszewski 2008; Krajcarz *et al*. 2012, 2014; Přichystal 2013, 2018; Brandl *et al*. 2016; Krajcarz and Sudoł-Procyk 2019; Šebela *et al*. 2017; Parish and Werra 2018; Werra and Siuda 2022; Sudoł-Procyk *et al*. 2018, 2021a, 2021b, 2022; Mandera *et al*. 2024).

The silicification process of limestones is controlled mainly by the composition of the host limestones and the concentration of dissolved silica, regardless of the original silica source (Maliva 2001). Silicification means replacement of $CaCO_3$ with SiO_2, combined with the infilling of the empty voids within host limestones and the transformations of various silica phases under the controlling factors: time, pressure, pH and nucleation rates (Laschet 1984; Gao and Land 1991; Lawrence 1993). Generally, cherts originate from diagenetic replacement of their host limestones (see e.g.: Bustillo and Ruiz-Ortiz 1987; Hesse 1989; Maliva and Siever 1989; Knauth 1992, 1994; Lawrence 1994; McBride *et al*. 1999; Bustillo *et al*. 2009) under the strong influence of their lithology and porosity (Bustillo 2010). However, according to some researchers, cherts may also form syngenetically (e.g.: Keheila 2000; Lindgreen and Jakobsen 2012). For the interpretation of the diagenetic environment, the determination of the silica source is important. This can be biogenic, volcanic, hydrothermal, terrestrial and mixed (e.g.: Adachi *et al*. 1986; Yamamoto 1987; Murray 1994; Beauchamp and Baud 2002; Chen *et al*. 2006; Hofmann and Bolhar 2007; Van den Boorn

et al. 2007, 2010; Kidder and Tomescu 2016; Lin *et al*. 2018; Shen *et al*. 2018; Lei *et al*. 2019).

This paper presents the results of geochemical analyses of chert concretions and bedded cherts samples collected from: (i) both the southern and the northern parts of the Kraków-Częstochowa Upland (S-KCU and N-KCU), whose petrographic characterizations have already been presented by Matyszkiewicz *et al*. (2015b), Kochman *et al*. (2020a) and Kochman and Matyszkiewicz (2023), (ii) the southeastern part of the Franconian Alb (southeastern FA) and (iii) the Bayerwald (BW), the latter two characterized in detail by Kochman and Matyszkiewicz (2025; Text-fig. 1). Analysis of the results enabled these authors to discuss the origin of the siliceous rocks and to identify the sources of silica. Moreover, references were presented to the epigenetic silicification of the Upper Jurassic sediments from the KCU, including the chert concretions and the bedded cherts, previously described and discussed by Kochman *et al*. (2020b) and Kochman and Matyszkiewicz (2023).

HISTORY OF STUDIES

Until the end of the XXth century, descriptions (mostly macroscopic) of chert concretions were contained in rather scarce publications concerning the development of Upper Jurassic limestones (see e.g.: Dżułyński 1952; Alexandrowicz 1955; Rajchel 1971; Matyszkiewicz 1989a, 1997a) as well as their technical analyses as potential raw materials (Stawin 1969, 1970). A few mineralogical and geochemical papers provided the results of studies on samples collected from individual outcrops of Upper Jurassic carbonates hosting siliceous concretions (Gaweł 1925; Pawlikowski *et al*. 1978; Świerczewska 1997).

Even more scarce were studies and papers on siliceous beds hosted in Upper Jurassic calciturbidites, which were found in the S-KCU as late as in 1989 (Matyszkiewicz 1989b; Świerczewska 1989) and described in detail even later (Matyszkiewicz 1996; Matyszkiewicz and Olszewska 2007; Matyszkiewicz *et al*. 2015b). More attention has been paid to epigenetic siliceous rocks from the Upper Jurassic succession, unfortunately, described mainly macroscopically (see: Morozewicz 1909; Kuźniar and Żelechowski 1927; Rajchel 1971; Heliasz 1980; Matyszkiewicz 1987).

The lack of geochemical analyses together with relatively poor knowledge of the microfacies development of the Upper Jurassic limestones from the KCU, studies on which commenced as late as at the end of the XXth century, resulted in highly speculative conclusions concerning: (i) the origin of silica in chert concretions, bedded cherts, and epigenetic siliceous rocks, (ii) the age of these sediments and (iii) the nature of silicification process itself.

New studies on siliceous rocks carried on using advanced laboratory methodologies have been undertaken in only the last dozen or so years (Sitarz *et al*. 2014; Matyszkiewicz *et al*. 2015a, 2016; Kochman *et al*. 2020a, 2020b; Krzyżak *et al*. 2020; Fajt *et al*. 2024; Kochman and Matyszkiewicz 2023, 2025). As a result, modern petrographic descriptions have been composed, closely referring to the microfacies development of the host limestones and to the results of various modern laboratory methods: fluid inclusions, geochemical analyses, X-ray diffraction, nuclear magnetic resonance and Mössbauer spectroscopy.

In the chert concretions from the S-KCU, Sitarz *et al*. (2014) first identified the presence of moganite and found its contents to be higher in comparison with those in samples from both the Neogene and the Quaternary sediments. However, these authors stated also that it is difficult to draw far-reaching conclusions about the age of these cherts based upon the contents of moganite.

A significant progress was made by Matyszkiewicz *et al*. (2015a) in understanding the genesis of epigenetic siliceous rocks from the N-KCU (Sokole Góry area). The study materials were: (i) silicified limestones located in close vicinity of joints and fractures, (ii) crusts growing on the top surface of the Upper Jurassic limestones succession and (iii) rims enclosing the chert concretions. The results enabled the authors to reconstruct the course of the silicification process, to identify several silicification stages in the Upper Jurassic limestones and to disclose the relationships of silicification and circulation of hydrothermal solutions driven by the regional tectonic events. Specifically, at least two silicification stages were identified, closely related to tectonic activity along the Kraków-Lubliniec Fault Zone within the Paleozoic basement. The first stage of inferred Early Cretaceous (Valanginian) age affected the erosional top surface of the denuded Upper Jurassic succession under subtropical climatic conditions and resulted in the formation of pedogenic silcretes as well as some inhibition of the karstification process. The source of silica was silica-enriched descending solutions generated in the weathering zone. The second stage was triggered by the next tectonic activity event in the Cenozoic, which gave rise to the formation of new, numerous dislocations and fracture systems subsequently filled with quartz sands. These fracture systems became the transfer conduits of ascending, warm, hydrothermal

solutions, which dissolved the limestones and remobilized silica from the sands. That silica subsequently precipitated onto the silcretes and/or as rims enclosing the chert concretions (Matyszkiewicz *et al*. 2015a).

Important information about silicification was gained from studies on the Oxfordian neptunic dykes filled with brachiopod fossils, which were described in the Oxfordian limestones from the S-KCU (Matyszkiewicz *et al*. 2016). The high crystallinity index (CI) values (see Murata and Norman 1976) together with the temperatures exceeding 100°C revealed by fluid inclusions (FI) studies indicated the hydrothermal origin of the silica related to extensional tectonic events in the S-KCU, initiated in the Late Jurassic (Matyszkiewicz *et al*. 2016). Similarly, silica from chert concretions found along the southwestern margin of the Holy Cross Mts. was sourced mainly by episodic influxes of SiO_2-rich fluids during various stages of Late Jurassic extensional tectonic events, as documented by Migaszewski and co-authors (for details, see Durakiewicz *et al*. 2001; Sharp *et al*. 2002; Migaszewski *et al*. 2006, 2022). Silicification of material infilling the neptunic dykes proceeded in at least two stages of hydrothermal activity and was presumably genetically linked to the tectonic events identified in that region in the Late Cretaceous and in the Cenozoic. These new studies also enabled the identification of several silicification stages in the KCU and related these processes both to tectonic events and to the circulation systems of the hydrothermal solutions.

Further conclusions on the course of the silicification and its products in the Upper Jurassic carbonates were brought about by the results of studies on the possible identification of siliceous raw materials used in the production of prehistoric tools encountered by archaeologists (Kochman *et al*. 2020a; Matyszkiewicz and Kochman 2020). The microscopic observations of thin sections combined with the determination of the crystallinity index CI based upon the X-ray diffraction patterns indicated diagnostic features, which aimed to distinguish various types of siliceous raw materials: the chert concretions, bedded cherts, and epigenetic siliceous rocks used in the manufacturing of archaeological artifacts and to suggest the potential sources of the silica.

Observations of chert concretions from the S-KCU have demonstrated their presence in both of the varieties of the lithostratigraphic succession members: (i) those rich in calcified siliceous sponges and (ii) those rich in microbial structures but low in or even devoid of sponges. Similarly, in the calciturbidites encountered in the uppermost Upper Jurassic strata, siliceous sponges were practically absent or extremely rare whereas chert concretions occurred below and/or above the bedded cherts. The opposite relationship was observed in the pseudonodular limestones (Matyszkiewicz and Kochman 2016), where calcified siliceous sponges were abundant and chert concretions were absent. Such a feature gave rise to the rejection of the commonly accepted concept about the dominant role of siliceous sponge skeletons as the main source of silica for chert concretions (Alexandrowicz 1960). Similarly, radiolarian exoskeletons have been proposed as a potential source of silica for bedded cherts hosted in calciturbidites (Matyszkiewicz 1996), in accordance with the silicification model proposed by Bustillo and Ruiz-Ortiz (1987). However, very thick-bedded chert layers made the origin of silica from radiolarian exoskeletons very doubtful. Moreover, the presence of concentric growth layers indicated the multi-stage nature of the silicification process and suggested the supply of silica from external, abiotic sources.

The next progress in the recognition of silicification products was made by fluid inclusion (FI) studies. Microthermometric and geochemical analyses clearly indicated the abiotic, hydrothermal origin of silica from samples collected in the S-KCU exposures (Kochman *et al*. 2020b). Specifically, the FI observations in quartz crystals derived from epigenetic siliceous rocks revealed crystallization from hydrothermal brines at temperatures of about 70–90°C. Inclusions observed in the rims enclosing the early diagenetic chert concretions indicated somewhat higher temperatures: about 80–110°C. The hydrothermal origin of the epigenetic siliceous rocks was confirmed also by the results of geochemical analyses. Moreover, it was found that the epigenetic siliceous rocks from the S-KCU were formed under conditions similar to those described from the N-KCU (Matyszkiewicz *et al*. 2015a; Kochman *et al*. 2020b). The undoubtedly younger age of epigenetic siliceous rocks in comparison with chert concretions was demonstrated by the latter being crystallization nuclei for epigenetic silica as well as by the infilling of the cracks cutting through the chert concretions with epigenetic silica. The cracks were presumably generated during the main faulting stage of the Upper Jurassic sediments in the Cenozoic (Matyszkiewicz *et al*. 2015a; Kochman *et al*. 2020a).

Krzyżak *et al*. (2020) and Fajt *et al*. (2024) applied the low-field neutron magnetic resonance (NMR) relaxometry method to distinguish chert concretions from bedded cherts. Analysis of the obtained relaxation parameters revealed that the two types of siliceous rocks had different porosity pa-

rameters. The total porosity of these rocks was about 1–2% and included mostly mesopores (2–50 nm in diameter) and macropores (over 50 nm in diameter). However, the bedded cherts were dominated by macropores whereas the chert concretions showed more a balanced proportion of meso- and macropores. Furthermore, the results presented by Fajt *et al*. (2024) indicated some differences between cherts which had originated from various locations.

As revealed by the studies of Kochman and Matyszkiewicz (2023), silicification of the Upper Jurassic limestones in the N-KCU had a two-stage nature and was strictly controlled by tectonic events and the circulation of hydrothermal solutions. The first stage occurred during very early burial diagenesis and was controlled by local redox conditions, leading to the formation of chert concretions which had the low crystallinity index of chalcedony (CI < 0.7). The second, much longer stage followed the early diagenesis of carbonate sediments after their chemical compaction. The siliceous rocks produced during that stage did not contain moganite and revealed a much higher degree of ordering in the chalcedony structure (CI = 6.0–6.6), corresponding to previously determined values for sediments from the S-KCU (Świerczewska 1989, 1997; Kochman *et al*. 2020a). The geochemical indicators pointed to the contribution of low-temperature hydrothermal solutions to the formation of siliceous rocks. Variations of REE ratios and enrichments suggested mixing of these solutions with seawater at the final stage of hydrothermal activity. The results of these studies proved that silicification was a two-stage process controlled by influxes of low-temperature hydrothermal solutions related to the Late Jurassic extensional tectonic events.

The latest research (see Kochman and Matyszkiewicz 2025) revealed the significant petrographic similarity of chert concretions and bedded cherts from the KCU, the southeastern FA and the BW. Concretions from both the BW and the KCU showed similar sizes, textures and colors, indicating similar conditions of formation. However, in the BW, some specific chert concretions were found, which had no equivalents in the KCU. Such concretions were silicification products of: (i) pseudonodular textures resulted from pressure dissolution of carbonate sediment (cf. Matyszkiewicz and Kochman 2016) and (ii) limestones subjected first to dolomitization and then to chemical compaction. In the southeastern FA, where carbonate sediments represent the stratigraphic interval from the Middle Kimmeridgian to the Lower Tithonian, some chert concretions and tabular cherts revealed morphological similarity to sediments from the turn of the Oxfordian/Kimmeridgian, common in the KCU. Petrographic observations of chert concretions and bedded cherts from both the southeastern FA and the BW showed that silicification was a multi-stage, late-diagenetic process. Moreover, the results of Mössbauer spectroscopy confirmed the multistage nature of that process and the diverse sources of silica. Generally, the results presented above challenge earlier concepts (e.g. Thewalt and Dörfner 2011) that silica contained in these concretions was derived mainly from opaline skeletons of siliceous sponges. Instead, the main sources of silica were local hydrothermal phenomena.

GEOLOGICAL SETTING

Kraków-Częstochowa Upland

The Upper Jurassic (Oxfordian–Lower Kimmeridgian) sediments constitute some parts of the KCU which belong to the Silesia-Kraków Monocline (see e.g.: Dżułyński 1952; Wierzbowski 1965, 1966; Kutek *et al*. 1977; Heliasz *et al*. 1984, 1987; Matyszkiewicz 1989a, 1994, 1996, 1997a, 1997b, 1999; Kutek 1994; Krajewski 2001; Krajewski and Matyszkiewicz 2004, 2009; Matyja and Wierzbowski 2004, 2006; Ziółkowski 2007; Krajewski *et al*. 2018; Matyszkiewicz *et al*. 2006, 2012, 2015b). The maximum thickness of Upper Jurassic strata preserved in the S-KCU is about 250 m in the eastern part and decreases gradually westward (Matyszkiewicz *et al*. 2012), whereas in the N-KCU it exceeds 450 m (Heliasz *et al*. 1984, 1987). The sediments occur as bedded and unbedded facies, composing the carbonate microbial-sponge megafacies, which developed along the northern margin of the Tethys Ocean, ranging from Portugal to the Caucasus Mts. (Trammer 1985, 1989; Matyszkiewicz 1997a; Matyszkiewicz *et al*. 2012). This megafacies hosts chert concretions and bedded cherts, which are related to particular limestone varieties.

The chert concretions occur mostly in biostromal bedded limestones but are present also in the fine-detrital platy deposits of gravity flows and, exceptionally, in massive (unbedded) limestones. In the bedded limestones, chert concretions are distributed usually as horizons parallel to the bedding surfaces (Matyszkiewicz 1996; Matyszkiewicz *et al*. 2015b) whereas in the transitional zones from bedded to massive limestones, these are randomly scattered within the host rocks and gradually disappear (Alexandrowicz 1955; Matyszkiewicz 1989a; Kochman *et al*. 2020a). Similarly, a random distribution of chert concretions is observed also in de-

bris flow deposits (Matyszkiewicz, 1996). Bedded cherts are much less frequent in the KCU where their occurrence is limited to gravity flow calciturbidites formed at the turn of the Oxfordian/Kimmeridgian (Matyszkiewicz 1996; cf. Marcinowski 1970).

The epigenetic siliceous rocks, which occur in the uppermost part of the Upper Jurassic succession, reveal significant variability in their development, and their distribution is unrelated to any specific limestone facies (Kuźniar and Żelichowski 1927; Rajchel 1971; Heliasz 1980; Matyszkiewicz 1987; Matyszkiewicz *et al*. 2015a; Kochman *et al*. 2020b). Four types of epigenetic siliceous rocks were distinguished: (i) concentric and irregular rims of silicified limestone around the chert concretions; (ii) irregular bodies within limestones from the topmost parts of the Upper Jurassic succession; (iii) coatings on fault surfaces and/or on Cretaceous erosion surfaces cutting the Upper Jurassic sediments and (iv) loose fragments of silicified limestones embedded within the regolith (Kochman *et al*. 2020a, 2020b). Epigenetic siliceous rocks are brownish, dark-brown, dark-gray, and locally even cherry-red in color, show high porosity and have sharply defined boundaries between the rims composed of silicified limestones and the enclosed chert concretions.

Southeastern Franconian Alb and Bayerwald

The Upper Jurassic sediments from both the BW and the southeastern FA also represent the carbonate microbial-sponge megafacies (e.g.: Gwinner 1971; Keupp *et al.* 1990) and are up to about 400 m thick. However, in the top part of the Upper Jurassic succession from the southeastern FA, shallow-marine sediments of Upper Kimmeridgian and Lower Tithonian age have been identified (e.g.: Zeiss 1964, 2012; Niebuhr and Pürner 2014), which have not been preserved in the KCU.

The Upper Jurassic succession from the FA is clearly dominated by bedded facies, mostly by thick-bedded limestones, whereas thin-bedded limestones, usually intercalated by marls, are less common, as are massive facies. The Upper Jurassic stratigraphy in the FA includes 17 formations (Niebuhr and Pürner 2014) of ages from the Middle Oxfordian to the Upper Tithonian. In the studied SE part of the FA, both chert concretions and thin-bedded cherts are observed, mostly in the Tangrintel Formation (Upper Kimmeridgian–Lower Tithonian; cf. Rutte 1962; Weber 1978; Meyer 1977; Binsteiner 2005; Niebuhr and Pürner 2014). Less common are chert concretions in the Treuchtlingen Formation (upper part of the Lower Kimmeridgian–middle part of the Upper Kimmeridgian; Meyer 1975, 2003a, b, c; Niebuhr and Pürner 2014) and in the Painten Formation (bottom part of the Lower Tithonian; Streim 1961; Viohl and Zapp 2007; Niebuhr and Pürner 2014) whereas thin-bedded cherts are known from the Torleite Formation (middle-topmost parts of the Upper Kimmeridgian; Streim 1961; Zeiss 1964; Binsteiner 2005; Niebuhr and Pürner 2014).

The Upper Jurassic sediments from the BW are different. These are relics of the carbonate microbial-sponge megafacies, which represent a stratigraphic interval from the Middle Oxfordian to the Lower Kimmeridgian (the so-called Ortenburg Formation; cf. Zeiss 1977; Meyer 1977; Gröschke 1985; Niebuhr 2014) and comprise thick-bedded limestones with numerous chert concretions. These deposits reveal a distinct similarity to the Upper Jurassic bedded limestones from the KCU, particularly from the S-KCU (Kochman and Matyszkiewicz 2025).

PETROGRAPHY OF CHERT CONCRETIONS AND BEDDED CHERTS

The petrographic characterization of both the chert concretions and the bedded cherts has already been presented in a number of papers (Kochman *et al*. 2020a, 2020b; Matyszkiewicz and Kochman 2020; Kochman and Matyszkiewicz 2023, 2025). It was found that chert concretions from similar stratigraphic intervals of the Upper Jurassic carbonates from the KCU, the BW, and from the lower part of that succession in the southeastern FA reveal similar petrographic features, which reflect the similar development of the microbial-sponge megafacies in Poland and in Germany. Only a few, less important, specific features were observed in samples from particular locations, such as variable shares of silica polymorphs in some sediments.

Chert concretions from the KCU

Macroscopic description

The chert concretions from the KCU are usually developed as ellipsoidal, spheroidal, or, rarely, irregular bodies with diameters of up to several tens of centimeters (Text-fig. 2A–C). Their colors vary from the most common brown through gray and bluish up to black, and may change even within a single specimen. Some chert concretions have empty voids, up to several centimeters across, entirely or partially

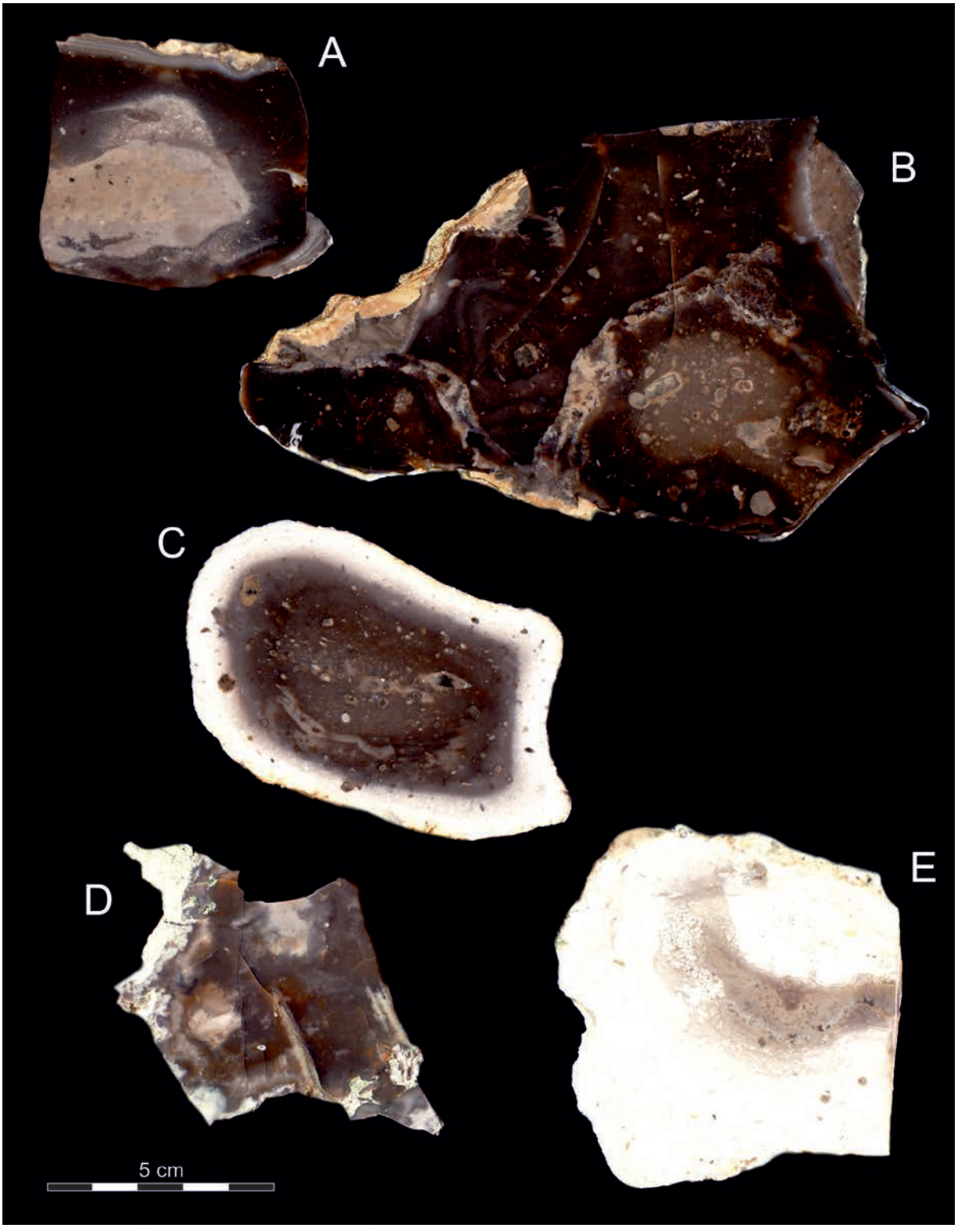

Text-fig. 2. A – chert concretion from bedded limestones. S-KCU, Piekary outcrop, sample KA-2; B – chert concretion with preserved hexactinellid siliceous skeleton and fine, unrecognizable bioclasts. S-KCU, Dąbrowa Szlachecka outcrop, sample KB-8; C – spheroidal chert concretion with white rim and skeletal fragments of siliceous sponge in its core. S-KCU, Bonarka Quarry, sample B-10; D – irregular chert concretion from calciturbidite below silicified bedded chert. S-KCU, Ujazd outcrop, sample SA-3; E – chert concretion with sponge cast in the center; concretion color becomes increasingly lighter towards its edge. N-KCU, Siedlec outcrop, sample PC-2C.

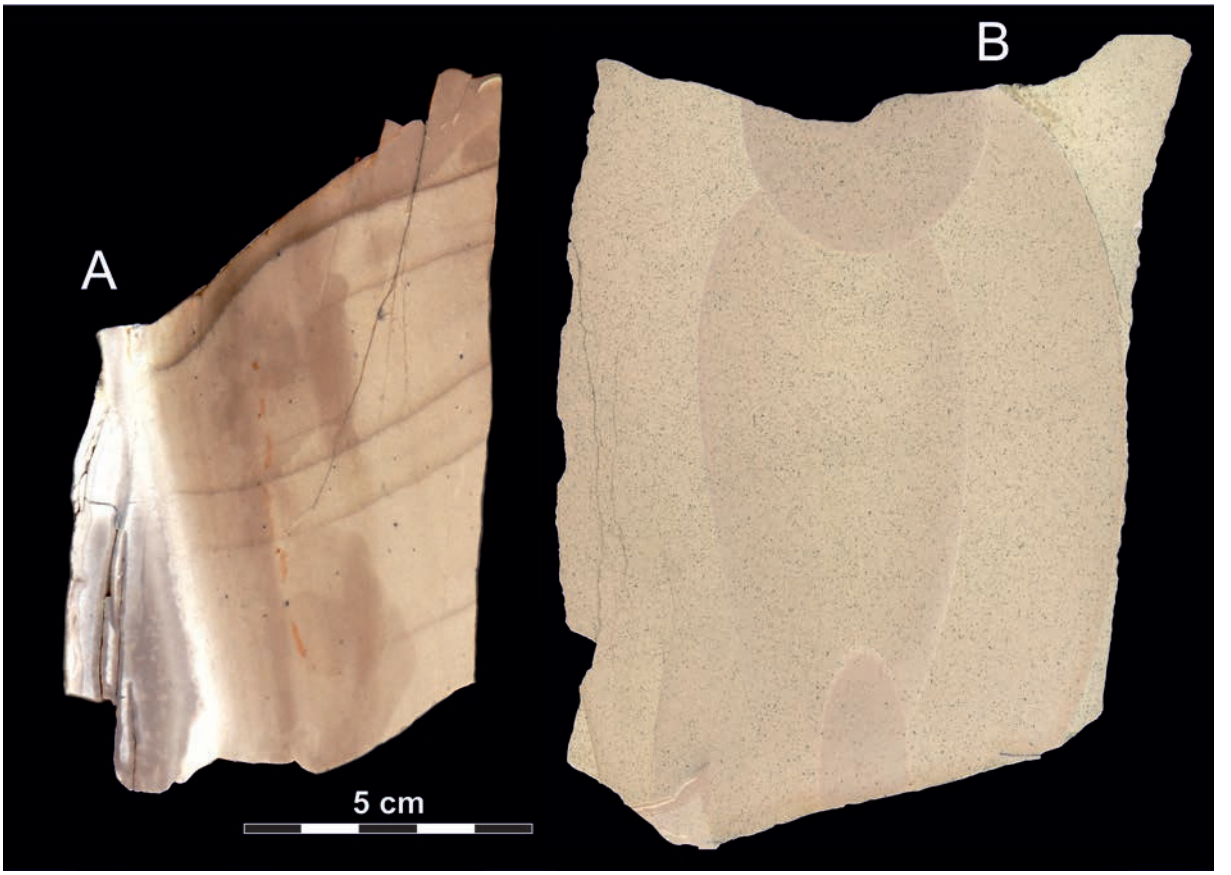

Text-fig. 3. A – bedded chert in silicified calciturbidite; silicified primary lamination seen in carbonate mud; fragment of laminated bedded chert with lighter spot is silicified bioturbation enclosed in primary, fine-grained carbonate mud. S-KCU, Wielkanoc Hill, sample SC-2"; B – fragment of bedded chert with silica growth bands precipitated onto the surface of chert concretion. N-KCU, Siedlec outcrop, sample PC-4 (cf. Matyszkiewicz and Kochman 2020).

filled with coarse-crystalline quartz. However, chert concretions hosted in calciturbidites do not contain such geodes (Text-fig. 2E–D; Kochman *et al*. 2020a). In the vicinity of fault zones, chert concretions are strongly cracked and filled with secondary silica.

Microscopic description

The chert concretions are composed mostly of cryptocrystalline SiO_2 sometimes accompanied by micro- and/or macrocrystalline quartz (megaquartz). Silicified bioclasts seen in some chert concretions reveal well-defined shapes and are composed of fibrous SiO_2, chalcedony, microcrystalline quartz, or megaquartz. Locally observed geodes are also filled with megaquartz. In some chert concretions originated from the S-KCU, moganite has been identified (Sitarz *et al*. 2014; Kochman *et al*. 2020) but its recognition under the microscope is practically impossible.

Bedded cherts from the KCU

Macroscopic description

The bedded cherts are developed as horizons with a thickness of up to 40 centimeters and a length of up to several meters. Usually, from 2 to 3 such horizons are observed in a single outcrop. Their upper surfaces are usually flat whereas the bottom ones have common bulges. Some bedded cherts may host occluded chert concretions and demonstrate concentric growth layers (Kochman *et al*. 2020a). The latter show diverse colors: creamy, gray, brownish or dark-creamy (Text-fig. 3A, B). Generally, the internal parts of bedded cherts have darker colors, which become increasingly lighter toward the outside. Bedded cherts represent silicified calciturbidites, specifically the perfectly sorted T_a and T_b layers of the Bouma sequence (Matyszkiewicz 1996).

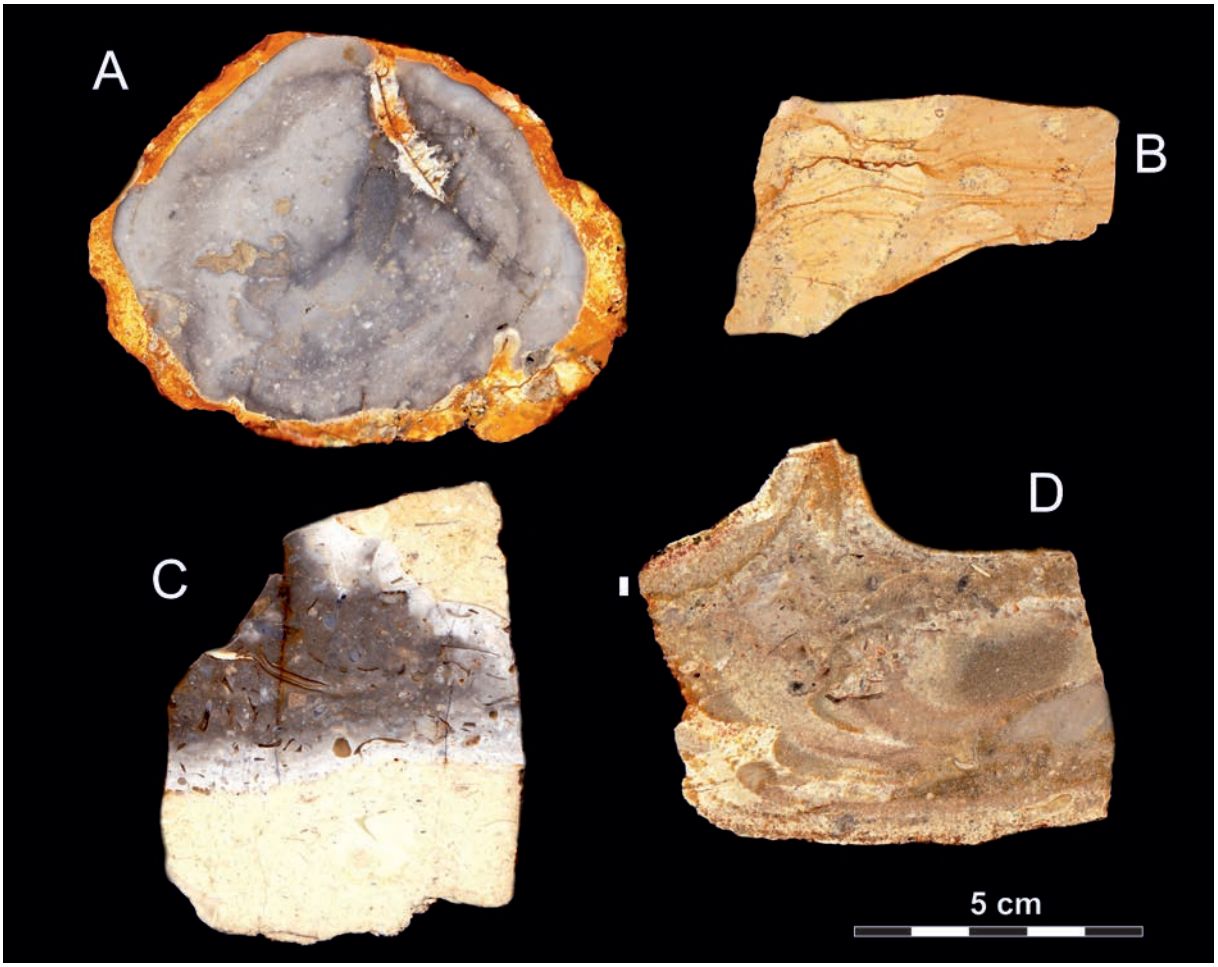

Text-fig. 4. A – spheroidal chert concretion with partially preserved skeleton fragments of hexactinellid siliceous sponge. BW, Münster outcrop, sample M7; B – strongly fractured chert concretion with preserved stylolites filled with Fe-oxides. BW, Flintsbach outcrop, sample F3; C – chert concretion in tempestite; numerous fragments of shallow-water fauna are embedded in poorly sorted carbonate tempestite and in chert concretion. Southeastern FA, Kelheim outcrop, sample K1/3; D – fragment of tabular chert from regolith; convolute disturbances seen in lower left part; brownish color originates from disseminated dolomite. Southeastern FA , Hemau outcrop, sample H3.

Microscopic description

Silicified calciturbidites are composed of cryptocrystalline silica and microcrystalline quartz, with locally scattered megaquartz aggregates, which fill pore spaces of millimeter size (Matyszkiewicz 1996).

Chert concretions from the southeastern FA and the BW

Macroscopic description

The chert concretions located in the lower part of the Upper Jurassic succession from the southeastern FA and the BW are hosted in bedded limestones developed as wackestones-packstones (Text-fig. 4A, B). Usually, these are spheroidal, ellipsoidal and/or irregular, sometimes even branched bodies (Kochman and Matyszkiewicz 2025) of diameters from several to about 10 centimeters. Variable colors and morphology enabled the authors to distinguish two types of these concretions. The first type comprises concretions with dark-gray cores grading into light-gray zones at the contact with the cortex, although the opposite pattern has also been noticed. The second type of concretions have light-gray cores whereas their peripheries are light-creamy or even almost white, with irregular, brownish-cherry spots and scattered, dark dots, up to 2 millimeters across. Chert concretions occur both individually and as aggregates composed of

a number of individuals randomly distributed within the limestones (Kochman and Matyszkiewicz 2025).

Microscopic description

The chert concretions represent silicified wackestones-packstones. Usually, their cores contain skeletons of siliceous sponges. The contours of bioclasts are marked by chalcedony and microcrystalline quartz, as well as rare relics of a non-silicified fossil fauna. The carbonate matrix is replaced by cryptocrystalline silica. Sometimes, the limestone-chert interfaces follow the stylolites (Kochman and Matyszkiewicz 2025).

In the top part of the Upper Jurassic succession from the southeastern FA, chert concretions reveal a specific development which has no analogues in the KCU. First of all, such concretions show several generations of silica as well as pseudomorphs after dolomite crystals filled with Fe-oxides, which are preserved in the core (Kochman and Matyszkiewicz 2025). Similarly to the chert concretions found in the lower part of the Upper Jurassic succession, those from the upper part are built of cryptocrystalline SiO_2 accompanied by microcrystalline quartz and/or megaquartz.

Bedded cherts from the southeastern FA

Macroscopic description

The bedded cherts from the upper part of the Upper Jurassic carbonate succession in the FA (so-called ”tabular cherts”; Text-fig. 4C, D) are silicified tempestites (Kochman and Matyszkiewicz 2025) located mainly in thin-bedded limestones as distinctly laminated, light-brown plates, from 1 to 5 centimeters thick. Both top and bottom surfaces of laminae are usually flat, but some can be undulating. Laminae are arranged as parallel sets or show convolutional disturbances and contain silicified fossil fragments, as well as indistinct grading. Comparison of bedded cherts from the KCU and the FA demonstrates that the latter reveal much lower thicknesses and poorer sorting of carbonate sediment, then subjected to silicification. Sometimes, only a single tempestite plate is observed, with a thickness of up to 1 centimeter (Kochman and Matyszkiewicz 2025).

Microscopic description

The silicified tempestites are composed of cryptocrystalline silica, accompanied by microcrystalline quartz and megaquartz, which fill pore spaces of millimeter size (Kochman and Matyszkiewicz 2025). Silicified laminae, 1–2 centimeters thick, are packstones-grainstones of grain size up to about 2 millimeters. Both the top and bottom surfaces of silicified laminae are uneven, with silica protruding into the enclosing limestone up to a distance of about 1 millimeter.

MATERIALS AND METHODS

Chemical analyses were carried on 137 samples, 100 of which originated from the KCU (61 from the S-KCU and 39 from the N-KCU), 20 from the southeastern FA and 17 from the BW (Text-fig. 1). Samples of chert concretions constituted the vast majority (87 samples, in which 37 from the S-KCU, 30 from the N-KCU, 3 from the southeastern FA and 17 from the BW). Sampling was carried on 5 outcrops in the S-KCU (Piekary, Dąbrowa Szlachecka, Guminek Hill, Liban Quarry, and Bonarka Quarry), 3 outcrops in the N-KCU (Olsztyn, Julianka and Rudniki), 2 outcrops in the BW (Münster and Flintsbach) and 1 in the southeastern FA (Emmerthal). Samples of bedded cherts (totalling 27 specimens) originated from the following regions: 18 from the S-KCU (Ujazd, Sikornik and, Wielkanoc Hill outcrops), 5 from the N-KCU (Siedlec outcrop) and 4 from the southeastern FA (Hemau and Kelheim outcrops). Samples of chert concretions hosted in gravity flow sediments included 23 items, in which 6 came from the S-KCU (Ujazd outcrop), 4 from the N-KCU (Siedlec outcrop) and 13 from the southeastern FA (Hemau and Kelheim outcrops).

The major and trace element composition, including rare earth elements (REE), was analyzed at Activation Laboratories Ltd. (ACTLABS) in Ancaster (Canada) using fusion-inductively coupled plasma (FUS-ICP), fusion-inductively coupled plasma-mass spectrometry (FUS-MS), and thermal desorption-mass spectrometry (TD-MS) methods.

The REE were conventionally divided into three subgroups: light REE (LREE) including La through Eu, medium REE (MREE) from Sm to Dy and heavy REE (HREE), from Gd to Lu. The results of REE analyses were normalized using the PAAS-normalized abundances (Post Archean Australian Shales; Taylor and McLennan 1985; McLennan 1989; Piper and Bau 2013). The PAAS-normalized patterns effectively highlight the REE fractionation trends and anomalies (e.g., Eu, Ce, Pr, Gd), which may reflect variability of the conditions of deposition of hydrothermal solution influxes and/or redox conditions during chert formation (Shimizu and Masuda 1977;

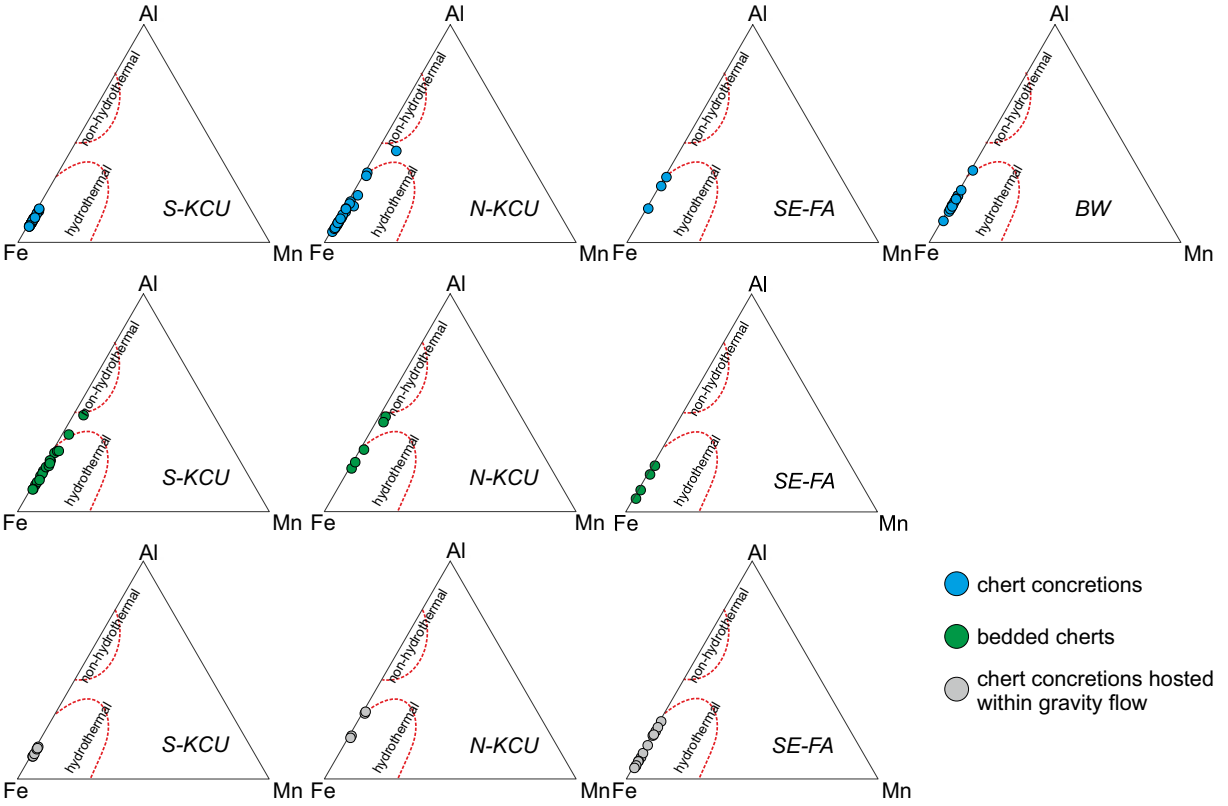

Text-fig. 5. Ternary Al-Fe-Mn diagram for chert concretions, bedded cherts, and chert concretions hosted within gravity flow deposits; hydrothermal and non-hydrothermal fields defined after Adachi *et al.* (1986).

Taylor and McLennan 1985; Sholkovitz 1990; Bau and Dulski 1996). The Eu, Ce, Pr, and Gd anomalies were calculated using the methodology after Dulski (1994), Bau and Dulski (1996), Wang *et al*. (2012) and Nothdurft *et al*. (2004) with the following equations: $Eu/Eu^{*}=Eu_{SN}/(0.5Sm_{SN}+0.5Gd_{SN})$, $Ce/Ce^{*}=Ce_{SN}/(0.5La_{SN}+0.5Pr_{SN})$, $Pr/Pr^{*}=Pr_{SN}/(0.5Ce_{SN}+0.5Nd_{SN})$, $Gd/Gd^{*}=Gd_{SN}/(0.5Eu_{SN}+0.5Tb_{SN})$. The REE ratios and enrichments, especially $LREE_{SN}/HREE_{SN}$, La_{SN}/Yb_{SN}, La_{SN}/Sm_{SN}, and Sm_{SN}/Yb_{SN}, were computed because such indices enable one to evaluate the relative LREE enrichments in relation to HREE, the distribution of LREE, MREE, and HREE as well as the identification of Ce, Eu, Pr, and Gd anomalies.

ANALYTICAL RESULTS – GEOCHEMICAL CHARACTERIZATIONS

Major and trace elements

The results of major and trace element analyses are listed in Appendix (Tables 1–10). The major chemical component of all samples is SiO_2, with minor contribution of Al_2O_3, Fe_2O_3, and CaO. The contents of SiO_2 are inversely proportional to these of CaO. The remaining oxides and trace elements occur in very low amounts, typically close to or even below the detection limits of the analytical methods mentioned above, however, with local exceptions.

Chert concretions

In the chert concretions from the S-KCU, the contents of SiO_2 are generally high being about 97 wt.%, on average. The highest contents – 95.86–98.46 wt.% – occur in the samples from the Piekary outcrop but the results in the samples from the Guminek Hill and the Liban Quarry are only slightly lower. In the samples from the N-KCU outcrops, the SiO_2 contents are more diverse in particular outcrops. For example, in the Olsztyn outcrop, the SiO_2 contents are very similar, within a narrow range, from 97.25 to 98.35 wt.%. The samples from the Julianka outcrop reveal a wider range of values: from 64.22 to 98.91 wt.%, but contents over 97 wt.% prevail. The samples from the

Rudniki outcrop show the highest variability of SiO_2 contents, from very low to very high: 36.03 to 98.02 wt.%, respectively.

In the samples from the BW, the SiO_2 contents generally exceed 97 wt.% in most of the analyzed specimens. However, in the Flintsbach samples, the distribution of SiO_2 values is relatively similar (95.35–98.75 wt.%) whereas in the Münster samples, higher variability was found (86.74–99.15 wt.%). Finally, in the samples from the southeastern FA, the contents of SiO_2 are relatively high: from 94.10 to 97.37 wt.%.

In chert concretions from all the sampled outcrops, the contents of minor components: Al_2O_3, Fe_2O_3, and TiO_2 are low but some regional variations are observed. The Al_2O_3 contents are low (0.05–0.40 wt.%), and the maximum values occur in the samples from the Bonarka Quarry (S-KCU) and in those from both the Olsztyn and the Rudniki outcrops (N-KCU). The Fe_2O_3 values are more variable, from 0.06 to 2.12 wt.% and the maximum values are detected in the Bonarka Quarry (S-KCU) and in the Rudniki outcrop (N-KCU) whereas the minimum values are in the samples from the Dąbrowa Szlachecka outcrop (S-KCU) as well as from the Julianka and the Olsztyn ones (N-KCU). The trace TiO_2 contents (usually < 0.03 wt.%) show the maximum values in the samples from Bonarka Quarry and from the Piekary outcrop (S-KCU) as well as from the Rudniki outcrop (N-KCU). In the samples from both the BW and the southeastern FA, minor elements values are quite stable – the Al_2O_3 contents fall into the range of 0.16–0.40 wt.% in the BW and of 0.26–0.30 wt.% in the southeastern FA), the Fe_2O_3 contents change from 0.60 to 1.45 wt.%, and those of TiO_2 are even lower: 0.002–0.007 wt.%. Generally, the analyzed samples of chert concretions reveal low contents of Al_2O_3 and TiO_2 as well as a moderate variability of Fe_2O_3 contents, which demonstrates quite uniform chemical composition with local anomalies in the samples from the Bonarka Quarry and the Rudniki outcrop.

The analyzed trace elements show moderate but variable contents in chert concretions. In the samples from the S-KCU, the contents of alkaline and rare elements: Ba, Rb, Sr, U, Nb, Th, and Y vary from low to moderate values. Specifically, the Ba contents change from 5 to 42 $mg \cdot kg^{-1}$, and those of Sr from 2 to 22 $mg \cdot kg^{-1}$ whereas the contents of heavy and transition metals: Pb, Ni, Co, Cu, Cr, Zn, and V are more diverse, with local enrichments in Cu (up to 16.5 $mg \cdot kg^{-1}$), Cr (up to 15 $mg \cdot kg^{-1}$) and Ni (up to 19 $mg \cdot kg^{-1}$). In the samples of chert concretions from the N-KCU, higher variability of trace elements is observed. The alkaline elements, particularly Sr, show high local enrichments (up to 101 $mg \cdot kg^{-1}$). Also the contents of transition metals (Cu, Cr, Zn) are distinctly anomalous: e.g. Cu up to 39.2 $mg \cdot kg^{-1}$ and Cr up to 45 $mg \cdot kg^{-1}$. The chert concretions from the BW reveal similar variability trends with distinct, local enrichments in Cu (up to 32.8 $mg \cdot kg^{-1}$) and Cr (up to 50 $mg \cdot kg^{-1}$), particularly in the samples from the Münster outcrop. The contents of Ba and Sr increase up to 49 and 15 $mg \cdot kg^{-1}$, respectively, whereas Y contents are the highest among all the analyzed samples – up to 12.4 $mg \cdot kg^{-1}$. In the chert concretions from the southeastern FA, low to moderate contents of trace elements are detected with the relatively stable values of Ba (10–13 $mg \cdot kg^{-1}$) and Sr (3–6 $mg \cdot kg^{-1}$). Also the heavy metals show low contents although local enrichments can be found of Cr (up to 26 $mg \cdot kg^{-1}$) and Cu (up to 11 $mg \cdot kg^{-1}$).

The Al/(Al+Fe+Mn) ratios from the S-KCU vary from 0.07 to 0.15 and are from 0.04 to 0.42 in the N-KCU. In both the BW and the southeastern FA, this ratio changes from 0.10 to 0.33 and from 0.16 to 0.30, respectively. The values of the Al_2O_3/TiO_2 ratio appear to be at their the lowest in the S-KCU (from 6.84 to 60) but they increase in the N-KCU (from 4.14 to 170). In the BW, this ratio is from 51.43 to 100 and in the southeastern FA it is somewhat higher: from 54 to 130). The Fe_2O_3/TiO_2 ratios are the highest in the N-KCU (50–90, with high variability) and the lowest in the S-KCU (64–470).

Bedded cherts

The bedded cherts from the S-KCU reveal an average content of 88.27 wt.% SiO_2 but the diversity of the silica contents in that region is significant with minimum and maximum values of 58.74 and 98.44 wt.%, respectively. In the bedded cherts from the N-KCU, the average content of SiO_2 is 87.15 wt.% with minimum and maximum values 72.85 and 96.47 wt.%, respectively. The samples from the southeastern FA (Kelheim and Hemau outcrops) show the highest and the most stable values of SiO_2 among all the analyzed localities: average 96.60, minimum 94.77 and maximum 98.17 wt.% SiO_2.

The minor elements: Al_2O_3, Fe_2O_3, and TiO_2 are low with some insignificant regional variations. The contents of Al_2O_3 vary from 0.09 to 0.24 wt.% with average values falling into the narrow range of 0.15–0.17 wt.%. The highest contents are observed in the samples from the Sikornik and the Ujazd outcrops (S-KCU) and from the Kelheim outcrop (southeastern FA). The contents of Fe_2O_3 show moderate variability

(0.14–1.51 wt.%) and reach maximum values in the samples from the Ujazd outcrop and Wielkanoc Hill (S-KCU) as well as from the Kelheim outcrop (southeastern FA) whereas the minimum contents occur in the N-KCU sites (0.15–0.76 wt.%). The contents of TiO_2 are very low (usually < 0.005 wt.%), i.e., rather at the level of trace components. Generally, the bedded cherts reveal low contents of Al and Ti, and moderate values of Fe, which suggests quite uniform composition of the minor elements with local enrichments in Fe_2O_3 at the given sampling sites.

The bedded cherts from the S-KCU, the N-KCU, and the southeastern FA demonstrate varying contents of trace elements. In the S-KCU, both the alkaline and the rare element (Ba, Rb, Sr, U, Nb, Th and Y) values are diverse, particularly Ba (6–41 $mg \cdot kg^{-1}$) and Sr (2–78 $mg \cdot kg^{-1}$). The heavy and the transition metals (Pb, Ni, Co, Cu, Cr, Zn, and V) show moderate contents with local enrichments in Pb encountered in the samples from the Sikornik outcrop and Wielkanoc Hill. In the N-KCU, a more uniform distribution of these metals is evident. Specifically, the contents of Ba, Rb, Sr, U, Nb, Th, and Y are low and moderately variable. The contents of both the heavy and the transition metals (Pb, Cu, Cr, and Zn) reveal moderate and stable contents: (e.g. Pb < 0.5–0.7 $mg \cdot kg^{-1}$) with no distinct anomalies. The highest diversity of trace elements is observed in the bedded cherts from the southeastern FA where high variability is indicated for both the alkaline and the rare elements (particularly Ba: 34–429 $mg \cdot kg^{-1}$ and Sr: 4–17 $mg \cdot kg^{-1}$) as well as for some heavy and transition metals (Cu: 7.5–28.9 $mg \cdot kg^{-1}$, Cr: 6–46 $mg \cdot kg^{-1}$) whereas the others: Pb, Ni, Co, Zn, and V show moderate contents. However, the samples from all the localities demonstrate low and stable Zr, Ga, and Hf contents.

The Al/(Al+Fe+Mn) ratios in bedded cherts are as follows: 0.10–0.44 in the S-KCU, 0.20–0.44 in the N-KCU and 0.06–0.21 in the southeastern FA. The Al_2O_3/TiO_2 ratios (25–47) are similar in the samples from the KCU, but distinctly lower in comparison with those from the southeastern FA (30–200). The Fe_2O_3/TiO_2 ratios are the highest in the southeastern FA (110–1,240, with high variability), whereas the lowest values (38–160) are observed in the N-KCU.

Chert concretions hosted in gravity flow deposits

In the chert concretions developed within the gravity flow deposits from the S-KCU, the SiO_2 contents are high and stable, from 97.94 to 99.02 wt.% with an average of 98.60 wt.%. Similarly high SiO_2 contents are observed in the samples from the N-KCU: from 97.03 to 98.36 wt.% with an average of 97.79 wt.%. Generally, the SiO_2 distribution is relatively uniform within the narrow range of extremes (only about 1.3 wt.%). In the samples from the southeastern FA, the SiO_2 contents are more variable: from 83.7 to 98.93 wt.% with an average of 96.15 wt.%. The lowest SiO_2 value (83.7 wt.%) was detected in a sample from the Kelheim outcrop, whereas most analyzed samples revealed very high SiO_2 contents, exceeding 95 wt.%.

In all the analyzed samples of chert concretions hosted in gravity flows, the contents of Al_2O_3, Fe_2O_3, and TiO_2 are low but locally variable. Specifically, the Al_2O_3 contents range from 0.07 to 0.38 wt.% with an average value about 0.14 wt.% in the S-KCU and somewhat higher (0.16–0.19 wt.%) in the N-KCU. The samples from the southeastern FA reveal the highest Al_2O_3 variability. The contents of Fe_2O_3 vary from 0.39 to 1.49 wt.% with the highest values found in the southeastern FA and the more stable ones (0.85–1.03 wt.%) in the S-KCU. The contents of TiO_2 are generally low (0.001–0.005 wt.%), except for a single sample from the Hemau outcrop where 0.135 wt.% was detected. Generally, the samples of chert concretions from the gravity flow deposits show low amounts of Al_2O_3 and TiO_2, and the moderately variable Fe_2O_3. This indicates quite a uniform composition of the minor components, however, with local enrichments in Fe_2O_3 and TiO_2 in some samples from the southeastern FA.

Generally, the chert concretions hosted in gravity flow deposits from the S-KCU, the N-KCU, and the southeastern FA reveal low and relatively stable contents of trace elements but local enrichments are observed, as well. In both the S-KCU and the N-KCU, the contents of both the alkaline and the rare elements (Ba, Rb, Sr, U, Nb, Th, Y) are low (Ba 4–8 $mg \cdot kg^{-1}$, Sr 2–4 $mg \cdot kg^{-1}$, the remaining elements: < 0.6 $mg \cdot kg^{-1}$), which suggests quite a uniform geochemical background. Similarly, the rare elements: Zr, Ga, and Hf show low and stable values with no distinct anomalies. Both the heavy and the transition metals (Pb, Ni, Co, Cu, Cr, Zn, and V) indicate moderate variability of contents. In the S-KCU, local enrichments in Cr occur (up to 58 $mg \cdot kg^{-1}$) whereas in the N-KCU its contents do not exceed 8 $mg \cdot kg^{-1}$. The remaining trace elements contents are also low, as e.g. Cu (3–7.3 $mg \cdot kg^{-1}$) and Pb (< 0.7 $mg \cdot kg^{-1}$). The highest variability of trace elements is indicated in the southeastern FA, where both the alkaline and the rare elements together with the heavy metals show much higher contents. Specifically, Ba and Sr demonstrate wide ranges of values (Ba:

18–334 mg·kg^{-1}, Sr: 3–27 mg·kg^{-1}) whereas local enrichments are observed in Pb (up to 8.2 mg·kg^{-1}), Cu (6.5–15.3 mg·kg^{-1}) and Cr (5–39 mg·kg^{-1}). The contents of the other trace elements: Nb, Y, Zr, Ga, and Hf remain low or moderate, with low variability.

The Al/(Al+Fe+Mn) ratios vary from 0.10 to 0.15 in the samples from the S-KCU, from 0.19 to 0.31 in those from the N-KCU and from 0.05 to 0.26 in the southeastern FA. The Al_2O_3/TiO_2 ratios are the lowest in the S-KCU (25–40), but increase in the N-KCU (34–63), and are their highest in the southeastern FA (27–100). Finally, the Fe_2O_3/TiO_2 ratios are at their highest in the southeastern FA (6–1,490, with high variability) and lowest in the N-KCU (78–240).

Rare earth elements

The results of REE analyses and the calculated anomalies are presented in Appendix (Tables 11–20). These values show a wide range of variation between the analyzed samples. Generally, depletion of REE is observed. The total analyzed REE contents are very low in all the types of chert with LREE prevailing over HREE.

Chert concretions

In the chert concretions from the S-KCU, variability of the total REE content is observed with the highest values found in the samples from the Piekary (average 4.46 mg·kg^{-1}) and the Dąbrowa Szlachecka (3.67 mg·kg^{-1}) outcrops whereas the lowest contents are in the specimens from Guminek Hill (1.47 mg·kg^{-1}). In most of the analyzed samples, the La_{SN}/Yb_{SN} ratio exceeds 1, which indicates moderate LREE enrichments relative to HREE. Distinct enrichment in LREE is observed in the samples from Bonarka Quarry whereas in those from the Dąbrowa Szlachecka and the Wielkanoc Hill outcrops, the La_{SN}/Yb_{SN} ratios are close to 1 or slightly lower, which suggests more balanced REE distribution or moderate enrichments in LREE. The La_{SN}/Sm_{SN} ratios are close to 1, with minor deviations. In the samples from the Dąbrowa Szlachecka outcrop, LREE are enriched in comparison with MREE whereas the samples from the Piekary outcrop are slightly enriched in MREE. In most of the analyzed samples, values of the Sm_{SN}/Yb_{SN} ratios exceed 1, which indicates enrichment in MREE related to HREE, except for the samples from the Dąbrowa Szlachecka outcrop, where relative enrichment in HREE is evident and a clear enrichment in MREE is absent. The average Eu/Eu^* ratio is about 0.8 for all samples, except for these from Bonarka Quarry where a positive Eu anomaly (about 1.24, on average) occurs. Moreover, in all the studied samples, negative Ce anomalies are indicated with the most diverse Ce/Ce^* values detected in the Piekary outcrop.

In the N-KCU, the total REE contents are lower than in the S-KCU. The highest average REE values (2.01 mg·kg^{-1}) are observed in the Rudniki samples whereas the lowest ones (1.68 mg·kg^{-1}) come from the Julianka outcrop. The lowest and the moderate values of the La_{SN}/Yb_{SN} ratios are in the samples from the Olsztyn and the Julianka outcrops, which suggests moderate enrichment in LREE or the lack of distinct LREE enrichment in relation to HREE. The highest and more variable values of this ratio are noticed in the Rudniki samples, which proves the strong and irregular enrichment in LREE relative to HREE. The La_{SN}/Sm_{SN} ratios reveal the highest variability among all the analyzed indicators. Specifically, samples from the Julianka and the Olsztyn outcrops demonstrate the trend of higher LREE to MREE enrichments, in comparison with those from the Rudniki site. The values of Sm_{SN}/Yb_{SN} ratios are below 1 in most samples collected in the Olsztyn and the Julianka outcrops, i.e., these samples are relatively enriched in HREE over MREE but in samples from the Rudniki outcrop, the values of this indicator often exceed 1.5, which documents strong enrichment in MREE related to HREE. The average Eu/Eu^* ratio values show significant differences between particular locations: Olsztyn – 1.17; Julianka – 0.88 and Rudniki – 1.05. The highest diversity occurs in samples from the Julianka outcrop whereas the lowest one is observed in those from the Rudniki site. The Ce anomalies are negative in all the analyzed samples. The lowest average Ce/Ce^* value (0.31) was calculated in samples from the Julianka outcrop, which also shows the lowest variability of values of this indicator.

In the samples collected in the BW, an average total REE content is 2.64 mg·kg^{-1}. The values of the La_{SN}/Yb_{SN} ratios in the Flintsbach outcrop are below 1.5, indicating moderate enrichment in LREE related to HREE. On the contrary, in the samples from the Münster outcrop, highly variable values of that indicator are observed, from very low to high, which means both the enrichment and the depletion in LREE, in given samples. The La_{SN}/Sm_{SN} ratio values are highly variable between particular localities and even within single outcrops. In detail, the samples from the Münster site demonstrate higher enrichment in LREE over MREE whereas the Flintsbach samples show relative depletion of LREE related to MREE. The Sm_{SN}/Yb_{SN} ratios exceed 1 in the Flintsbach

samples indicating domination of MREE over HREE whereas the Münster samples reveal general enrichment in MREE but also a significant variability of that indicator. The values of the Eu/Eu^* ratio differ among studied localities: the Flintsbach samples give an average value of 0.81, while values obtained from the Münster outcrop are higher (1.63). However, all analyzed samples exhibit overall negative Eu anomalies. The Ce/Ce^* ratios in both the Flintsbach and the Münster outcrops are roughly similar (about 0.37), with lower variability observed in samples from the former site.

In the southeastern FA, the lowest total REE contents occur (1.10 $mg \cdot kg^{-1}$, on average). The La_{SN}/Yb_{SN} ratios indicate moderate enrichment in LREE over HREE. However, the values of the La_{SN}/Sm_{SN} indicator prove relative depletion in LREE related to MREE. The Sm_{SN}/Yb_{SN} ratio demonstrates high variability but enrichment in MREE related to HREE occurs in only a single sample. The values of Ce/Ce^* ratios vary from 0.27 to 1.12 (0.74, on average) and show high diversity, from the positive Ce anomaly in a single sample to the negative anomalies in the two remaining ones. Unfortunately, some analytical constraints precluded the Eu/Eu^* calculation for samples from the southeastern FA.

In all the analyzed samples of chert concretions, positive Pr anomalies occur. The only exceptions are: a single sample from the Olsztyn outcrop and two others from the Julianka one (in N-KCU). The average Pr/Pr^* values are: 1.25 in the S-KCU, 1.28 in the N-KCU, 1.44 in the BW and 1.18 in the southeastern FA. Moreover, distinct positive Gd/Gd^* anomalies, between 1.22 and 1.49, are observed in all the studied regions.

Bedded cherts

In the bedded cherts from the S-KCU, the highest total REE contents are detected. The highest average value (5.55 $mg \cdot kg^{-1}$) is in the samples from the Ujazd outcrop whereas the lowest one (3.58 $mg \cdot kg^{-1}$) occurs in that from the Wielkanoc Hill. The La_{SN}/Yb_{SN} ratios exceed 1 (average about 1.3) in the samples from the Ujazd outcrop, which suggests a moderate enrichment in LREE over HREE. In the samples from the remaining localities, values of that indicator are around 1 or slightly over 1, which suggests a uniform distribution of all REE and the lack of distinct enrichments in LREE. The La_{SN}/Sm_{SN} ratios, around 1, are detected in all the analyzed samples, which suggests a balance between LREE and MREE. The highest values of the Sm_{SN}/Yb_{SN} ratios are indicated in the Ujazd samples, demonstrating the enrichment in MREE over HREE. In samples from the remaining sites, the values of this indicator are around 1, i.e. no enrichments in MREE related to HREE occur. The Eu/Eu^* ratios are mostly close to neutral, but their average values vary in particular samples, from 1.03 in the Ujazd outcrop, through 0.95 at Wielkanoc Hill to 0.87 in the Sikornik outcrop. Negative Ce anomalies are present in all the analyzed samples with an average Ce/Ce^* value of 0.26. The highest variability of that ratio is observed in the samples from Wielkanoc Hill and the lowest in those from the Sikornik outcrop.

In the bedded cherts from the N-KCU, the total REE contents are low (3.59 $mg \cdot kg^{-1}$, on average). The values of both the La_{SN}/Yb_{SN} and the La_{SN}/Sm_{SN} ratios exceed 1, which shows moderate enrichment in LREE over both the HREE and MREE. The Sm_{SN}/Yb_{SN} ratios also oscillate around 1 suggesting balanced distribution of MREE versus HREE. In samples from the Siedlce outcrop, typical is the lack of a distinct Eu anomaly ($Eu/Eu^* = 1.08$, on average) together with a negative Ce one ($Ce/Ce^* = 0.31$, on average).

In samples from the southeastern FA, particularly from the Kelheim outcrop, some analytical problems precluded the determination of the full REE range. The total REE contents in the samples from the Kelheim site are about 1.24 $mg \cdot kg^{-1}$ and those in the Hemau samples are 2.52 $mg \cdot kg^{-1}$. Moreover, the Kelheim samples reveal high values of both the La_{SN}/Yb_{SN} and the La_{SN}/Sm_{SN} ratios, which points out to high enrichment in LREE over both the MREE and the HREE. On the contrary, the Sm_{SN}/Yb_{SN} ratio (0.51) reveals a relative enrichment in HREE over MREE. In the samples from the Hemau outcrops, the values of the La_{SN}/Yb_{SN} and La_{SN}/Sm_{SN} ratios are variable indicating changes in the environmental conditions as one sample shows enrichment in HREE and the other – in LREE. In the samples from the Kelheim site, the Eu and Ce anomalies were determined in only a single sample ($Eu/Eu^* = 2.10$ and $Ce/Ce^* = 1.14$). Two samples from the Hemau site reveal variations in the Eu/Eu^* ratios: in one sample it is 1.14 and in the second it is 0.36. The Ce anomaly for both samples appears to be negative ($Ce/Ce^* = 0.53$, on average).

All the analyzed samples of bedded cherts exhibit positive Pr anomalies. The average values of the Pr/Pr^* ratio are: 1.38 for the samples from the S-KCU, 1.34 for those from the N-KCU and 1.36 for the southeastern FA samples. Moreover, a positive Gd anomaly is detected in the analyzed bedded cherts (Gd/Gd^* values from 0.70 to 1.90).

Chert concretions hosted in gravity flows deposits

The chert concretions hosted within gravity flows deposits sampled in the S-KCU reveal the highest total REE contents with average values up to 1.77 mg·kg^{-1}. The La_{SN}/Yb_{SN} ratio values are close to 1, i.e. no enrichment in LREE occurs whereas the La_{SN}/Sm_{SN} ratios are slightly lower than 1, which suggests small enrichment in MREE related to LREE. The Sm_{SN}/Yb_{SN} ratios somewhat over 1 indicate insignificant enrichment in MREE. The analyzed samples demonstrate variable values of the Eu/Eu* ratio in a single location. The Eu anomalies are generally neutral with the average ratio Eu/Eu* = 1.01. In all the analyzed samples, negative Ce anomalies occur with an average value of Ce/Ce* = 0.34 and with low variability between particular samples.

In the N-KCU, the average content of REE reaches 0.83 mg·kg^{-1}. All the calculated ratios: La_{SN}/Yb_{SN}, La_{SN}/Sm_{SN} and Sm_{SN}/Yb_{SN} exceed 1, which demonstrates enrichment in LREE related to HREE and in MREE over HREE. Although no clear Eu anomaly is observed, Eu/Eu ratios vary within single outcrops. All the samples show also negative Ce anomalies with an average value of Ce/Ce* = 0.49 and with low variations of values between the individual samples.

In the southeastern FA, the average total REE contents are 0.59 mg·kg^{-1} for the Kelheim outcrop and 2.48 mg·kg^{-1} for the Hemau one. The La_{SN}/Yb_{SN} ratio in a single sample from the Kelheim site indicates the lack of LREE enrichment over HREE whereas the Sm_{SN}/Yb_{SN} ratio suggests a moderate enrichment in MREE related to HREE. In the samples from the Hemau site, the La_{SN}/Yb_{SN} ratios demonstrate enrichment in LREE over HREE, whereas the average La_{SN}/Sm_{SN} ratio (about 0.72) suggests a relative enrichment in MREE related to LREE, and the average values of the Sm_{SN}/Yb_{SN} ratio over 4 point to strong domination of MREE in relation to HREE. Unfortunately, analysis of Eu anomalies was rather limited due to the small number of samples in which the full range of REE could be detected. In a sample from the Kelheim outcrop, the Eu/Eu* ratio is 1.91 whereas in the samples from the Hemau site the values of that indicator are variable: two samples show negative Eu anomalies and a single one has a positive Eu anomaly. The Ce anomalies differ between various locations from the southeastern FA. In the Kelheim samples, a lack of anomalies was found (average Ce/Ce* = 1.06) whereas in the Hemau samples, negative anomalies occurred (Ce/Ce* = 0.69, on average).

All the analyzed samples of chert concretions hosted within gravity flows reveal positive Pr anomalies except for two specimens from the Kelheim outcrop. The average Pr/Pr* ratio values are: 1.27 in the S-KCU, 1.18 in the N-KCU and 1.11 in the southeastern FA. Moreover, the samples from both the S-KCU and the N-KCU reveal positive Gd anomalies with average values of 1.11 for the S-KCU and 1.98 for the N-KCU. On the contrary, the Gd anomalies in the southeastern FA are negative (average value 0.84).

DISCUSSION

Petrographic observations

The petrography of both the chert concretions and the bedded cherts reflects the depositional conditions of the carbonate sediments and the nature of the diagenetic processes, which led to the replacement of calcium carbonate by silica. In most of the analyzed samples of chert concretions and bedded cherts, the predominant mineral is microcrystalline silica, whereas megaquartz, fibrous quartz, and/or chalcedony occur mostly as the infillings of pore spaces and/or bioclasts (particularly those large in size) (Kochman *et al*. 2020a; Matyszkiewicz and Kochman 2020; Kochman and Matyszkiewicz 2023, 2025).

The dominant microcrystalline silica shows low crystallinity and a high packing degree of quartz crystals (cf. Adachi *et al*. 1986; Yamamoto 1987; Chen *et al*. 2006; Van Kranendonk 2006; He *et al*. 2014; Shen; 2018; Lei *et al*. 2019), which suggests a hydrothermal origin of chert concretions and bedded cherts. The solubility of silica is only poorly affected by the pH until it reaches values about 9 (Guo *et al*. 2022). The presence of hydrothermal solutions can decrease pH in the seawater, which facilitates the dissolution of carbonate minerals. As a result, the influx of hydrothermal solutions, followed by their mixing with the seawater may give rise to the replacement of carbonates with both the microcrystalline and the cryptocrystalline quartz at temperatures above 100°C (cf. Shen *et al*. 2018). Hydrothermal fluids can be significantly diluted in oxic seawater, up to 1,000–10,000 times or even more (Nozaki *et al*. 1997). The cherts deposited in deep-water environments can by more easily influenced by hydrothermal fluids than those deposited in shallow seawater (He *et al*. 2013; Zhang *et al*. 2020).

On the contrary, the megaquartz crystals, typically infilling neptunic dykes crystallized at much higher temperatures (cf. Matyszkiewicz *et al*. 2016), similar to epigenetic siliceous rocks (Matyszkiewicz 1987; Kochman *et al*. 2020b). Their formation was

presumably related to secondary heating and the resultant recrystallization of microcrystalline quartz at higher temperatures (above 100°C up to even 350°C) in the presence of fluids relatively low in silica (Bello *et al*. 2025; cf. Zakharov *et al*. 2021).

In some chert concretion samples from the S-KCU, Sitarz *et al*. (2014) and Kochman *et al*. (2020a) identified moganite. This is a microcrystalline silica polymorph (cf. Flörke *et al*. 1984; Miehe *et al*. 1984; Heaney and Post 1992; Miehe and Graetsch 1992; Bustillo 2002; Graetsch and Grünberg 2012; Zhang and Moxon 2014) structurally similar to and commonly accompanying fine-crystalline quartz (cf. Flörke *et al*. 1976, 1984; Heaney and Post 1992). Moganite may occur in many siliceous rocks however, its amounts and stability are controlled by diagenetic conditions and temperature (Heaney and Post 1992; Bustillo 2002). This silica variety appears to be metastable and may be transformed into α-quartz over time or due to changing environmental conditions (Heaney and Post 1992; Rodgers and Cressey 2001). Moganite reveals higher stability at low temperatures, and shows higher dissolution rates together with lower thermodynamic stability in comparison with quartz (Gislason *et al*. 1997). The low contents of moganite in some chert concretions may suggest that their formation took place in a thermally stable environment, at low temperatures and limited hydrothermal activity. However, it must be emphasized that the role of moganite, present in various amounts in the studied cherts, remains poorly understood (Shepelenko *et al*. 2025).

Insights from major and trace elements geochemistry

The abundance analysis of major components may be applied to the reconstruction of the conditions of formation of cherts (e.g., Adachi *et al*. 1986; Yamamoto 1987; Murray 1994; Wang *et al*. 2012; He *et al*. 2014; Yu *et al*. 2019). For example, Kato and Nakamura (2003) postulated that cherts have a relatively simple major element composition while trace elements and REEs represent minor constituents, such as hydrothermal precipitates, volcanic detritus, and terrigenous clasts. Hence, these are the key indicators of the depositional environment. Other authors (see Boström and Peterson 1969; Adachi *et al*. 1986; Yamamoto 1987; Murray 1994) have demonstrated that Al and Ti are excellent indicators of terrigenous input whereas Fe represents the contribution of hydrothermal fluids. Marine hydrothermal sediments commonly show Fe/Ti ratios exceeding 20, which prove the contribution of hydrothermal components in marine sediments (Liang *et al*. 2022). Therefore, the correlation between Fe_2O_3 and SiO_2 suggests that the formation of given cherts was strongly controlled by hydrothermal processes (Adachi *et al*. 1986; Qiu and Wang 2011).

Analysis of the major element composition reveals that the analyzed cherts show high chemical stability. All the types of cherts are dominated by SiO_2 (commonly > 90 wt.%) with simultaneously low contents of Al_2O_3, Fe_2O_3, and TiO_2 as well as very low contents of trace elements. Chemical differences between the samples from various regions are low and are limited mainly to local anomalies (enrichments) of Fe_2O_3 and some trace elements contents. Thus, the processes responsible for chert formation were presumably similar in all the studied regions.

The chert concretions from the KCU, the BW, and the southeastern FA reveal high chemical homogeneity. Specifically, these cherts show very high SiO_2 contents, usually within the range of 94–98 wt.% together with low contents of Al_2O_3 (0.05–0.40 wt.%) and TiO_2 (< 0.03 wt.%). Such values are typical of cherts generated in environments having a limited supply of terrigenous material and a dominant input of silica of chemical or hydrothermal origin. The moderate variability of Fe_2O_3 contents may indicate local differences in redox conditions or enrichment in Fe derived from hydrothermal solutions. Important is also a moderate enrichment in Ba, which may result from a still significant influence of low-temperature hydrothermal solutions on the silicification process. The local enrichments in Ba, especially in the S-KCU (Matyszkiewicz *et al*. 2015a, 2016), confirm an episodic influx of such solutions whereas the results of isotope analyses of Nd and Sr point out to their continental provenance (Matyszkiewicz *et al*. 2016). Additionally, the local enrichments in Cu, Cr and Ni (noticed in Bonarka Quarry, in the Rudniki, and in the Münster outcrops) may be related to a limited inflow of hydrothermal solutions enriched in metals or may reflect variable redox conditions in these depositional environments. Moreover, the low to non-detectable contents of trace metals such as Co, Cr, Cu, Ni, Zn, and Pb indicate a hydrothermal origin of the Fe-Mn mineralization (Chiari *et al*. 2012). On the other hand, locally increased contents of Pb and Cu (Matyszkiewicz *et al*. 2015a) may additionally confirm the influence of relic hydrothermal solutions, presumably related to regional faulting events (Sibson 1987; Aranburu *et al*. 2002).

The bedded cherts from the KCU and the southeastern FA show distinct differences in SiO_2 contents,

from relatively low (58.74 wt.%) up to almost pure silica (98.44 wt.%). The highest and the least variable SiO_2 values (94.77–98.17 wt.%) occur in the southeastern FA, which suggests a lower supply of detrital material and more homogeneous diagenetic conditions. Both the low contents of TiO_2 and the moderate concentrations of Al_2O_3 and Fe_2O_3 indicate the dominance of silica precipitated from the seawater and the low share of terrigenous components (Adachi *et al.* 1986; Murray 1994). Simultaneously, moderate variability of Fe_2O_3 contents (0.14–1.51 wt.%) may reflect the local differences in redox conditions of the diagenetic environment or the presence of ferruginous minerals. Hence, Fe is mostly of hydrothermal origin and is commonly applied as an indicator of hydrothermal influx into marine sediments (Murray 1994). The presence of Fe compounds in siliceous rocks from both the N-KCU (Matyszkiewicz *et al*. 2015a) and the southeastern FA was noticed in the earlier publications and confirmed by the results of Mössbauer analyses (Kochman and Matyszkiewicz 2025). It must be emphasized that the Fe minerals: goethite and hematite were found in epigenetically silicified limestones from the N-KCU, although in minor or trace amounts (Matyszkiewicz *et al*. 2015a). The processes forming such mineralization were related to the circulation of hydrothermal solutions in fracture systems and the resultant precipitation of silica together with metal compounds, including Fe-minerals. Traces of Fe mineralization are visible as brown or reddish-brown stains in silicified limestones. The Fe-minerals (goethite, hematite) are present also in brownish and chocolate-colored, successive rims embedding chert concretions from the southeastern FA, which suggests formation of individual rims in various diagenetic environments, under different chemical conditions and several stages of silicification controlled by various silica sources (Kochman and Matyszkiewicz 2025).

The moderate enrichment of bedded cherts in Fe_2O_3 observed in some outcrops (Ujazd, Wielkanoc Hill, and Kelheim) may document the episodes of increased Fe availability related to the circulation of Fe-rich solutions during early diagenesis (Yamamoto 1987; He *et al*. 2014). On the other hand, the bedded cherts from the N-KCU reveal a homogeneous trace element composition with low Ba, Rb, and Sr contents as well as stable amounts of transition metals (Cu, Cr, Zn), which points to stable, low-energy diagenetic environment.

The highest geochemical diversity is observed in the southeastern FA, where bedded cherts reveal a very wide range of Ba contents (34–429 $mg \cdot kg^{-1}$) possibly indicating local enrichments related to the influx of hydrothermal solutions. Moreover, the high contents of Cu (up to 28.9 $mg \cdot kg^{-1}$) and Cr (up to 46 $mg \cdot kg^{-1}$) correlate with the presence of reducing conditions and, potentially, with the contribution of organic matter. The latter might have catalyzed the sorption and immobilization of metals during the transformation of silica gel into chalcedony and microquartz (cf. Williams *et al.* 1985; Hesse 1989). Additionally, the presence of transition metals (Cu, Cr, and Ni) demonstrates that diagenesis might have locally proceeded under reducing conditions with the participation of organic matter, which is consistent with the formation models of laminated cherts proposed by Hesse (1989) and Knauth (1994).

The analyzed chert concretions hosted within gravity flow deposits reveal very high contents of SiO_2 (97.03–99.02 wt.%) with low diversity of values between the S-KCU and the N-KCU. However, the samples from the southeastern FA show higher variability of SiO_2 contents (83.70–98.93 wt.%) probably reflecting some regional differences in the nature of the silicification. The oxides contents: Al_2O_3 (0.07–0.38 wt.%) and TiO_2 (< 0.005 wt.%, excluding the Hemau sample) are very low, which indicates a negligible participation of terrigenous material. Furthermore, the trace element contents in chert concretions hosted within gravity flows are generally low and stable in both the S-KCU and the N-KCU, which points to their formation in an environment of limited chemical exchange. The low contents of alkaline and rare elements as well as transition metals suggest the rather insignificant influence of hydrothermal solutions. The highest diversity of trace element composition is observed in the southeastern FA, where Ba contents (18–334 $mg \cdot kg^{-1}$) are distinctly elevated and local anomalies of transition metals (Cu, Cr, Pb) are evident. This suggests a more complex nature of diagenesis processes related to both the episodic influxes of hydrothermal solutions and the local changes of redox regime within the gravity flow deposits (Boström and Peterson 1969; Hesse 1989; He *et al*. 2014). Simultaneously, the high purity of SiO_2, together with the low contents of trace elements indicate the chemical-diagenetic origin of these concretions, typical of limited circulation of solutions and low supply of terrigenous material (Williams *et al.* 1985; Hesse 1989; Knauth 1994).

In some samples, an increase of Sr contents was detected presumably reflecting the presence of small amounts of limestone in the analyzed materials. On the contrary, distinct depletion in Sr was noticed in siliceous rocks of high SiO_2 contents from the N-KCU (Matyszkiewicz *et al*. 2015a).

Geochemical indicators of silica origin

The geochemical indicators: Al/(Al+Fe+Mn), Al_2O_3/TiO_2 and Fe_2O_3/TiO_2 enable the identification of silica sources in siliceous rocks. Siliceous rocks are characterized by low values of the Al/(Al+Fe+Mn) and the Al_2O_3/TiO_2 ratios, and by high values of the Fe_2O_3/TiO_2 ratio (see e.g.: Boström and Peterson 1969; Boström 1983; Sugisaki 1984; Adachi *et al*. 1986; Aitchison and Flood 1990; Murray 1994; Wang *et al*. 2012; Yu *et al*. 2019). Moreover, petrological evidence demonstrates that siliceous rocks were formed in carbonates deposited in a marine environment affected by intensive hydrothermal processes. The low values of the Al/(Al+Fe+Mn) ratio suggest periodical influxes of hydrothermal solutions into the seawater from vents (e.g.: Boström 1983; Adachi *et al*. 1986; Murray 1994; Kochman *et al*. 2020b; Wang *et al*. 2012; Migaszewski *et al*. 2022; Yeşilot Kaplan 2023). The values of that ratio depend on the volume of hydrothermal solution input into the sediments and decrease with the increasing hydrothermal activity, from 0.6 in sediments of biological provenance to 0.01 in hydrothermal deposits (Adachi *et al*. 1986; Yamamoto 1987).

For various types of cherts collected in both the S-KCU and the N-KCU, the values of the Al/(Al+Fe+Mn) ratio remain relatively low, from 0.04 to 0.44. Moreover, diverse ranges of values of that indicator are observed in chert concretions and in chert concretions hosted in gravity flows, as well as similar values are indicated for bedded chert in both the KCU parts. In the samples from Germany, lower values of the Al/(Al+Fe+Mn) ratio are quoted: from 0.10 to 0.33 in the BW and from 0.05 to 0.30 in the southeastern FA. Similar values of the Al/(Al+Fe+Mn) ratio, particularly in the bedded cherts from both the S-KCU and the N-KCU as well as in the chert concretions from the BW and the southeastern FA, prove stable depositional conditions in similar marine environments (cf. Murray 1994). Comparable relationships are observed for the Al_2O_3/TiO_2 ratio, which is commonly used for evaluation of the origin of detrital material and the influence of hydrothermal processes in sediments (Adachi *et al*. 1986; Murray 1994). Additionally, low values of this ratio indicate that the formation of cherts was controlled by local hydrothermal pulses, which played an important role in the silicification process (cf. Hein *et al*. 1978; Adachi *et al*. 1986). Comparison of the Al/(Al+Fe+Mn) and the Al_2O_3/TiO_2 values calculated for various types of cherts demonstrates the decreasing amounts of detrital material in their formation process, in the following order: bedded cherts – chert concretions hosted within gravity flows – chert concretions, which may correspond to a mixed model of chert origin. The Fe/Ti ratios in marine hydrothermal sediments commonly exceed 20 hence that indicator appears to be a reliable proxy for hydrothermal activity in marine sediments (Boström 1983; Liang *et al*. 2022). The wide range of the Fe_2O_3/TiO_2 ratio values found in various types of cherts may reflect local enrichments in Fe of hydrothermal origin (Adachi *et al*. 1986; Murray 1994).

The results of geochemical analyses of cherts sampled in various outcrops are presented as ternary Al-Fe-Mn plots after Adachi *et al*. (1986) (Text-fig. 5). The distribution of elements shown in the plots is typical of rocks formed under the influence of hydrothermal solutions. The plots enable researchers not only to identify the hydrothermal origin of the cherts in question but also to differentiate them from biogenic and terrigenous cherts. The distribution patterns of elements in these plots are typical of rocks formed by the action of hydrothermal solutions, which supports the conclusions drawn from both the petrographic observations and the geochemical analyses.

REE geochemistry and interpretation of anomalies

REE geochemistry is a powerful tracer of sedimentary and diagenetic processes in siliceous deposits (Piper 1974; Murray *et al*. 1991; Bau and Dulski 1996). REE are commonly applied as indicators of marine sedimentary paleoenvironments due to their low susceptibility to late diagenetic processes (Douville *et al*. 1999). Both the REE abundance patterns and the relative fractionations are valuable environmental indicators for cherts of various ages and are tools suitable for identification of silica sources (e.g., Murray *et al*. 1990; Girty *et al*. 1993; He *et al*. 2019). Variations in REE patterns between chert concretions, bedded cherts, and chert concretions hosted within gravity flow deposits may reflect variations in sedimentary environments, composition of pore solutions and intensity of diagenetic processes (Bau 1991; Kamber and Webb 2001; Bolhar *et al*. 2004).

In some samples, particularly the cherts collected in the BW and the southeastern FA (Text-figs 6–8), determination of the full range of REE was impossible, which precluded the identification of geochemical anomalies. Among the values of the Ce/Ce^*, Eu/Eu^*, and Pr/Pr^* ratios, those below 0.8 are indicative of negative anomalies whereas those above 1.2

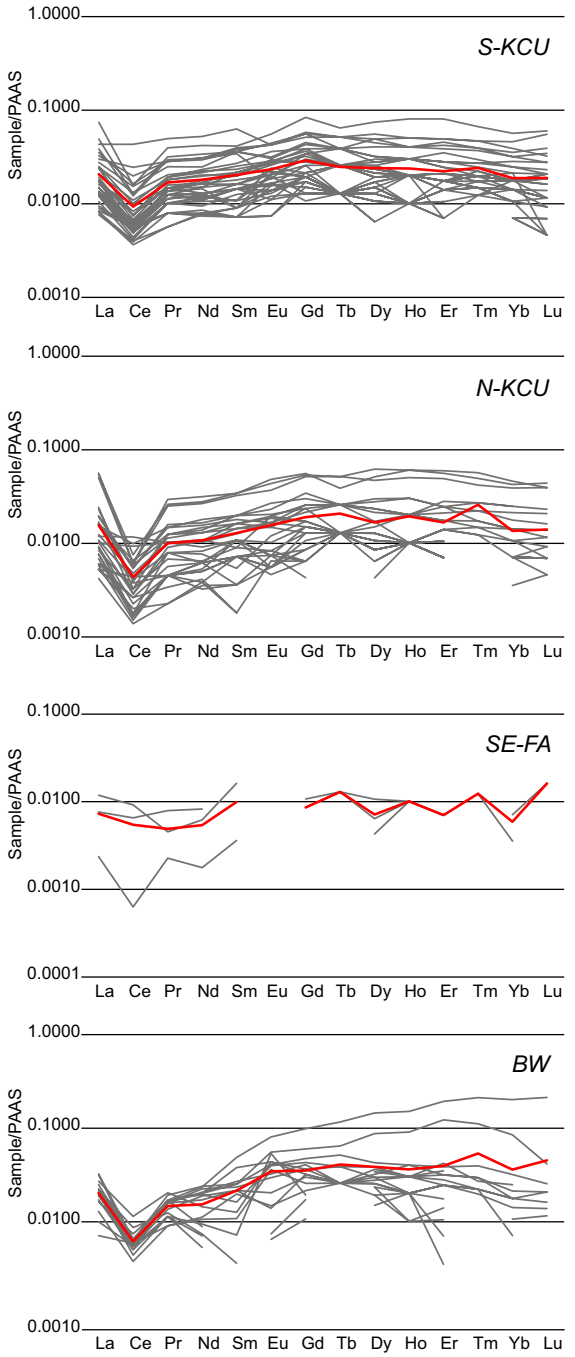

Text-fig. 6. PAAS-normalized REE patterns of chert concretions (the red line indicates the average values for the given region).

represent positive ones. Moreover, anomalous values within the range ±0.2 to 1 are related to measurement errors (cf. Grawunder *et al*. 2014; Migaszewski *et al*. 2016).

In most of the analyzed samples, LREE are enriched relative to MREE, which suggests that during the formation of cherts, REE are supplied by the seawater or diagenetic solutions showing domination of LREE over MREE and selective removal of HREE (Hatije *et al*. 2024). The diversity of La_{SN}/Yb_{SN} and Sm_{SN}/Yb_{SN} ratios reflects both the mixing of hydrothermal solutions with the seawater and the local diagenetic conditions (Chen *et al*. 2006; German *et al*. 1990, 1999; Qiu and Wang 2011). Generally, marine sediments affected by hydrothermal solutions reveal distinct geochemical features (Bolhar *et al*. 2005; Bau *et al*. 2014; Wang *et al*. 2022), including LREE enrichment and positive Eu anomalies. Sediments formed with the input of hydrothermal solutions usually inherit the REE patterns of the parent solutions, as e.g. the positive Eu anomalies (German *et al*. 1990; Mills and Elderfield 1995; Bau and Dulski 1999; Chen *et al*. 2006; Wang *et al*. 2012). However, the REE patterns change with the increasing influx of ambient seawater (Wang *et al*. 2012; He *et al*. 2019). Thus, the low La abundances in some samples of chert concretions and bedded cherts likely resulted mainly from their high precipitation rates, and/or the scavenging of REE by Fe-Mn oxyhydroxides in the hydrothermal vent systems (e.g.: Olivarez and Owen 1989; German *et al*. 1990; Chen *et al*. 2006).

Ce/Ce anomalies*

The presence of Ce anomalies is closely associated with the prevailing redox conditions of the seawater. Unlike the other trivalent REE, Ce is susceptible to oxidative removal from the seawater, reflecting its redox-sensitive behavior. Due to its relatively stable values during diagenesis, the Ce/Ce^* ratio is a valuable indicator for identifying the diagenetic environments (Shimizu and Masuda 1977; Murray *et al*. 1992; Bau and Dulski 1996; Alibo and Nozaki 1999; He *et al*. 2019; Yeşilot Kaplan 2023). Specifically, in an oxidizing environment, Ce^{3+} ion can be oxidized to Ce^{4+}, which shows lower solubility and, thus, can isomorphically substitute for Mn^{4+} in Fe- and Mn-oxides leading to the negative Ce anomaly (Shimizu and Masuda 1977; German and Elderfield 1990; Junguo *et al*. 2011). On the contrary, both the suboxic and anoxic marine environments typically lack the pronounced Ce anomalies because Fe-Mn-oxides undergo reductive dissolution under such conditions (German *et al*. 1991). Values of negative Ce anomalies ($Ce/Ce^* < 1$) indicate the formation of cherts under the oxidizing conditions whereas positive Ce anomalies ($Ce/Ce^* > 1$) suggest the anoxic environments (Gao *et al*. 2020; Deng *et al*. 2022).

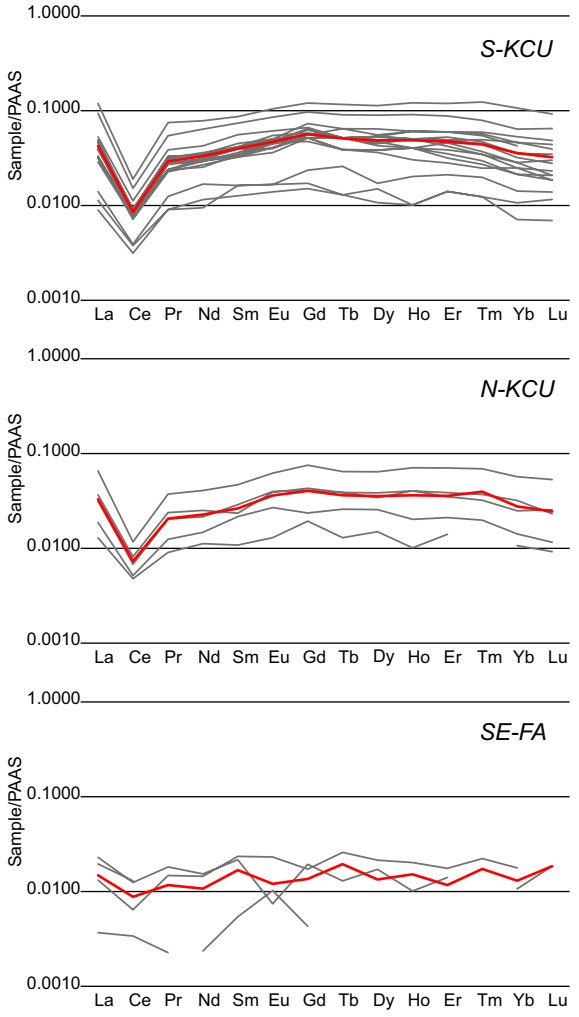

Text-fig. 7. PAAS-normalized REE patterns of bedded cherts (the red line indicates the average values for the given region).

Negative Ce anomalies are ubiquitous in well-oxygenated, open-ocean waters whereas the studies on REE distribution in modern, anoxic deep waters demonstrate either lowered or even absent negative Ce anomalies (German and Elderfield 1990; German *et al*. 1991). The Ce/Ce^* ratio values change also with the seawater depth, hence, in the open-ocean waters these values usually fall into the range of 0.2–0.3, but in the sediments from the nearshore zone, their increase to 0.8–1.0 is observed. If hydrothermal activity is present in the sedimentary basin, the values of negative Ce anomalies increase, while HREE are strongly depleted in relation to LREE (Elderfield *et al*. 1990). The influence of terrestrial sediments tends to elevate the Ce/Ce^* ratio (Murray *et al*. 1991). However, the negative Ce anomalies commonly result from the enrichment in La of sediments affected by hydrothermal solutions and are, therefore, not necessarily a consequence of anomalous Ce behavior (Bau and Dulski 1996; Yu *et al*. 2019). The negative Ce anomalies cause the appearance of positive Pr anomalies (Bau and Dulski 1996).

Negative Ce anomalies (Ce/Ce^* = 0.26–0.69; Text-figs 6–8) are observed in all the studied regions, which documents the dominance of highly oxic conditions during the silicification. The clear, negative Ce anomalies observed in the S-KCU, the N-KCU, and the BW support the presence of well-oxygenated seawater and the limited action of hydrothermal solutions (De Baar *et al*. 1985; Bau and Dulski 1996). However, the analyses of samples from some outcrops (Piekary, Julianka) reveal weaker or even vanishing Ce anomalies, which may reflect locally decreased oxygen contents or episodic influx of hydrothermal solutions enriched in Fe and Mn. In the southeastern FA, the negative Ce anomaly is less evident and can be caused by a limited supply of oxidized seawaters or a local influx of low-oxygenated hydrothermal solutions (Murray *et al*. 1991; Chen *et al*. 2006; He *et al*. 2019). The high Ce/Ce^* values detected in some samples may suggest an episodic contribution of reducing hydrothermal solutions, which disturbed local REE distributions in pore solutions. Under such conditions, Ce^{3+} could not be effectively oxidized to Ce^{4+}, which led to the partial vanishing of the negative Ce anomalies.

The Pr/Pr^* ratios over 1 found in all the analyzed samples confirm that the observed Ce anomalies are real and do not result from enrichment in La. This supports the idea of mixing the seawater with hydrothermal solutions during silica precipitation (Bau and Dulski 1996; Wang *et al*. 2012).

Gd/Gd^* anomalies

The positive Gd anomalies are typical of oxygen-rich marine environments (De Baar *et al*. 1985; Bau and Dulski 1996) because the Gd^{3+} ion forms stable complexes with organic and carbonate ligands, thus, it remains longer in solution than adjacent members of the REE series, i.e. Tb and Eu. The positive Gd anomalies in the seawater can be associated also with marine carbonates (Bau and Dulski 1996). Solutions of slightly acidic to almost neutral pH usually show positive Gd anomalies whereas basic solutions reveal negative Gd anomalies. Thus, the lack of negative Gd anomalies in samples suggests low amounts or absence of complex organic compounds during chert formation (Lee and Byrne 1993). The presence of

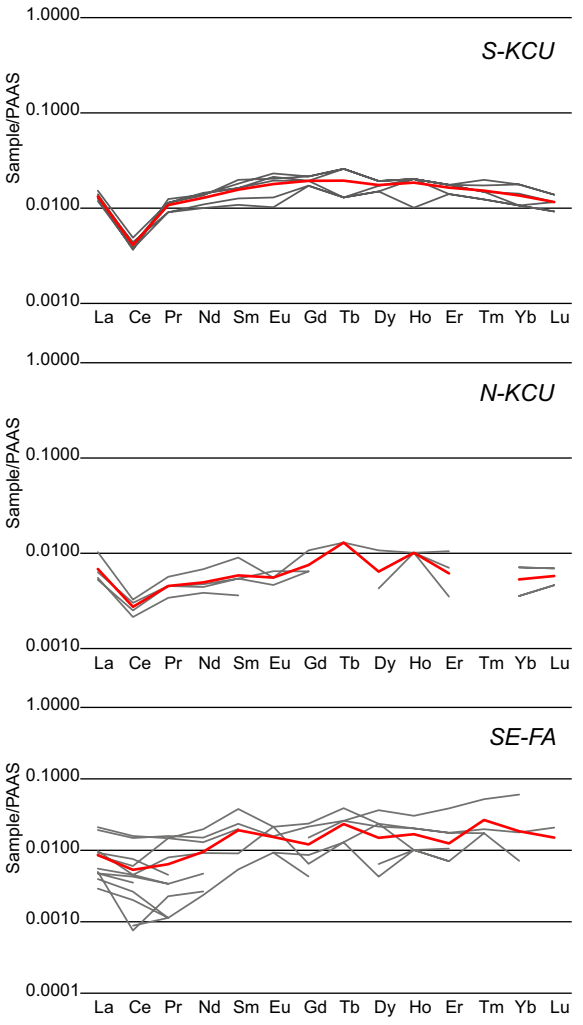

Text-fig. 8. PAAS-normalized REE patterns of chert concretions hosted within gravity flow deposits (the red line indicates the average values for the given region).

distinct positive Gd anomalies, particularly in samples having low contents of trace elements, indicates the dominance of well-oxygenated marine conditions as well as the low amount of organic matter available during silicification. Moreover, the positive Gd anomalies, typical of well-oxygenated seawater, confirm that the main source of silica was the seawater, whereas the role of hydrothermal solutions was only local and episodic (De Baar *et al*. 1985; Bau and Dulski 1996).

Eu/Eu anomalies*

The Eu anomalies are an important indicator of the input of hydrothermal solutions into a sedimentary basin (e.g.: Danielson *et al*. 1992; Bau and Dulski 1996; Douville *et al*. 1999; Chen *et al*. 2006; Wang *et al*. 2012; He *et al*. 2019; Deng *et al*. 2022; Yeşilot Kaplan 2023). The Eu anomalies depend on the following factors: (i) redox potential, (ii) pH and (iii) activity of ligands such as sulfates, carbonates, and chlorides (Sverjensky 1984; German and Elderfield 1990; Bau and Möller 1992). The Eu/Eu* ratios exceeding 1 suggest a strong influence of hydrothermal fluids on silica deposition. Fractionation of Eu in relation to the remaining REE together with reduction of Eu^{3+} to Eu^{2+} may proceed at temperatures over 200–250°C (e.g., Sverjensky 1984; Bau 1991; Kato and Nakamura 2003). At low temperatures, close to those prevailing on the Earth's surface, the dominant ion is Eu^{3+}, except for the most reducing, alkaline pore waters within anoxic marine sediments. The high-temperature fluids preferentially extract Eu^{2+} from oceanic crust by water-rock reaction under the acidic conditions (Elderfield *et al*. 1988), which leads to Eu enrichment in hydrothermal fluids (Bau 1991; Douville *et al*. 1999). Above approximately 250°C and at elevated pressures, the Eu^{2+} ion becomes a dominant component. The values of Eu anomalies reflect the degree of mixing of hydrothermal and seawater components, and indicate that only a minor proportion of REE was derived from hydrothermal fluids, while the majority originated from the ambient seawater (Chavagnac *et al*. 2005).

The low-temperature hydrothermal solutions (100–150°C) of redox potential close to magnetite/hematite or sulfide/sulfate stability ranges may contain significant amounts of both the Eu^{2+} and Eu^{3+} ions, which gives rise to weak, positive Eu anomalies. This, in turn, suggests that cherts essentially precipitated from the low-temperature hydrothermal solutions (Kato and Nakamura 2003) or due to the action of complicated, multistage diagenetic processes (Shen *et al*. 2018). The lack of distinct, positive Eu anomalies may also indicate that silicification might have proceeded as a result of waning hydrothermal solutions, near the end of hydrothermal activity periods and/or in the distal parts of fracture systems, away from the main solution transfer conduits and/or at an enhanced influence of seawater (German *et al*. 1990; Wang *et al*. 2012, He *et al*. 2019).

In the studied regions, the positive Eu anomalies occur mostly in the chert concretions from the S-KCU and the BW (Text-fig. 6), whereas in the bedded cherts, mostly neutral Eu anomalies are known from the S-KCU and the N-KCU (Text-fig. 7). Concerning the chert concretions hosted within gravity flows deposits, the positive Eu anomalies prevail in both the

S-KCU and the southeastern FA (Text-fig. 8). The positive Eu anomalies (Eu/Eu^* up to 1.2) disclosed in both the Bonarka Quarry and the Münster site point out to the local influence of hydrothermal solutions or to remobilization of REE during diagenesis (German and Elderfield 1990; Bau 1991) as well as indicate the reducing conditions in the sedimentary basin (Danielson *et al*. 1992; Bau and Dulski 1996). The lack of clear, positive Eu anomalies in the remaining studied localities implies that chert formation might have proceeded from the waning hydrothermal solutions, close to the end of hydrothermal episodes and/or in the distal parts of fracture systems, away from the principal conduit zones. Alternatively, silicification processes might have continued with a minor contribution of hydrothermal solutions or under the increased influence of the seawater (German *et al*. 1990; Bau and Möller 1992; Wang *et al*. 2012; He *et al*. 2019). The clear, positive Eu anomalies occur close to the hydrothermal vents (within about 10 km distance, see Chen *et al*. 2006). On the other hand, the presence of negative Eu anomalies in a few samples of bedded cherts, suggests precipitation from the seawater-dominant solutions, away from the hydrothermal vents clusters. Differences in the values of Eu anomalies between particular locations presumably reflect differences in the temperatures of hydrothermal solutions responsible for that silicification process (Kato and Nakamura 2003).

CONCLUSIONS

The geochemical analyses of siliceous rocks from the studied regions in Poland and Germany did not reveal any significant differences in their chemical composition. Minor variations were only occasionally found in both the individual samples and the samples derived from a single outcrop. The results of studies on cherts from the KCU, the BW, and southeastern FA provide evidence that their formation proceeded in several stages of diagenesis, under the significant influence of hydrothermal solutions. The composition of cherts is dominated by SiO_2, whereas the contents of Al_2O_3, TiO_2, Fe_2O_3, and trace elements are low, which advocates a limited contribution of terrigenous material and a predominance of silica derived from hydrothermal sources. Petrographic observations provide the presence of microcrystalline quartz accompanied by occasionally encountered coarse-crystalline quartz, which suggests episodic input of higher-temperature solutions, in accordance with the periodic nature of hydrothermal activity.

The obtained results of REE analyses correlate well with those of major and trace elements. The REE patterns confirm the mixed nature of the environments in which the cherts were formed. The negative Ce anomalies disclosed in the samples from all the localities, suggest oxidizing environmental conditions during silicification, whereas the positive Eu anomalies found in some selected samples indicate the local influence of hydrothermal solutions and partial reducing conditions within the sediments. Differences in the values of Eu anomalies between various sampling sites reflect the variations of temperatures and the intensity of activity of the hydrothermal solutions during silicification. The Eu anomalies show that siliceous rocks formed far from hydrothermal centers. Subtle geochemical differences between some samples presumably result from the varying controls of the chert-forming hydrothermal solutions, e.g., their temperatures (cf. Kato and Nakamura 2003).

Similarly, the values of geochemical indicators: $Al/(Al+Fe+Mn)$, Al_2O_3/TiO_2 and Fe_2O_3/TiO_2 integrated with the REE patterns indicate that chert formation was controlled by low-temperature hydrothermal solutions and chemical precipitation of silica at limited supply of terrigenous material. These results support a mixed model of chert origin, which includes both hydrothermal activity and the contribution of seawater under variable redox conditions.

The results of geochemical analyses corroborate the relationship between silicification of the Upper Jurassic carbonates from the KCU and the episodes of tectonic activity, which triggered migration of silica-carrying hydrothermal solutions along fault zones (Gołębiowska *et al*. 2010; Kochman and Matyszkiewicz 2012; Matyszkiewicz *et al*. 2015a, 2016). Similar conclusions are drawn for the origin of siliceous rocks encountered in the Upper Jurassic carbonates from the southeastern FA and the BW (Kochman and Matyszkiewicz 2025). Therefore, hydrothermal activity was the more likely main silica source for the siliceous rocks formed in the Upper Jurassic successions from the studied fragments of the northern margin of the Tethys Ocean.

Acknowledgements

The paper presents a next part of the results of studies carried on within the grant "Processes controlling the formation of chert nodules and bedded cherts in the Upper Jurassic sediments from the Kraków-Częstochowa Upland" funded by the National Science Centre, Poland, contract No. UMO-2017/27/B/ST10/00594 for the period 2018–2021, principal

investigator Jacek Matyszkiewicz, and the subsidy granted to the AGH University of Krakow by the Ministry of Science and Higher Education.. The author acknowledges with gratitude the insightful comments and valuable suggestions of Professor A. Gałuszka, Professor A. Muszyński, and an anonymous reviewer, which greatly improved this manuscript.

REFERENCES

Adachi, M., Yamamoto, K. and Sugisaki, R. 1986. Hydrothermal chert and associated siliceous rocks from the Northern Pacific: their geological significance as indication of ocean ridge activity. *Sedimentary Geology*, **47**, 125–148.

Aitchison, J.C. and Flood, P.G. 1990. Geochemical constraints on the depositional setting of Palaeozoic cherts from the New England orogen, NSW, eastern Australia. *Marine Geology*, **94**, 79–95.

Alexandrowicz, S.W. 1955. Notes on the origin of the Vistula Gap at Tyniec (near Cracow). *Biuletyn Instytutu Geologicznego*, **97**, 271–295. [In Polish with English summary]

Alexandrowicz, S.W. 1960. Geological structure of the vicinity of Tyniec. *Biuletyn Instytutu Geologicznego*, **152**, 5–93. [In Polish with English summary]

Alibo, D.S. and Nozaki, Y. 1999. Rare earth elements in seawater: particle association, shale-normalization, and Ce oxidation. *Geochimica et Cosmochimica*, **63**, 363–372.

Aranburu, A., Fernandez-Mendiola, P.A., Lopez-Horgue, M.A. and Garcia-Mordejar, J. 2002. Syntectonic hydrothermal calcite in a faulted carbonate platform margin (Albian of Jorrios, northern Spain). *Sedimentology*, **49**, 875–890.

Bau, M. 1991. Rare-earth element mobility during hydrothermal and metamorphic fluid-rock interaction and the significance of the oxidation state of europium. *Chemical Geology*, **93**, 219–230.

Bau, M. and Dulski, P. 1996. Distribution of yttrium and rare-earth elements in the Penge and Kuruman iron formations, Transvaal Supergroup, South Africa. *Precambrian Research*, **79**, 37–55.

Bau, M. and Dulski, P. 1999. Comparing yttrium and rare earths in hydrothermal fluids from the Mid-Atlantic Ridge: implications for Y and REE behaviour during near-vent mixing and for the Y/Ho ratio of Proterozoic seawater. *Chemical Geology*, **155**, 77–90.

Bau, M. and Möller, P. 1992. Rare earth element fractionation in metamorphogenic hydrothermal calcite, magnesite and siderite. *Mineralogy and Petrology* **45**, 231–246.

Bau, M., Schmidt, K., Koschinsky, A., Hein, J., Kuhn, T. and Usui, A. 2014. Discriminating between different genetic types of marine ferro-manganese crusts and nodules based on rare earth elements and yttrium. *Chemical Geology*, **381**, 1–9.

Beauchamp, B. and Baud, A. 2002. Growth and demise of Permian biogenic chert along northwest Pangea: evidence for end-Permian collapse of thermohaline circulation. *Palaeogeography, Palaeoclimatology, Palaeoecology*, **184**, 37–63.

Bello, A.M., Amao, A.O., Koeshidayatullah, A.I, Alnazghah, M., Alrowaie, M.A., Herlambang, A. and Al-Ramadan, K. 2025. Petrological and geochemical characteristics of Ordovician cherts in the Qasim Formation, NW Saudi Arabia: Understanding the roles of biogenic and volcanic activities. *Journal of Asian Earth Sciences*, **280**, 106483.

Binsteiner, A. 2005. Die Lagerstätten und der Abbau Bayerischer Jurahornstein sowie deren Distribution im Neolithikum Mittel- und Osteuropas. *Jahrbuch des Römisch-Germanischen Zentralmuseums*, **52**, 43–155.

Bolhar, R., Kamber, B.S., Moorbath, S. Fedo, C.M. and Whitehouse, M.J. 2004. Characterisation of early Archaean chemical sediments by trace element signatures. Earth and Planetary Science Letters, **222**, 43–60.

Bolhar, R., Van Kranendonk, M.J. and Kamber, B.S. 2005. A trace element study of siderite-jasper banded iron formation in the 3.45 Ga Warrawoona Group, Pilbara Craton – Formation from hydrothermal fluids and shallow water. *Precambrian Research*, **137**, 93–114.

Boström, K. 1983. Genesis of ferromanganese deposits-diagnostic criteria for recent and old deposits. In: Rona, P.A., Boström, K., Laubier, L. and Smith, K.L. (Eds), Hydrothermal Processes at Seafloor Spreading Centers, 473–483. Plenum Press; New York.

Boström, K. and Peterson, M.N.A. 1969. The origin of aluminum-poor ferromanganoan sediments in areas of high heat flow on the East Pacific rise. *Marine Geology*, **7**, 427–447.

Brandl, M., Hauzenberger, C., Martinez, M.M., Filzmoser, P. and Werra, D.H. 2016. The application of the multi-layered chert sourcing approach (MLA) for the characterisation and differentiation of 'Chocolate Silicites' from the Holy Cross Mountains, South-Central Poland. *Archaeologia Austriaca*, **100**, 119–149.

Budziszewski, J. 2008. Current research on the occurrence and prehistoric exploitation of chocolate flint. In: Borkowski, W., Libera, J., Sałacińska, B. and Sałaciński, S. (Eds), Krzemień czekoladowy w pradziejach. Materiały z konferencji w Orońsku, 08–10.10.2003. Studia nad gospodarką surowcami krzemiennymi w pradziejach 7, 33–106. Instytut Archeologii UMCS and Państwowe Muzeum Archeologiczne; Warszawa–Lublin. [In Polish with English summary]

Bukowy, S. 1956. Geology of the area between Kraków and Korzkiew. *Biuletyn Państwowego Instytutu Geologicznego,* **108**, 17–82. [In Polish with English summary]

Bustillo, M.A. 2002. Occurrence and significance of the moganite in silica rocks: A review. *Journal of Iberian Geology*, 2002, **28**, 157–166.

Bustillo, M.A. 2010. Silicification of continental carbonates. In: Alonso-Zarza, A.M. and Tanner, L.H. (Eds), Carbonates

in continental settings: processes, facies and applications, Developments in Sedimentology, 62, 153–174. Elsevier; Amsterdam.

Bustillo, M.Á. and Ruiz-Ortiz, P.A. 1987. Chert occurrences in carbonate turbidites: examples from the Upper Jurassic of the Betic Mountains (southern Spain). *Sedimentology*, **34**, 611–621.

Bustillo, M.Á., Castañeda, N., Capote, M., Consuegra, S., Criado, C., Díaz-del-Río, P., Orozco, T., Pérez-Jiménez, J.L. and Terradas, X. 2009. Is the macroscopic classification of flint useful? A petroarchaeological analysis and characterization of flint raw materials from the Iberian Neolithic mine of Casa Montero. *Archaeometry,* **51**, 175–196.

Chavagnac, V., German, C.R., Milton, J.A. and Palmer, M.R. 2005. Sources of REE in sediment cores from the Rainbow vent site (36°14′N, MAR). *Chemical Geology*, **216**, 329–352.

Chen, D.Z., Qing, H.R., Yan, X. and Li, H. 2006. Hydrothermal venting and basin evolution (Devonian, South China): Constraints from rare earth element geochemistry of chert. *Sedimentary Geology*, **183,** 203–216.

Chiari, M., Baumgartner, P.O., Bernoulli, D., Bortolotti, V., Marcucci, M., Photiades, A. and Principi, G. 2012. Late Triassic, Early and Middle Jurassic Radiolaria from ferromanganese-chert 'nodules' (Angelokastron, Argolis, Greece): evidence for prolonged radiolarite sedimentation in the Maliac-Vardar Ocean. *Facies*, **59**, 391–424.

Danielson, A., Möller, P. and Dulski, P. 1992. The europium anomalies in banded iron formations and the thermal history of the oceanic crust. *Chemical Geology*, **97**, 89–100.

De Baar, H.J.W., Brewer, P.G. and Bacon, M.P. 1985. Anomalies in rare earth distributions in seawater: Gd and Tb. *Geochimica et Cosmochimica Acta*, **49**, 1961–1969.

Deng, T., Li, Y. and Hu, X.M. 2022. Origin of Carnian Ma'angtang cherts, northwestern Sichuan Basin, South China: Field, petrographic, and geochemical perspectives. *Journal of Asian Earth Sciences,* **228**, 105–143.

Doben, K., Doppler, G., Freudenberger, W., Jerz, H., Meyer, R.K.F., Mielke, H., Ott, W.D., Rohrmüller, J., Schmidt-Kaler, H., Schwerd, K. and Unger, H.J. 1996. Geologische Karte von Bayern 1:500 000. Bayerisches Geologisches Landesamt; Augsburg.

Douville, E., Bienvenu, P., Charlou, J.L., Donval, J.P., Fouquet, Y., Appriou, P. and Gamo, T. 1999. Yttrium and rare earth elements in fluids from various deep-sea hydrothermal systems. *Geochimica et Cosmochimica Acta*, **63**, 627–643.

Dulski, P. 1994. Interferences of oxide, hydroxide and chloride analyte species in the determination of rare earth elements in geological samples by inductively coupled plasma-mass spectrometry. *Fresenius' Journal of Analytical Chemistry*, **350**, 194–203.

Durakiewicz, T., Migaszewski, Z.M., Sharp, Z.D. and Atudorei, V.N. 2001. The significance of Upper Jurassic flints in studies on the origin of siliceous rocks. *Przegląd Geologiczny*, **49**, 225–228. [In Polish with English summary]

Dżułyński, S. 1952. The origin of the Upper Jurassic limestones in the Cracow area. *Rocznik Polskiego Towarzystwa Geologicznego*, **21**, 125–180. [In Polish with English summary]

Elderfield, H., Whitfield, M., Burton, J.D., Bacon, M.P. and Liss, P.S. 1988. The oceanic chemistry of the rare-earth elements. *Philosophical Transactions of the Royal Society of London - Series A: Mathematical and Physical Sciences*, **325**, 105–126.

Elderfield, H., Upstill-Goddard, R. and Sholkovitz, E.R. 1990. The rare earth elements in rivers, estuaries, and coastal seas and their significance to the composition of ocean waters. *Geochimica et Cosmochimica Acta*, **54**, 971–991.

Flörke, O.W., Jones, J.B. and Schmincke, H.U. 1976. A new microcrystalline mineral from Gran Canaria. *Zeitschrift für Kristallographie – Crystalline Materials*, **143**, 156–165.

Flörke, O.W., Flörke, U. and Giese, U. 1984. Moganite: a new microcrystalline silica mineral. *Neues Jahrbuch für Mineralogie Abhandlungen*, **149**, 325–336.

Fajt, M., Mazur-Rozmus, W., Stefańska, A., Kochman, A. and Krzyżak, A.T. 2024. Chert outcrops differentiation by means of low-field NMR relaxometry. *Scientific Reports*, **14**, 25280.

Gao, G.Q. and Land, L.S. 1991. Nodular chert from the Arbuckle Group, Slick Hills, SW Oklahoma – a combined field, petrographic and isotopic study. *Sedimentology*, **38**, 857–870.

Gao, P., He, Z.L., Lash, G.G., Li, S.J., Xiao, X.M., Han, Y.Q. and Zhang, R.Q. 2020. Mixed seawater and hydrothermal sources of nodular chert in Middle Permian limestone on the eastern Paleo-Tethys margin (South China). *Palaeogeography, Palaeoclimatology, Palaeoecology,* **551**, 109740.

Gaweł, A. 1925. Beiträge zur Kenntniss der Feuersteine und Hornsteine aus dem südpolnischen Gebiete. *Bulletin International de L'Académie Polonaise des Sciences et des Lettres. Classe des Sciences Mathématiques et Naturelles*, **V–VIA**, 231–242.

German, C.R. and Elderfield, H. 1990. Application of the Ce anomaly as a paleoredox indicator: The ground rules. *Paleoceanography*, **5**, 823–833.

German, C.R., Klinkhammer, G.P., Edmond, J.M., Mitra, A. and Elderfield, H. 1990. Hydrothermal scavenging of rare earth elements in the ocean. *Nature*, **345**, 516–518.

German, C.R., Holliday, B.P. and Elderfield, H. 1991. Redox cycling of rare earth elements in the suboxic zone of the Black Sea. *Geochimica et Cosmochimica Acta*, **55**, 3553–3558.

German, C.R., Hergt, J., Palmer, M.R. and Edmond, J.M. 1999. Geochemistry of hydrothermal sediment core from the OBS vent field, 21°N East Pacific Rise. *Chemical Geology*, **155**, 65–75.

Ginter, B. and Kozłowski, J.K. 1990. Technika obróbki i typologia wyrobów kamiennych paleolitu, mezolitu i neolitu, 252 pp. PWN; Warszawa.

Girty, G.H., Hanson, A.D., Yoshinobu, A.S., Knaack, C. and Johnson, D. 1993. Provenance of Paleozoic mudstones in a contact metamorphic aureole determined by rare earth element, Th, and Sc analyses, Sierra Nevada, California. *Geology*, **21**, 363–366.

Gislason, S.R., Heaney, P.J., Oelkers, E.H. and Schott, J. 1997. Kinetic and thermodynamic properties of moganite, a novel silica polymorph. *Geochimica et Cosmochimica Acta*, **61**, 1193–1204.

Gołębiowska, B., Pieczka, A., Rzepa, G., Matyszkiewicz, J. and Krajewski, M. 2010. Iodargyrite from Zalas (Cracow area, Poland) as an indicator of Oligocene–Miocene aridity in Central Europe. *Palaeogeography, Palaeoclimatology, Palaeoecology*, **296**, 130–137.

Grawunder, A., Merten, D. and Büchel, G. 2014. Origin of middle rare earth element enrichment in acid mine drainage-impacted areas. *Environmental Science and Pollution Research*, **21**, 6812–6823.

Graetsch, H.A. and Grünberg, J.M. 2012. Microstructure of flint and other chert raw materials. *Archaeometry*, **54**, 18–36.

Gröschke, M. 1985. Stratigraphie und Ammonitenfauna der Jurare likte zwischen Straubing und Passau (Niederbayern). *Palaeontographica, Abteilung A*, **191**, 1–68.

Guo, P., Li, C., Wen, H., Wei, Y. and Lei, H. 2022. Genesis of Continental Siliceous Rocks and Their Tectonic-climatic Significance. *Acta Sedimentologica Sinica,* **40**, 450–464.

Gwinner, M.P. 1971. Carbonate rocks of the Upper Jurassic in SW-Germany. In: Müller, G. (Ed), Sedimentology of parts of Central Europe, 193–207. Kramer; Frankfurt a. M.

He, T.C., Lin, H.F., Chen, Y.Q., Li, D., Yang, A.H., Wang, D. and Wu, H.B. 2013. Geochemical characteristics and origin of Ediacaran Piyuancun chert in the Lantian section, Xiuning, southern Anhui Province. *Geological Journal of China Universities*, **19**, 620–633.

Hatije, V., Schijf, J., Johannesson, K.H., Andrade, R., Caetano, M., Brito, P., Haley, B.A., Lagarde, M. and Jeandel, M. 2024. The global biogeochemical cycle of the rare earth elements. *Global Biogeochemical Cycles*, **38**, e2024GB008125.

He, L.J., Huang, F., Liu, Q.Y., Li, C.R. and Wang, J.Y. 2014. Tectono-thermal Evolution of Sichuan Basin in Early Paleozoic. *Journal of Earth Sciences & Environment*, **36**, 10–17.

He, J., Ding, W., Huang, W., Cao, Z., Chen, E., Dai, P. and Zhang, Y. 2019. Petrological, geochemical, and hydrothermal characteristics of Ordovician cherts in the southeastern Tarim Basin, NW China, and constraints on the origin of cherts and Permian tectonic evolution. *Journal of Asian Earth Sciences*, **170**, 294–315.

Heaney, P.J. and Post, J.E. 1992. The widespread distribution of a novel silica polymorph in microcrystalline quartz varieties. *Science*, **255**, 441–443.

Hein, J.R., Scholl, C.W., Barron, J.A., Jones, M.G. and Miller, J. 1978. Diagenesis of late Cenozoic diatomaceous deposits and formation of the bottom-simulating reflector in the southern Bering Sea. *Sedimentology*, **25**, 155–181.

Heliasz, Z. 1980. Limestones silicifications in the Julianka area, near Częstochowa. *Prace Naukowe Uniwersytetu Śląskiego w Katowicach, 383, Geologia,* **4**, 92–101. [In Polish with English summary]

Heliasz, Z., Ptak, B., Więckowski, R. and Zieliński, T. 1984. Detailed geological map of Poland, 1:50 000, sheet Janów (846). Wydawnictwa Geologiczne; Warszawa. [In Polish]

Heliasz, Z., Ptak, B., Więckowski, R. and Zieliński, T. 1987. Explanation to detailed geological map of Poland sheet Janów (846) 1:50 000, 66 pp. Wydawnictwa Geologiczne; Warszawa. [In Polish]

Hesse, R. 1989. Silica diagenesis: origin of inorganic and replacement cherts. *Earth-Science Reviews*, **26**, 253–284.

Hofmann, A. and Bolhar, R. 2007. Carbonaceous Cherts in the Barberton Greenstone Belt and Their Significance for the Study of Early Life in the Archean Record. *Astrobiology*, **7**, 355–388.

Janák, V. and Přichystal, A. 2007. Distribution of silicites of the Kraków-Częstochowa Jurassic in Moravia and Upper Silesia in the Neolithic and at the beginning of the Eneolithic. *Památky archeologické*, **98**, 5–30. [In Czech with English summary]

Junguo, H., Yongzhang, Z. and Hongzhong, L. 2011. Study on Geochemical Characteristics and Depositional Environment of Pengcuolin Chert, Southern Tibet. *Journal of Geography and Geology*, **3**, 178–188.

Kaczanowska, M. and Kozłowski, J.K. 1976. Studia nad surowcami krzemiennymi południowo-wschodniej części Wyżyny Krakowsko-Częstochowskiej. *Acta Archaeologica Carpathica*, **16**, 201–216.

Kaczanowska, M., Kozłowski, J.K. and Pawlikowski, M. 1979. Dalsze badania nad surowcami krzemiennymi południowej części Wyżyny Krakowsko-Częstochowskiej. *Acta Archaeologica Carpathica*, **19**, 179–187.

Kamber, B.S. and Webb, G.E. 2001. The geochemistry of late Archaean microbial carbonate: implications for ocean chemistry and continental erosion history. *Geochimica et Cosmochimica Acta*, **65**, 2509–2525.

Kato, Y. and Nakamura, K. 2003. Origin and global tectonic significance of early Archeancherts from the Marble Bar greenstone belt, Pilbara Craton, Western Australia. *Precambrian Research*, **125**, 191–243.

Keheila, E.A. 2000. Carbonate facies, sequential analysis and sedimentary cycles of the lower Eocene Thebes Formation at Gebel Duwi (Red Sea coast) and south Wadi Quena, Egypt; Chert breccia tempestites as evidence of synsedimentary silicification. *Bulletin of the Faculty of Science, F.*, Geology, **29**, 51–76.

Keupp, H., Koch, R. and Leinfelder, R. 1990. Steuerungsproz-

esse der Entwicklung von Oberjura-Spongiolithen Süddeutschlands: Kenntnisstand, Probleme und Perspektiven. *Facies*, **23**, 141–174.

Kidder, D.L. and Tomescu, I. 2016. Biogenic chert and the Ordovician silica cycle. *Palaeogeography, Palaeoclimatology, Palaeoecology*, **458**, 29–38.

Knauth, L.P. 1992. Origin and diagenesis of cherts: An isotopic perspective. In: Clauer, N. and Chaudhuri, S. (Eds), Isotopic signatures and sedimentary records, *Lecture Notes in Earth Sciences,* **43**, 123–152.

Knauth, L.P. 1994. Petrogenesis of chert. In: Heaney, P.J., Prewitt, C.T. and Gibbs, G.V. (Eds), Silica: Physical behavior, geochemistry, and materials applications, *Reviews in Mineralogy*, **29**, 233–258. Mineralogical Society of America; Washington.

Kochman, A. and Matyszkiewicz, J. 2012. Microbial laminites with coprolites from Upper Jurassic carbonate buildups complex (Kraków-Częstochowa Upland; Poland). *Annales Societatis Geologorum Poloniae*, **82**, 331–347.

Kochman, A. and Matyszkiewicz, J. 2023. The development and origin of the two-stage silicification of Upper Jurassic limestones from the northern part of the Kraków-Częstochowa Upland (Southern Poland). *Geology, Geophysics and Environment*, **49**, 225–243.

Kochman, A. and Matyszkiewicz, J. 2025. Chert concretions and bedded cherts from the southeastern Franconian Alb, Bayerwald and Kraków-Czestochowa Upland as potential raw materials for artifact manufacturing in the Paleolithic, Mesolithic and Neolithic – a comparative petrographic study. *Geological Quarterly*, **69**, 12.

Kochman, A., Matyszkiewicz, J. and Wasilewski, M. 2020a. Siliceous rocks from the southern part of the Kraków-Częstochowa Upland (Southern Poland) as potential raw materials in the manufacture of stone tools – a characterization and possibilities of identification. *Journal of Archaeological Science: Reports*, **30**, 102195.

Kochman, A., Kozłowski, A. and Matyszkiewicz, J. 2020b. Epigenetic siliceous rocks from the southern part of the Kraków-Częstochowa Upland (Southern Poland) and their relation to Upper Jurassic early diagenetic chert concretions. *Sedimentary Geology*, **401**, 105636.

Kopacz, J. and Pelisiak, A. 1992. Studies on utilization of Jurassic flint, variety G, in the Neolithic. *Sprawozdania Archeologiczne*, **44**, 109–116. [In Polish with English summary]

Krajcarz, M.T. and Sudoł-Procyk, M. 2019. The mine of chocolate flint in the Udorka Valley (Kraków-Częstochowa Upland), Field Trip Guide. In: Werra, D.H., Sudoł-Procyk, M., Jedynak, A., Kaptur, K. and Krajcarz, M.T. (Eds), UISPP Commission on Flint Mining in Pre- and Protohistoric Times „The Filint Mining Studies: Archaeological Excavations – Extraction Methods – Chipping Floors– Distribution of Raw Materials and Workshop Products", Program – Abstracts – Field Guide, 19–21th, 33–37. Archeological Museum and Reserve „Krzemionki"; Ostrowiec Świętokrzyski.

Krajcarz, M.T., Sudoł, M., Krajcarz, M. and Cyrek, K. 2012. From far or from near? Sources of Kraków-Częstochowa banded and chocolate silicite raw material used during the Stone Age in Biśnik Cave (southern Poland). *Anthropologie*, **50**, 411–425.

Krajcarz, M.T., Sudoł, M., Krajcarz, M. and Cyrek, K. 2014. Outcrops of striped flint on the Ryczów Upland (Kraków-Częstochowa Upland). In: Piotrowska, D., Piotrowski, W., Jedynak, A. and Kaptur, K. (Eds), Górnictwo z epoki kamienia: Krzemionki – Polska – Europa. W 90. Rocznicę odkrycia kopalni w Krzemionkach, Silex et Ferrum Vol. 1, 77–95. Muzeum Historyczno-Archeologiczne w Ostrowcu Świętokrzyskim; Ostrowiec Świętokrzyski. [In Polish with English summary]

Krajewski, M. 2001. Upper Jurassic chalky limestones in the Zakrzówek Horst, Kraków, Kraków-Wieluń Upland (South Poland). *Annales Societatis Geologorum Poloniae*, **71**, 43–51.

Krajewski, M. and Matyszkiewicz, J. 2004. Development and facial architecture of the Upper Jurassic complexes of buildups in the SW part of the Kraków Upland. In: Partyka, J. (Ed), Zróżnicowanie i przemiany środowiska przyrodniczo-kulturowego Wyżyny Krakowsko-Częstochowskiej, Tom I, Przyroda, 27–34. Ojcowski Park Narodowy; Ojców. [In Polish with English summary]

Krajewski, M. and Matyszkiewicz, J. 2009. Upper Jurassic deposits in the Częstochowa Upland. In: Stefaniak, K., Tyc, A., Socha, P. (Eds), Karst of the Częstochowa Upland and of the Eastern Sudetes: palaeoenvironments and protection, Studies of the Faculty of Earth Sciences, 56. University of Silesia; Sosnowiec – Wrocław.

Krajewski, M., Olchowy, P. and Rudziński, D. 2018. Sedimentary successions in the Middle–Upper Oxfordian reef deposits from the southern part of the Kraków-Częstochowa Upland (Southern Poland). *Geological Quarterly*, **62**, 653–668.

Krukowski, S. 1920. Pierwociny krzemieniarskie górnictwa, transportu i handlu w holocenie Polski. *Wiadomości Archeologiczne*, **5**, 185–206.

Krzyżak, A.T., Mazur, W., Matyszkiewicz, J. and Kochman, A. 2020. Identification of Proton Populations in Cherts as Natural analogues of pure silica materials by means of low field NMR. *Journal of Physical Chemistry C*, **124**, 5225–5240.

Kutek, J. 1994. Jurassic tectonic events in south-eastern cratonic Poland. *Acta Geologica Polonica*, **44**, 167–221. [In Polish with English summary]

Kutek, J., Wierzbowski, A., Bednarek, J., Matyja, B.A. and Zapaśnik, T. 1977. Z problematyki stratygraficznej osadów górnojurajskich Jury Polskiej. *Przegląd Geologiczny*, **25**, 438–445. [In Polish with English summary]

Kuźniar, W. and Żelechowski, W. 1927. Materiały do poznania stosunku Karpat do ich przedgórza na przestrzeni do Morawskiej Ostrawy po Kraków. *Przegląd Górniczo-Hutniczy*, **19**, 327–334, 355–360, 393–402, 434–444, 465–471.

Laschet, C. 1984. On the Origin of Cherts. *Facies*, **10**, 257–290.

Lawrence, M.J.F. 1993. Sedimentology and petrography of early diagenetic chert and dolomite in the Late Cretaceous–Early Tertiary Amuri Limestone Group, eastern Marlborough, New Zealand. *New Zealand Journal of Geology and Geophysics*, **36**, 9–25.

Lawrence, M.J.F. 1994. Conceptual model for early diagenetic chert and dolomite, Amuri Limestone Group, north-eastern South Island, New Zeland. *Sedimentology*, **41**, 479–478.

Lech, J. 1980. Geologia krzemienia jurajskiego-podkrakowskiego na tle innych skał krzemionkowych. Wprowadzenie do badań z perspektywy archeologa. *Acta Archaeologica Carpathica*, **20**, 165–230. [In Polish]

Lech, J. 1981. Górnictwo krzemienie społeczności wczesnorolniczych na Wyżynie Krakowskiej – koniec VI tysiąclecia – 1 połowa IV tysiąclecia p.n.e., 284 pp. Polska Akademia Nauk. Instytut Historii Kultury Materialnej i Zakład Narodowy imienia Ossolińskich, Wydawnictwo Polskiej Akademii Nauk; Wrocław-Warszawa-Kraków-Gdańsk-Łódź.

Lee, J.H. and Byrne, R.H. 1993. Complexation of trivalent rare earth elements (Ce, Eu, Gd, Tb, Yb) by carbonate ions. *Geochimica et Cosmochimica Acta*, **57**, 295–302.

Lei, Z., Dashtgard, S., Wang, J., Li, M., Feng, Q., Yu, Q., Zhao, A. and Du, L. 2019. Origin of chert in Lower Silurian Longmaxi Formation: Implications for tectonic evolution of Yangtze Block, South China. *Palaeogeography, Palaeoclimatology, Palaeoecology*, **529**, 53–66.

Liang, Y.T., Tang, X., Zhang, J.C., Liu, Y., Zhang, Y., Yuan, K., Lin, T., Ding, J.H. and Wang, Y. 2022. Origin of Lower Carboniferous cherts in southern Guizhou, South China. *Palaeogeography, Palaeoclimatology, Palaeoecology*, **590**, 110863.

Lin, L., Yu, Y., Gao, J. and Hong, W. 2018. The origin and geochemical characteristics of Permian chert in the Eastern Sichuan Basin, China. *Carbonates and Evaporites*, **33**, 613–624.

Lindgreen, H. and Jakobsen, F. 2012. Marine sedimentation of nano-quartz forming flint in North Sea Danian chalk. *Marine and Petroleum Geology*, **38**, 73–82.

Maliva, R.G. 2001. Silicification in the Belt Supergroup (Mesoproterozoic), Glacier National Park, Montana, USA. *Sedimentology*, **48**, 887–896.

Maliva, R.G. and Siever, R. 1989. Nodular chert formation in carbonate rocks. *Journal of Geology*, **97**, 421–433.

Mandera, S., Sudoł-Procyk, M., Malak, M., Skrzatek, M. and Krajcarz, M.T. 2024. New deposit of chocolate flint in Załęże gully (Kraków-Częstochowa Upland, Poland) – Raw material characterization and its availability for prehistoric communities. *Journal of Archaeological Science: Reports*, **53**, 104328.

Marcinowski, R. 1970. Turbidites in the Upper Oxfordian limestones at Jaskrów in the Polish Jura Chain. *Bulletin of the Polish Academy of Sciences, Earth Sciences*, **18**, 219–225.

Matyja, B.A. and Wierzbowski, A. 2004. Stratigraphy and facies development in the Upper Jurassic of the Kraków–Częstochowa Upland. In: Partyka, J. (Ed), Zróżnicowanie i przemiany środowiska przyrodniczo-kulturowego Wyżyny Krakowsko-Częstochowskiej, Tom I, Przyroda, 13–26. Ojcowski Park Narodowy; Ojców. [In Polish with English summary]

Matyja, B.A. and Wierzbowski, A. 2006. Julianka, coral colonization of the cyanobacteria-sponge bioherms at the turn of the Oxfordian and Kimmeridgian. In: Wierzbowski, A., Aubrecht, A., Golonka, J. Gutowski, J., Krobicki, M., Matyja, B.A., Pieńkowski, G. and Uchman, A. (Eds), Jurassic of Poland and adjacent Slovakian Carpathians, Field trip guidebook of 7th International Congress on the Jurassic System, 203–206. Polish Geological Institute; Warszawa.

Matyszkiewicz, J. 1987. Epigenetic silification of the Upper Oxfordian limestones in the vicinity of Kraków. *Annales Societatis Geologorum Poloniae*, **57**, 59–87.

Matyszkiewicz, J. 1989a. Sedimentation and diagenesis of the Upper Oxfordian cyanobacterial-sponge limestones in Piekary near Kraków*, Annales Societatis Geologorum Poloniae*, **59**, 201–232.

Matyszkiewicz, J. 1989b. Utwory osuwiskowe w wapieniach górnego oksfordu w Ujeździe. In: Rutkowski, J. (Ed), Przewodnik LX Zjazdu Polskiego Towarzystwa Geologicznego, Kraków 14–16 września 1989, 83–88. Wydawnictwo AGH, Kraków. [In Polish]

Matyszkiewicz, J. 1994. Remarks on the deposition and diagenesis of pseudonodular limestones in the Cracow Area (Oxfordian; Southern Poland). *Berliner Geowissenschaftliche Abhandlungen*, **E13**, 419–439.

Matyszkiewicz, J. 1996. The Significance of Saccocoma-calciturbidites for the analysis of the Polish Epicontinental Late Jurassic Basin: an example from the Southern Cracow-Wieluń Upland (Poland). *Facies*, **34**, 23–40.

Matyszkiewicz, J. 1997a. Microfacies, sedimentation and some aspects of diagenesis of Upper Jurassic sediments from the elevated part of the Northern peri-Tethyan Shelf, a comprative study on the Lochen area (Schwäbische Alb) and the Cracow area (Cracow-Wielun Upland, Poland). *Berliner Geowissenschaftliche Abhandlungen*, **E21**, 1–111.

Matyszkiewicz, J. 1997b. Stromatactis cavities and stromatactis-like cavities in the Upper Jurassic carbonate buildups at Młynka and Zabierzów (Oxfordian, southern Poland). *Annales Societatis Geologorum Poloniae*, **67**, 45–55.

Matyszkiewicz, J. 1999. Sea-bottom relief versus differential compaction in ancient platform carbonates: a critical reassessment of an example from Upper Jurassic of the Cra-

cow-Wieluń Upland. *Annales Societatis Geologorum Poloniae*, **69**, 63–79.

Matyszkiewicz, J. and Kochman, A. 2016. Pressure dissolution features in Oxfordian microbial-sponge buildups with pseudonodular texture, Kraków Upland. *Annales Societatis Geologorum Poloniae*, **86**, 355–377.

Matyszkiewicz, J. and Kochman, A. 2020. The provenance of siliceous rocks from the Kraków-Częstochowa Upland (Poland) used as raw-materials in the manufacture of siliceous artefacts from Central-Eastern Europe; An old problem in new light. *Journal of Archaeological Science: Reports*, **34**, Part A, 102600.

Matyszkiewicz, J. and Olszewska, B. 2007. Osady podmorskich spływów grawitacyjnych pogranicza oksfordu i kimerydu w Ujeździe. *Volumina Jurassica*, **4**, 109–117. [In Polish]

Matyszkiewicz, J., Kochman, A. and Duś, A. 2012. Influence of local sedimentary conditions on development of microbialites in the Oxfordian carbonate buildups from the southern part of the Kraków-Częstochowa Upland (south Poland). *Sedimentary Geology*, **263–264**, 109–132.

Matyszkiewicz, J., Kochman, A., Rzepa, G., Gołębiowska, B., Krajewski, M., Gaidzik, K. and Żaba, J. 2015a. Epigenetic silicification of the Upper Oxfordian limestones in the Sokole Hills (Kraków-Częstochowa Upland): relationship to facies development and tectonics. *Acta Geologica Polonica*, **65**, 181–203.

Matyszkiewicz, J., Felisiak, I., Hoffmann, M., Kochman, A., Kołodziej, B., Krajewski, M. and Olchowy, P. 2015b. In: Haczewski, G. (Ed), Transgressive Callovian succession and Oxfordian microbial-sponge carbonate buildups in the Kraków Upland. Guidebook for field trips accompanying 31 IAS meeting of sedimentology held in Kraków, 51–73. Polskie Towarzystwo Geologiczne; Kraków.

Matyszkiewicz, J., Krajewski, M., Kochman, A., Kozłowski, A. and Duliński, M. 2016. Oxfordian neptunian dykes with brachiopods from the southern part of the Kraków-Częstochowa Upland (Southern Poland) and their links to hydrothermal vents. *Facies*, **62**, 12.

McBride, E.F., Abdel-Wahab, A. and El-Younsy, A.M. 1999. Origin of spheroidal chert nodules, Drunka Formation (Lower Eocene), Egypt. *Sedimentology*, **46**, 733–755.

McLennan, S.M. 1989. Rare earth elements in sedimentary rocks: influence of provenance and sedimentary processes. In: Lipin, R. and McKay, G.A. (Eds), Geochemistry and Mineralogy of Rare Earth Elements, 21, 169–200. De Gruyter; Berlin, Munich, Boston.

Meyer, R.K.F. 1975. Mikrofazielle Untersuchungen in Schwamm-Biohermen und -Biostromen des Malm Epsilon (Ober-Kimmeridge) und obersten Malm Delta der Frankenalb. *Geologische Blätter für Nordost-Bayern*, **25**, 149–177.

Meyer, R.K.F. 1977. Stratigraphie und Fazies des Frankendolomits und der Massenkalke (Malm), 3. Teil: Südliche Frankenalb. *Erlanger Geologische Abhandlungen*, **104**, 1–41.

Meyer, R.K.F. 2003a. Kurzerläuterung zur Geologischen Karte 1:25 000 7035 Schamhaupten. Bayerisches Geologisches Landesamt; München.

Meyer, R.K.F. 2003b. Kurzerläuterung zur Geologischen Karte 1:25 000 7135 Kösching. Bayerisches Geologisches Landesamt; München.

Meyer, R.K.F. 2003c. Kurzerläuterung zur Geologischen Karte 1:25 000 7033 Titting. Bayerisches Geologisches Landesamt; München.

Michniak, R. 1989. Nazewnictwo, geneza i występowanie krzemieni. *Przegląd Geologiczny*, **9**, 452–457. [In Polish]

Miehe, G. and Graetsch, H. 1992. Crystal structure of moganite: a new structure type for silica. *European Journal of Mineralogy*, **4**, 693–706.

Miehe, G., Graetsch, H. and Flörke. O.W. 1984. Crystal structure and growth of fabric of length-fast chalcedony. *Physics and Chemistry of Minerals*, **10**, 197–199.

Migaszewski, Z.M., Gałuszka, A., Durakiewicz, T. and Starnawska, E. 2006. Middle Oxfordian – Lower Kimmeridgian chert nodules in the Holy Cross Mountains, south-central Poland. *Sedimentary Geology*, **187**, 11–28.

Migaszewski, Z.M., Gałuszka, A. and Dołęgowska, S. 2016. Rare earth and trace element signatures for assessing an impact of rock mining and processing on the environment: Wiśniówka case study, south-central Poland. *Environmental Science and Pollution Research*, **23**, 24943–24959.

Migaszewski, Z.M., Gałuszka, A. and Migaszewski, A. 2022. Geochemistry and petrology of striped chert as a provenance tool for artefacts from the Krzemionki Neolithic mining area (Poland). *Archaeometry*, **64**, 1093–1109.

Mills, R.A. and Elderfield, H. 1995. Rare earth element geochemistry of hydrothermal deposits from the active TAG Mound, 26°N Mid-Atlantic Ridge. *Geochimica et Cosmochimica Acta*, **59**, 3511–3524.

Morawski, W. 1976. Uwagi na marginesie referatu M. Kaczanowskiej i J.K. Kozłowskiego. *Acta Archaeologica Carpathica*, **16**, 217–219. [In Polish]

Morozewicz, J. 1909. O haczetynie i jego Bonarskim złożu. *Kosmos*, **34**, 610–624. [In Polish]

Murata, K.J. and Norman, M.B. 1976. An index of crystallinity for quartz. *American Journal of Science*, **276**, 1120–1130.

Murray, R.W. 1994. Chemical criteria to identify the depositional environment of chert: general principles and applications. *Sedimentary Geology*, **90**, 213–232.

Murray, R.W., Buchholtz Ten Brink, M.R., Jones, D.L., Gerlach, D.C. and Russ III, G.P. 1990. Rare earth elements as indicators of different marine depositional environments in chert and shale. *Geology*, **18**, 268–271.

Murray, R.W., Buchholtz Ten Brink, M.R., Gerlach, D.C., Russ III G.P. and Jones, D.L. 1991. Rare earth, major, and trace elements in chert from the Franciscan Complex and Monterey Group, Californian: Assessing REE sources to fine-

grained marine sediments. *Geochimica et Cosmochimica Acta,* **55**, 1875–1895.

Murray, R.W., Buchholtz Ten Brink, M.R., Gerlach, D.C., Russ III, G.P. and Jones, D.L. 1992. Interoceanic variation in the rare earth, major, and trace element depositional chemistry of chert: Perspectives gained from the DSDP and ODP record. *Geochimica et Cosmochimica Acta*, **56**, 1897–1913.

Niebuhr, B. 2014. Lithostratigraphie der mittel- bis oberjurassischen Reliktvorkommen zwischen Straubing und Passau (Niederbayern). *Schriftenreihe der Deutschen Gesellschaft für Geowissenschaften*, **83**, 73–82.

Niebuhr, B. and Pürner, T. 2014. Plattenkalk und Frankendolomit – Lithostratigraphie der Weißjura-Gruppe der Frankenalb (außeralpiner Oberjura, Bayern). *Schriftenreihe der Deutschen Gesellschaft für Geowissenschaften*, **83**, 5–72.

Nothdurft, L.D., Webb, G.E. and Kamber, B.S. 2004. Rare earth element geochemistry of Late Devonian reefal carbonates, Canning Basin, Western Australia: confirmation of a seawater REE proxy in ancient limestones. *Geochimica et Cosmochimica Acta*, **68**, 263–283.

Nozaki, Y., Zhang, J. and Amakawa, H. 1997. The fractionation between Y and Ho in the marine environment. *Earth and Planetary Science Letters*, **148**, 329–340.

Olivarez, A.M. and Owen, R.M. 1989. REE/Fe variations in hydrothermal sediments: Implications for the REE content of seawater. *Geochimica et Cosmochimica Acta*, **53**, 757–762.

Parish, R.M. and Werra, D.H. 2018. Characterizing 'Chocolate' Flint Using Reflectance Spectroscopy. *Archaeologia Polona*, **56**, 89–101.

Pawlikowski, M., Kunert-Radek, J. and Stępień, H., 1978. Somatostatin inhibits the mitogenic effect of thyroliberin. *Experientia*, **34**, 271–272.

Pelisiak, A. 2003. Ze studiów na wykorzystywaniem surowców krzemiennych ze środkowej części Wyżyny Krakowsko-Częstochowskiej w późnym neolicie w strefie karpackiej. Neolityczne pracownie w Strzegowej (Strzegowa, stan. 42). *Acta Archaeologica Carpathica*, **38**, 28–70.

Pelisiak, A. 2006. The exploitation and distribution of flints from the central part of Polish Jura in the Late Neolithic times. *Analecta Archaeologica Ressoviensia*, **1**, 73–86.

Pelisiak, A. 2008. The Jurassic flint type G in Central Europe in the Late Neolithic (3100–2300 BC). In: Furholt, M., Szmyt, M. and Zastawny, A. (Eds), The Baden Complex and the Outside World, 147–154. Studien zur Archäologie in Ostmitteleuropa 4. Habelt; Bonn.

Piper, D.Z. 1974. Rare earth elements in the sedimentary cycle: A summary. *Chemical Geology*, **144**, 285–304.

Piper, D.Z. and Bau, M. 2013. Normalized rare earth elements in water, sediments, and wine: identifying sources and environmental redox conditions. American *Journal of Analytical Chemistry*, **4**, 69–83.

Přichystal, A. 2013. Lithic raw materials in Prehistoric Times of Eastern Central Europe, 351 pp. Masaryk University; Brno.

Přichystal, A. 2018. Artefacts Made from Siliceous Rocks of Polish Origin on Prehistoric Sites in the Czech Republic. *Archaeologia Polona*, **56**, 35–48.

Pusch, J.B. 1830. Krótki rys geognostyczny Polski i Karpat Północnych czyli opisanie zewnętrznego ukształcenia i wewnętrznego składu ziemi tego Kraju, 104 pp. A.M. Kitajewski; Warszawa.

Qiu, Z. and Wang, Q. 2011. Geochemical evidence for submarine hydrothermal origin of the Middle–Upper Permian chert in Laibin of Guangxi, China. *Science China: Earth Sciences*, **54**, 1011–1023.

Rajchel, J.M. 1971. Badania sedymentologiczne krzemieni jurajskich pod Krakowem. *Sprawozdania z Posiedzeń Komisji Naukowych Polskiej Akademii Nauk. Oddział w Krakowie*, **14**, 625–645.

Rodgers, K.A. and Cressey, G. 2001. The occurrence, detection and significance of moganite (SiO_2) among some silica sinters. *Mineralogical Magazine*, **65**, 157–167.

Roemer, F. 1870. Geologie von Oberschlesien. Robert Nischkowsky; Breslau.

Rutte, E. 1962. Geologische Karte mit Erläuterung 1:25 000 7037 Kelheim. Bayerisches Geologisches Landesamt; München.

Rühle, E., Ciuk, E., Osika, R. and Znosko, J. 1977. Mapa geologiczna Polski bez utworów czwartorzędowych: 1:500 000. Wydawnictwa Geologiczne; Warszawa.

Schild, R. 1971. Location of the so-called chocolate flint extraction sites on the North-eastern footslopes of the Holy Cross Mountains. *Folia Quaternaria*, **39**, 1–61.

Sharp, Z.D., Durakiewicz, T., Migaszewski, Z.M. and Atudorei, V.N. 2002. Antiphase hydrogen and oxygen isotope periodicity in chert nodules. *Geochimica et Cosmochimica Acta*, **66**, 2865–2973.

Shen, B., Ma, H., Ye, H., Lang, X., Pei, H., Zhou, C., Zhang, S. and Yang, R. 2018. Hydrothermal origin of syndepositional chert bands and nodules in the Mesoproterozoic Wumishan Formation: Implications for the evolution of Mesoproterozoic cratonic basin, North China. *Precambrian Research*, **310**, 213–228.

Shepelenko, M., Livneh, T., Natalio, F. and Kronik, J. 2025. Infrared Absorption Spectrum of α-Moganite from First-Principles. *The Journal of Physical Chemistry C*, **129**, 1831–1840.

Shimizu, H. and Masuda, A. 1977. Cerium in chert as an indication of marine environment of its formation. *Nature*, **266**, 346–348.

Sholkovitz, E.R. 1990. Rare earth elements in marine sediments and geochemical standards. *Chemical Geology*, **88**, 333–347.

Sibson, R.H. 1987. Earthquake rupturing as a hydrothermal mineralizing agent. *Geology*, **15**, 701–704.

Sitarz, M., Wyszomirski, P., Handke, B. and Jeleń, P. 2014. Moganite in selected Polish chert samples: The evidence from

MIR, Raman and X-ray studies. *Spectrochimica Acta Part A: Molecular and Biomolecular Spectroscopy*, **122**, 55–58.

Staszic, S. 1815. O ziemiorodztwie Karpatów i innych gór i równin Polski. Drukarnia Rządowa; Warszawa.

Stawin, J. 1969. Własności użytkowe krzemieni krajowych w porównaniu z importowanymi. *Surowce Mineralne*, **2**, 103–122.

Stawin, J. 1970. Własności techniczne krajowych krzemieni. *Biuletyn Państwowego Instytutu Geologicznego*, **244**, 105–158.

Streim, W. 1961. Stratigraphie, Fazies und Lagerungsverhältnisse des Malms bei Dietfurt und Hemau (Südliche Frankenalb). *Erlanger Geologische Abhandlungen*, **38**, 1–49.

Sudoł-Procyk, M., Budziszewski, J., Krajcarz, M.T., Jakubczak, M. and Szubski, M. 2018. In: Werra, D.H. and Woźny, M. (Eds), Between History and Archaeology Papers in honour of Jacek Lech, The chocolate flint mines in the Udorka Valley (Częstochowa Upland) – a preliminary report on the field and lidar surveys. 89–102. Archaeopress Archaeology; Oxford.

Sudoł-Procyk, M., Brandl, M., Krajcarz, M.T., Malak, M., Skrzatek, M., Stefański, D., Trela-Kieferling, E. and Werra, D.H. 2021a. Chocolate flint: new perspectives on its deposits, mining, use and distribution by prehistoric communities in Central Europe. *Antiquity*, **95**, e25.

Sudoł-Procyk, M., Krajcarz, M.T., Malak, M. and Werra, D.H. 2021b. Preliminary characterization of the prehistoric mine of chocolate flint in Poręba Dzierżna, site 24 (Wolbrom commune, Lesser Poland Voivodeship). *Sprawozdania Archeologiczne*, **73**, 109–135.

Sudoł-Procyk, M., Malak, M., Binnebesel, H. and Krajcarz, M.T. 2022. Striped flint in archaeological materials around the outcrops of the Kraków-Częstochowa striped flint variety. *Archaeologia Polona*, **60**, 163–185.

Sugisaki, R. 1984. Relation between Chemical Composition and Sedimentation Rate of Pacific Ocean-Floor Sediments Deposited since the Middle Cretaceous: Basic Evidence for Chemical Constraints on Depositional Environments of Ancient Sediments. *The Journal of Geology*, **92**, 235–259.

Sujkowski, Z. 1926. O utworach jurajskich, kredowych i czwartorzędowych okolic Wolbromia. *Sprawozdania Państwowego Instytutu Geologicznego*, **3**, 382–434.

Sujkowski, Z. 1937. Skały kredowe między miastami Pilica i Szczekociny. *Sprawozdania Państwowego Instytutu Geologicznego*, **7**, 39–74.

Sulgostowska, Z. 2005. Kontakty społeczności późnopaleolitycznych i mezolitycznych między Odrą, Dźwiną i górnym Dniestrem: studium dystrybucji wytworów ze skał krzemionkowych, 344 pp. Instytut Archeologii i Etnologii PAN; Warszawa.

Sverjensky, D.A. 1984. Europium redox equilibria in aqueous solution. *Earth and Planetary Science Letters*, **67**, 70–78.

Świerczewska, A. 1989. Krzemienie z wapieni górnego oksfordu okolic Ujazdu. In: Rutkowski, J. (Ed.), Przewodnik LX Zjazdu Polskiego Towarzystwa Geologicznego, Kraków 14–16 września 1989, 88–90. Wydawnictwo AGH; Kraków.

Świerczewska, A. 1990. Sylifikacja diagenetyczna w wapieniach jurajskich Jury Krakowsko-Wieluńskiej. Unpublished PhD thesis, Polish Academy of Sciences; Warszawa.

Świerczewska, A. 1997. Early diagenetic silicification in the Upper Jurassic biohermal and interbiohermal facies. In: Schild, R. and Sulgostowska, Z. (Eds), Man and Flint, Proceedings of the VIIth International Flint Symposium Warszawa-Ostrowiec Świetokrzyski September 1995, 357–361. Institute of Archaeology and Ethnology Polish Academy of Sciences; Warszawa.

Šebela, L., Přichystal, A., Škrdla, P. and Humpolová, A. 2017. Unusual Middle Paleolithic Stone Tool from Southern Moravia with Possible Relations to Southern Poland. *Acta Archaeologica Carpathica*, **52**, 289–297.

Taylor, S.R. and McLennan, S.M. 1985. The Continental Crust: Its Composition and Evolution. 312 pp. Blackwell Scientific Publications; Oxford

Thewalt, V.U. and Dörfner, G. 2011. Kieselschwämme in Feuersteinen: Beobachtungen an Kieselknollen aus dem Weißen Jura der Schwäbischen Alb. *Jahreshefte der Gesellschaft für Naturkunde in Württemberg*, **167**, 213–226.

Trammer, J. 1985. Sponge bioherms in the Jasna Góra Beds (Oxfordian of the Polish Jura Chain). *Przegląd Geologiczny,* **33**, 78–81.

Trammer, J. 1989. Middle to Upper Oxfordian sponges of the Polish Jura. *Acta Geologica Polonica*, **39**, 49–91.

Van den Boorn, S.H.J.M., van Bergen, M.J., Nijman, W. and Vroon, P.Z. 2007. Dual role of seawater and hydrothermal fluids in Early Archean chert formation: Evidence from silicon isotopes. *Geology*, **10**, 939–942.

Van den Boorn, S.H.J.M., van Bergen, M.J., Vroon, P.Z., de Vries, S.T. and Nijman, W. 2010. Silicon isotope and trace element constraints on the origin of ~3.5 Ga cherts: Implications for Early Archaean marine environments. *Geochimica et Cosmochimica Acta*, **74**, 1077–1103.

Van Kranendonk, M.J. 2006. Volcanic degassing, hydrothermal circulation and the flourishing of early life on Earth: A review of the evidence from c. 3490–3240 Ma rocks of the Pilbara Supergroup, Pilbara Craton, Western Australia. *Earth-Science Reviews*, **74**, 197–240.

Viohl, G. and Zapp, M. 2007. Schamhaupten, an outstanding Fossil-Lagerstätte in a silicified Plattenkalk around the Kimmeridgian–Tithonian boundary (Southern Franconian Alb, Bavaria). *Neues Jahrbuch für Geologie und Paläontologie – Abhandlungen*, **245**, 127–142.

Wang, J., Chen, D., Wang, D., Yan, D., Zhou, X. and Wang, Q. 2012. Petrology and geochemistry of chert on the marginal zone of Yangtze Platform, western Hunan, South China, during the Ediacaran–Cambrian Transition. *Sedimentology*, **59**, 809–829.

Wang, Z., Xie, X. and Wen, Z. 2022. Formation conditions of Ediacaran–Cambrian cherts in South China: Implications for marine redox conditions and paleoecology. *Precambrian Research*, **383**, 106867.

Weber, K.H. 1978. Erläuterungen zur Geologischen Karte 1:25 000 7137 Abensberg. Bayerisches Geologisches Landesamt; München.

Werra, D.H. and Siuda, R. 2022. The use of phosphate minerals for determination of the provenance of flint used by prehistoric communities in East-Central Europe. *Quaternary International*, **615**, 5–17.

Wierzbowski, A. 1965. Problem granicy oksford–kimeryd w północnej części Jury Krakowsko-Częstochowskiej. *Annales Societatis Geologorum Poloniae*, **35**, 291–300.

Wierzbowski, A. 1966. Górny oksford i dolny kimeryd Wyżyny Wieluńskiej. *Acta Geologica Polonica*, **16**, 127–200.

Williams, L.A., Parks, G.A. and Crerar, D.A. 1985. Silica Diagenesis, I. Solubility Controls. *Journal of Sedimentary Research*, **55**, 301–311.

Wiśniowski, T. 1888. Wiadomości o krzemieniach jurajskich okolicy Krakowa. *Kosmos*, **13**, 175–184.

Yamamoto, K., 1987. Geochemical characteristics and depositional environments of cherts and associated rocks in the Franciscan and Shimanto Terranes. *Sedimentary Geology*, **52**, 65–108.

Yeşilot Kaplan, M. 2023. Geochemical, mineralogical and diagenetic characteristics of marine chert in the Hatay region, S-Turkey: its origin and depositional environment. *Carpathian Journal of Earth and Environmental Sciences*, **18**, 65–77.

Yu, Y., Lin, L., Deng, X., Wang, Y., Li, Y. and Guo, Y. 2019. Geochemical features of the Middle–Upper Permian cherts and implications for origin, depositional environment in the Sichuan Basin, SW China. *Geological Journal*, **55**, 1493–1506.

Zakharov, D.O., Marin-Carbonne, J., Alleon, J. and Bindeman, I.N. 2021. Triple Oxygen Isotope Trend Recorded by Precambrian Cherts: A Perspective from Combined Bulk and in situ Secondary Ion Probe Measurements. *Reviews in Mineralogy and Geochemistry*, **86**, 323–365.

Zaręczny, S. 1894. Atlas geologiczny Galicji. Tekst do zeszytu trzeciego. 290 pp. Akademia Umiejętności; Kraków.

Zeiss, A. 1964. Zur Malm Gamma/Delta-Grenze in Franken. *Geologische Blätter für Nordost-Bayern*, **14**, 104–115.

Zeiss, A. 1977. Jurassic stratigraphy of Franconia. *Stuttgarter Beiträge zur Naturkunde, Serie B*, **31**, 1–32.

Zeiss, A. 2012. Lithostratigraphische Einheiten des Jura in Nordbayern. *Geologische Blätter für Nordost-Bayern*, **62**, 247–260.

Zejszner, L. 1841. O formacji Jura nad brzegami Wisły, jako przyczynek do topografii Krakowa. *Rocznik Wydziału Lekarskiego Uniwersytetu Jagiellońskiego*, **4**, 3–36.

Zhang, M. and Moxon, T. 2014. Infrared absorption spectroscopy of SiO_2-moganite. *American Mineralogist*, **99**, 671–680.

Zhang, H., Fan, H., Wen, H., Zhu, X. and Tian, S. 2020. Oceanic chemistry recorded by cherts during the early Cambrian Explosion, South China. *Palaeogeography, Palaeoclimatology, Palaeoecology,* **558**, 109961.

Ziółkowski, P. 2007. Stratygrafia i zróżnicowanie facjalne górnej jury wschodniej części Wyżyny Krakowskiej. *Volumina Jurassica*, **4**, 25–38.

Manuscript submitted: 15th January 2026
Revised version accepted: 17th March 2026

APPENDIX

Table 1. Contents of major [wt.%] and trace elements [mg·kg^{-1}] in chert concretions from S-KCU

Location	Sample	SiO_2	Al_2O_3	Fe_2O_3 (T)	MnO	MgO	CaO	Na_2O	K_2O	TiO_2	P_2O_5	LOI	Total	Ba	Rb	Sr	Pb	Th	U	Nb	Y	Zr	Ni	Co	Cu	Cr	Zn	Ga	Hf	V	Al/(Al+Fe+Mn)	Al_2O_3/TiO_2	MnO/TiO_2	Fe_2O_3/TiO_2
	Unit	%	%	%	%	%	%	%	%	%	%	%	%	mg·kg^{-1}	mg·kg^{-1}	mg·kg^{-1}	mg·kg^{-1}	mg·kg^{-1}	mg·kg^{-1}	mg·kg^{-1}	mg·kg^{-1}	mg·kg^{-1}	mg·kg^{-1}	mg·kg^{-1}	mg·kg^{-1}	mg·kg^{-1}	mg·kg^{-1}	mg·kg^{-1}	mg·kg^{-1}	mg·kg^{-1}	mg·kg^{-1}				
	Detection Limit	0.01	0.01	0.01	0.001	0.01	0.01	0.01	0.01	0.001	0.01		0.01	2	0.2	2	0.5	0.05	0.01	0.1	0.1	1	0.5	0.1	0.2	1	0.2	0.1	0.1	1				
	Analytical Method	FUS-ICP	FUS-ICP	FUS-ICP	FUS-ICP	FUS-ICP	FUS-ICP	FUS-ICP	FUS-ICP	FUS-ICP	FUS-ICP	GRAV	FUS-ICP	FUS-ICP	TD-MS	FUS-ICP	TD-MS	FUS-MS	FUS-MS	TD-MS	TD-MS	FUS-ICP	TD-MS	TD-MS	TD-MS	TD-MS	TD-MS	TD-MS	FUS-MS	TD-MS				
PIEKARY	KA-1	98.26	0.1	1.26	0.013	0.02	0.14	0.05	0.04	0.006	0.01	0.92	100.8	6	0.4	3	1.5	0.42	0.91	0.2	0.8	17	3.8	0.8	5.2	7	6	0.4	0.4	2	0.07	16.67	2.17	210
	KA-2	98.2	0.13	1.37	0.013	0.01	0.09	0.05	0.04	0.019	< 0.01	0.67	100.6	7	0.3	3	0.9	0.58	0.31	0.7	1.3	42	4.3	0.9	4.7	11	3.8	0.5	1	1	0.09	6.84	0.68	72
	KA-3	98.32	0.1	1.1	0.011	< 0.01	0.25	0.04	0.04	0.004	0.01	0.75	100.7	10	0.3	4	1.1	0.26	0.23	0.1	1.1	9	4	0.8	5.3	5	4	0.4	0.2	2	0.08	25.00	2.75	275
	KA-3’	98.46	0.14	1.32	0.013	< 0.01	0.11	0.05	0.04	0.004	0.02	0.78	100.9	14	0.4	4	1	0.25	0.33	0.2	1.3	9	4.1	0.8	5.9	7	3.7	0.8	0.2	1	0.10	35.00	3.25	330
	KA-3”	97.95	0.17	0.98	0.011	0.01	0.18	0.06	0.05	0.015	0.02	1	100.4	17	0.5	4	1.6	0.34	0.33	0.7	1.5	21	2.8	0.6	4.3	5	5.4	0.6	0.5	1	0.15	11.33	0.73	65
	KA-4	97.5	0.13	1.07	0.011	0.01	0.34	0.05	0.05	0.007	0.04	1.05	100.3	9	0.4	5	0.9	0.24	0.3	0.4	2.1	16	3.4	0.7	5.1	6	4	0.6	0.3	2	0.11	18.57	1.57	153
	KA-5	95.86	0.11	0.87	0.01	0.01	1.56	0.04	0.04	0.004	0.03	2.27	100.8	9	0.5	5	2	0.18	0.26	0.2	1.5	6	3.4	0.8	6.4	4	11.6	0.5	0.1	1	0.11	27.50	2.50	218
	KA-6	97.93	0.14	1.45	0.014	0.02	0.08	0.06	0.05	0.009	< 0.01	1.04	100.8	5	0.4	2	2.1	0.27	0.38	1.1	0.8	11	4.6	0.9	4.8	4	7.4	0.5	0.2	2	0.09	15.56	1.56	161
	KA-6’	97.73	0.12	1.07	0.011	0.02	0.28	0.05	0.03	0.007	< 0.01	0.98	100.3	11	0.4	4	2	0.25	0.25	0.4	1	13	3.6	0.8	4.3	10	8.5	0.4	0.3	2	0.10	17.14	1.57	153
DĄBROWA SZLACHECKA	KB-1	97.47	0.1	1.21	0.012	< 0.01	0.11	0.05	0.02	0.006	< 0.01	1	99.98	9	0.3	2	0.6	0.14	0.67	0.7	0.6	7	3.5	0.7	5	7	3	0.4	0.1	1	0.08	16.67	2.00	202
	KB-3	86.82	0.12	0.71	0.01	0.06	7.38	0.03	0.02	< 0.001	0.01	5.76	100.9	37	0.3	22	1.7	0.14	0.44	0.7	8.7	5	< 0.5	0.1	1.2	2	10.5	< 0.1	0.1	2	0.14	n. c.	n. c..	n. c.
	KB-5	98.22	0.1	1.05	0.011	< 0.01	0.14	0.05	0.02	0.003	< 0.01	0.94	100.6	12	0.3	4	0.6	0.14	0.76	0.2	0.9	5	3.4	0.7	3.4	8	2.9	0.7	0.1	2	0.09	33.33	3.67	350
	KB-7B	91.12	0.16	1.29	0.01	0.03	4.21	0.05	0.04	< 0.001	0.02	3.62	100.6	42	0.7	17	2.6	0.17	0.46	0.2	2.5	5	4.6	0.8	9.2	6	8.1	0.4	0.1	3	0.11	n. c.	n. c.	n. c.
	KB-8	98.27	0.09	0.87	0.01	0.01	0.52	0.05	0.02	0.003	< 0.01	1.04	100.9	8	0.3	3	0.6	0.13	1.04	0.2	1	6	3	0.7	5.8	4	2.6	0.3	0.1	< 1	0.09	30.00	3.33	290
	KB-9	98.09	0.11	0.89	0.01	0.01	0.31	0.05	0.02	0.004	< 0.01	1.05	100.5	11	0.4	3	1.6	0.15	0.73	0.5	5.1	4	19.1	1.1	5	3	6.3	0.5	0.1	< 1	0.11	27.50	2.50	223
	KB-10	97.66	0.12	1.24	0.012	0.01	0.56	0.05	0.02	0.003	< 0.01	1.21	100.9	12	0.4	4	2.1	0.14	0.97	0.2	0.8	4	4.2	0.8	5.6	6	3.2	0.7	0.1	2	0.09	40.00	4.00	413
	KB-11	98.41	0.1	1.01	0.01	< 0.01	0.23	0.05	0.02	0.004	0.03	0.8	100.7	22	0.3	4	0.5	0.14	0.6	0.5	1.8	4	3.5	0.7	9.6	4	15.4	0.3	0.1	1	0.09	25.00	2.50	253
GUMINEK HILL	KC-1	97.77	0.18	1.15	0.012	0.01	0.3	0.04	0.03	0.003	< 0.01	0.39	99.88	16	0.9	4	1.2	0.14	0.09	0.1	0.7	3	3	0.6	4.7	5	3.4	0.4	0.1	1	0.13	60.00	4.00	383
	KC-2	98.52	0.12	0.89	0.01	< 0.01	0.35	0.03	0.02	0.004	0.01	0.41	100.4	12	0.8	3	1.1	0.11	0.29	0.5	0.7	5	2.7	0.8	3.7	4	2.3	0.4	0.1	< 1	0.12	30.00	2.50	223
	KC-3	98.82	0.12	0.94	0.01	< 0.01	0.08	0.03	0.02	0.002	< 0.01	0.36	100.4	11	0.7	3	1.3	0.11	0.48	0.2	0.4	5	3	0.7	16.5	6	3.4	0.4	0.1	1	0.11	60.00	5.00	470
	KC-5	97.96	0.15	1.41	0.014	0.02	0.26	0.06	0.04	0.004	< 0.01	0.84	100.8	5	1	2	2.1	0.14	0.74	0.3	0.5	8	3.8	0.7	4.7	4	2	1.7	0.2	< 1	0.10	37.50	3.50	353
LIBAN QUARRY	KD-1	98.61	0.15	0.97	0.01	0.02	0.17	0.05	0.04	0.004	0.01	0.67	100.7	21	0.5	6	< 0.5	0.11	0.22	0.2	0.7	4	3.6	0.7	3	4	4.1	0.6	0.1	1	0.13	37.50	2.50	243
	KD-2	97.72	0.13	1.27	0.013	0.02	0.15	0.05	0.03	0.006	0.02	0.84	100.3	11	0.5	4	< 0.5	0.13	0.47	0.3	1.4	6	3.8	0.8	7.7	7	3.8	0.7	0.1	3	0.09	21.67	2.17	212
BONARKA QUARRY	B-1	95.75	0.17	1.7	0.016	< 0.01	0.14	0.05	0.03	0.01	0.01	1.02	98.91	19	0.5	4	< 0.5	0.14	0.45	0.3	0.8	6	4.2	0.9	4.7	10	3	0.69	< 0.1	3	0.09	17.00	1.60	170
	B-2	96.07	0.15	1.84	0.016	0.01	0.3	0.06	0.03	0.014	0.01	0.8	99.29	21	0.5	6	0.6	0.14	0.57	0.5	0.8	8	4.3	0.9	4.9	11	3	0.59	< 0.1	2	0.07	10.71	1.14	131
	B-4	96.28	0.17	1.59	0.015	< 0.01	0.08	0.05	0.03	0.009	0.01	1.02	99.26	17	0.7	4	< 0.5	0.16	0.41	0.7	0.3	7	3.7	0.7	4.4	8	3	0.81	< 0.1	2	0.10	18.89	1.67	177
	B-5	95.72	0.19	1.55	0.014	0.01	0.23	0.06	0.03	0.01	< 0.01	1.04	98.86	34	0.8	7	0.5	0.15	0.32	0.7	1.1	6	4	0.8	4	7	3	0.59	< 0.1	2	0.11	19.00	1.40	155
	B-6	96.6	0.15	1.37	0.013	< 0.01	0.09	0.05	0.03	0.008	< 0.01	0.91	99.23	17	0.6	3	0.6	0.11	0.35	0.3	0.6	5	3.3	0.6	3.8	8	2	0.52	< 0.1	2	0.10	18.75	1.63	171
	B-7	95.73	0.16	1.96	0.018	< 0.01	0.2	0.06	0.03	0.008	0.01	0.66	98.84	31	0.5	10	0.9	0.1	0.24	0.3	1	4	5.4	1	4.7	9	4	0.52	< 0.1	2	0.07	20.00	2.25	245
	B-8	97.57	0.2	1.62	0.017	0.01	0.21	0.06	0.03	0.01	0.02	1.08	100.8	21	0.9	5	0.5	0.22	0.43	0.4	0.7	9	4.8	0.9	4.4	11	2	0.79	< 0.1	3	0.11	20.00	1.70	162
	B-9	96.11	0.16	1.44	0.013	< 0.01	0.2	0.05	0.03	0.007	< 0.01	1.09	99.1	19	0.6	4	0.6	0.06	0.44	0.3	0.6	4	3.7	0.7	3.6	9	2	0.56	< 0.1	2	0.10	22.86	1.86	206
	B-10	95.48	0.17	2.12	0.018	< 0.01	0.17	0.06	0.03	0.009	0.01	0.59	98.68	17	0.6	5	0.6	0.09	0.39	0.4	0.7	6	5.3	1.1	6.4	12	5	0.69	< 0.1	3	0.07	18.89	2.00	236
	B-11	94.93	0.18	2.12	0.018	0.01	0.34	0.06	0.03	0.007	0.02	0.83	98.55	30	0.7	7	0.7	0.07	0.44	0.4	0.9	5	5.3	1.1	5.2	15	4	0.68	< 0.1	2	0.08	25.71	2.57	303
	B-12	95.89	0.22	1.22	0.012	0.01	0.31	0.06	0.04	0.006	0.01	1.51	99.29	28	0.9	12	0.5	0.09	0.32	0.2	0.8	5	3.3	0.7	4	11	3	0.61	< 0.1	1	0.15	36.67	2.00	203
	B-13	95.39	0.16	2.03	0.018	< 0.01	0.11	0.06	0.03	0.006	< 0.01	0.84	98.67	17	0.8	4	< 0.5	0.06	0.52	0.3	0.5	4	4.6	0.9	9.1	9	22	0.85	< 0.1	2	0.07	26.67	3.00	338
	B-14	94.77	0.32	1.74	0.015	0.01	0.74	0.09	0.05	0.008	< 0.01	1.38	99.14	38	1.1	9	< 0.5	0.07	0.18	0.5	0.9	7	4.3	0.9	5.3	10	4	0.69	< 0.1	2	0.15	40.00	1.88	218
	B-15	97.15	0.17	1.31	0.016	< 0.01	0.3	0.05	0.03	0.006	0.04	1.06	100.1	33	0.7	5	< 0.5	0.08	0.72	0.4	0.4	7	3.7	0.7	4.2	11	3	0.62	< 0.1	1	0.11	28.33	2.67	218

Table 2. Contents of major [wt.%] and trace elements [mg·kg^{-1}] in chert concretions from N-KCU

Location	Sample	SiO_2	Al_2O_3	Fe_2O_3 (T)	MnO	MgO	CaO	Na_2O	K_2O	TiO_2	P_2O_5	LOI	Total	Ba	Rb	Sr	Pb	Th	U	Nb	Y	Zr	Ni	Co	Cu	Cr	Zn	Ga	Hf	V	Al/(Al+Fe+Mn)	Al_2O_3/TiO_2	MnO/TiO_2	Fe_2O_3/TiO_2
	Unit	%	%	%	%	%	%	%	%	%	%	%	%	mg·kg^{-1}	mg·kg^{-1}	mg·kg^{-1}	mg·kg^{-1}	mg·kg^{-1}	mg·kg^{-1}	mg·kg^{-1}	mg·kg^{-1}	mg·kg^{-1}	mg·kg^{-1}	mg·kg^{-1}	mg·kg^{-1}	mg·kg^{-1}	mg·kg^{-1}	mg·kg^{-1}	mg·kg^{-1}	mg·kg^{-1}	mg·kg^{-1}				
	Detection Limit	0.01	0.01	0.01	0.001	0.01	0.01	0.01	0.01	0.001	0.01		0.01	2	0.2	2	0.5	0.05	0.01	0.1	0.1	1	0.5	0.1	0.2	1	0.2	0.1	0.1	1				
	Analytical Method	FUS-ICP	FUS-ICP	FUS-ICP	FUS-ICP	FUS-ICP	FUS-ICP	FUS-ICP	FUS-ICP	FUS-ICP	FUS-ICP	GRAV	FUS-ICP	FUS-ICP	TD-MS	FUS-ICP	TD-MS	FUS-MS	FUS-MS	TD-MS	TD-MS	FUS-ICP	TD-MS	TD-MS	TD-MS	TD-MS	TD-MS	TD-MS	FUS-MS	TD-MS				
OLSZTYN	PA-2’	98.35	0.15	0.64	0.008	< 0.01	0.44	0.05	0.02	0.003	0.02	1.24	100.9	6	0.3	4	0.6	0.1	0.22	0.1	1.3	3	2.4	0.5	3.8	4	3.6	0.8	< 0.1	2	0.19	50.00	2.67	213
	PA-3	97.25	0.22	0.46	0.007	0.02	0.48	0.06	0.03	0.004	< 0.01	1.48	100	7	0.4	4	< 0.5	0.11	0.24	0.3	0.3	4	1.9	0.3	7.3	2	1.9	0.5	< 0.1	1	0.32	55.00	1.75	115
	PA-3’	97.51	0.27	0.6	0.012	0.01	0.48	0.04	0.02	0.005	0.02	1.6	100.6	11	0.6	3	1.3	0.14	0.19	0.2	1.2	4	3.5	2.1	4.2	3	13.2	1.1	< 0.1	4	0.31	54.00	2.40	120
	PA-4	97.75	0.12	1.18	0.012	0.01	0.28	0.05	0.02	0.003	< 0.01	0.86	100.3	5	0.3	3	0.6	0.09	0.36	0.2	0.5	4	3.9	0.7	4	6	2.4	0.7	< 0.1	2	0.09	40.00	4.00	393
JULIANKA	PB-1	98.1	0.11	1.11	0.011	0.01	0.29	0.05	0.02	0.003	< 0.01	0.92	100.7	5	0.3	3	< 0.5	0.06	0.31	0.4	0.6	4	3.1	0.7	17.3	4	1.1	0.6	< 0.1	< 1	0.09	36.67	3.67	370
	PB-2	98.39	0.09	0.83	0.009	0.01	0.39	0.04	0.02	0.004	0.04	0.75	100.6	7	0.3	6	< 0.5	0.08	0.38	0.2	1.4	4	2.4	0.5	39.2	5	2.7	0.3	0.1	< 1	0.10	22.50	2.25	208
	PB-3	98.33	0.07	0.99	0.01	< 0.01	0.25	0.04	0.01	0.002	0.02	0.67	100.4	5	0.2	3	< 0.5	< 0.05	0.45	0.3	0.6	3	2.8	0.6	2.8	4	1.7	0.3	< 0.1	< 1	0.07	35.00	5.00	495
	PB-4	97.24	0.16	1.5	0.015	0.02	0.57	0.05	0.03	0.004	0.03	0.92	100.5	10	0.4	5	< 0.5	0.08	0.39	0.3	1	5	4.4	0.9	5.6	17	1.8	0.6	0.1	< 1	0.10	40.00	3.75	375

Location	Sample	SiO_2	Al_2O_3	Fe_2O_3 (T)	MnO	MgO	CaO	Na_2O	K_2O	TiO_2	P_2O_5	LOI	Total	Ba	Rb	Sr	Pb	Th	U	Nb	Y	Zr	Ni	Co	Cu	Cr	Zn	Ga	Hf	V	Al/(Al+Fe+Mn)	Al_2O_3/TiO_2	MnO/TiO_2	Fe_2O_3/TiO_2
	Unit	%	%	%	%	%	%	%	%	%	%	%	%	mg·kg^{-1}	mg·kg^{-1}	mg·kg^{-1}	mg·kg^{-1}	mg·kg^{-1}	mg·kg^{-1}	mg·kg^{-1}	mg·kg^{-1}	mg·kg^{-1}	mg·kg^{-1}	mg·kg^{-1}	mg·kg^{-1}	mg·kg^{-1}	mg·kg^{-1}	mg·kg^{-1}	mg·kg^{-1}	mg·kg^{-1}				
	Detection Limit	0.01	0.01	0.01	0.001	0.01	0.01	0.01	0.01	0.001	0.01		0.01	2	0.2	2	0.5	0.05	0.01	0.1	0.1	1	0.5	0.1	0.2	1	0.2	0.1	0.1	1				
	Analytical Method	FUS-ICP	FUS-ICP	FUS-ICP	FUS-ICP	FUS-ICP	FUS-ICP	FUS-ICP	FUS-ICP	FUS-ICP	FUS-ICP	GRAV	FUS-ICP	FUS-ICP	TD-MS	FUS-ICP	TD-MS	FUS-MS	FUS-MS	TD-MS	TD-MS	FUS-ICP	TD-MS	TD-MS	TD-MS	TD-MS	TD-MS	TD-MS	FUS-MS	TD-MS				
EMMERTHAL	E2	94.1	0.3	0.85	0.008	0.04	1.78	0.07	0.04	0.005	0.01	2.15	99.35	11	0.9	6	< 0.5	0.09	0.11	0.2	0.4	3	4.9	0.7	5.1	6	4	0.58	< 0.1	2	0.26	60.00	1.60	170
	E2A	97.37	0.27	1.45	0.012	0.02	0.31	0.06	0.04	0.005	< 0.01	1.1	100.6	10	0.9	5	25	0.1	0.11	0.2	0.3	4	5.4	0.8	11	6	7	0.76	< 0.1	2	0.16	54.00	2.40	290
	E3	97.33	0.26	0.6	0.006	0.02	0.37	0.05	0.03	0.002	< 0.01	1.16	99.8	13	0.9	3	< 0.5	< 0.05	0.05	0.1	0.2	4	2.6	0.4	6.4	26	3	0.64	< 0.1	2	0.30	130.00	3.00	300
RUDNIKI	PB-5	97.78	0.16	1.27	0.017	0.03	0.77	0.05	0.02	0.003	0.02	0.79	100.9	11	0.3	8	< 0.5	0.05	0.13	0.5	0.5	5	4	0.8	4.1	6	2.1	0.6	< 0.1	2	0.11	53.33	5.67	423
	PB-6	89.13	0.15	0.71	0.013	0.06	5.59	0.04	0.01	0.002	< 0.01	4.47	100.2	14	0.3	26	< 0.5	< 0.05	0.21	< 0.1	1.5	3	1.7	0.6	10.2	2	6.4	0.3	< 0.1	< 1	0.17	75.00	6.50	355
	PB-7B	98.91	0.05	1.07	0.011	0.01	0.26	0.02	0.01	0.002	0.01	0.55	100.9	5	< 0.2	4	< 0.5	< 0.05	0.36	0.4	0.7	3	3	2.1	30.7	4	13.7	0.3	< 0.1	< 1	0.04	25.00	5.50	535
	PB-8	98.28	0.08	0.97	0.01	0.01	0.41	0.04	0.01	0.002	< 0.01	0.77	100.6	7	0.2	4	< 0.5	< 0.05	0.42	0.2	0.3	1	3.1	0.6	4.6	3	1.8	0.4	< 0.1	< 1	0.08	40.00	5.00	485
	PB-9	97.98	0.09	0.95	0.01	< 0.01	0.18	0.04	0.02	0.002	< 0.01	0.77	100.1	4	0.2	3	< 0.5	< 0.05	0.42	0.3	0.4	1	2.9	1	7.4	3	5.2	0.4	< 0.1	< 1	0.09	45.00	5.00	475
	PB-10	96.96	0.09	1.03	0.012	0.01	0.44	0.04	0.02	0.002	< 0.01	0.85	99.45	10	0.3	4	< 0.5	< 0.05	0.46	0.1	0.4	1	3	0.8	4.3	10	1.7	0.5	< 0.1	< 1	0.08	45.00	6.00	515
	PB-11B	68.55	0.08	0.28	0.009	0.13	17.54	0.03	< 0.01	0.001	0.01	13.36	99.98	5	< 0.2	75	< 0.5	< 0.05	0.27	< 0.1	3	< 1	1.2	0.5	3.9	45	6	0.4	< 0.1	< 1	0.22	80.00	9.00	280
	PB-12	85.02	0.09	0.54	0.009	0.06	7.43	0.03	0.01	0.002	< 0.01	5.81	99.01	8	0.2	26	< 0.5	< 0.05	0.06	< 0.1	1.3	2	1.6	0.4	2.1	6	4.7	0.2	< 0.1	1	0.14	45.00	4.50	270
	PB-13	97.29	0.08	0.79	0.009	0.01	0.7	0.04	0.01	0.001	< 0.01	0.76	99.69	8	0.2	5	< 0.5	< 0.05	0.13	0.2	0.4	2	2.5	0.7	5.5	4	3.3	0.4	< 0.1	< 1	0.09	80.00	9.00	790
	PB-14	93.3	0.17	0.9	0.011	0.03	3.12	0.05	0.03	0.001	< 0.01	2.65	100.2	11	0.4	12	< 0.5	< 0.05	0.04	< 0.1	0.5	2	2.3	0.7	4.3	4	2.8	0.3	< 0.1	< 1	0.16	170.00	11.00	900
	PB-15	98.28	0.09	0.97	0.01	0.01	0.19	0.03	0.02	< 0.001	< 0.01	0.95	100.6	5	0.2	3	< 0.5	< 0.05	0.41	0.1	0.2	3	2.9	0.6	3.8	7	1	0.6	< 0.1	< 1	0.08	n. c.	n. c.	n. c.
	PB-16	96.81	0.13	0.94	0.012	0.01	0.23	0.04	0.02	0.003	< 0.01	1.02	99.22	5	0.3	3	< 0.5	0.05	0.22	0.3	0.2	14	2.7	0.6	3.6	3	2.1	0.7	0.3	< 1	0.12	43.33	4.00	313
	PB-17A	64.22	0.05	0.24	0.01	0.14	20.04	0.02	< 0.01	0.001	0.04	15.34	100.1	12	0.2	74	< 0.5	< 0.05	0.35	< 0.1	2.8	< 1	< 0.5	0.3	4.5	2	4.1	< 0.1	< 0.1	1	0.17	50.00	10.00	240
	PB-17B	94.54	0.13	0.59	0.008	0.02	2.32	0.03	0.02	0.002	< 0.01	1.89	99.54	12	0.3	11	< 0.5	< 0.05	0.12	< 0.1	1	< 1	2.2	0.5	2.5	2	2	0.2	< 0.1	< 1	0.18	65.00	4.00	295
	R1	95.61	0.25	1.68	0.017	0.01	0.08	0.05	0.02	0.014	< 0.01	0.81	98.54	16	0.7	4	< 0.5	0.12	0.13	1	0.2	7	5.4	0.9	7.9	9	3	0.5	< 0.1	3	0.13	17.86	1.21	120
	R2A	96.25	0.24	1.29	0.012	0.01	0.1	0.04	0.02	0.029	< 0.01	0.97	98.96	13	0.5	4	< 0.5	0.3	0.19	1.1	0.2	12	4.2	0.6	5.2	11	2	0.48	0.2	3	0.16	8.28	0.41	44
	R2B	96.24	0.12	1.77	0.016	< 0.01	0.09	0.05	0.01	0.029	0.02	0.72	99.07	4	0.3	3	0.5	0.24	0.41	1	1	10	4.6	0.9	5.2	13	4	0.68	0.2	2	0.06	4.14	0.55	61
	R3/1	98.02	0.09	1.23	0.011	< 0.01	0.09	0.04	0.01	0.003	< 0.01	0.77	100.3	2	0.3	< 2	< 0.5	0.07	0.26	0.2	0.2	3	3.3	0.5	4.1	16	< 2	0.39	< 0.1	2	0.07	30.00	3.67	410
	R3/2	94.05	0.18	0.98	0.01	0.04	3.44	0.04	0.03	0.002	< 0.01	2.07	100.8	11	0.6	24	< 0.5	0.05	0.19	0.2	0.9	3	3.8	0.6	4.2	4	5	0.11	< 0.1	1	0.15	90.00	5.00	490
	R3/3	36.03	0.05	0.06	0.009	0.21	35.76	0.02	< 0.01	0.002	0.02	28.27	100.4	5	0.5	101	< 0.5	< 0.05	0.37	0.1	3.5	2	< 0.2	< 0.1	0.6	14	6	< 0.05	< 0.1	3	0.42	25.00	4.50	30
	R3/4	97.65	0.16	1.6	0.014	0.02	0.49	0.05	0.02	0.003	< 0.01	0.34	100.3	7	0.5	6	0.9	< 0.05	0.13	0.3	0.7	2	5.7	0.8	30.1	11	7	0.27	< 0.1	2	0.09	53.33	4.67	533
	R4	94.22	0.13	1.05	0.011	0.03	2.14	0.03	0.02	0.011	0.03	1.53	99.2	14	0.4	16	< 0.5	0.12	0.21	0.4	0.9	5	4.1	0.7	3.2	6	3	0.33	< 0.1	1	0.11	11.82	1.00	95

Table 3. Contents of major [wt.%] and trace elements [mg·kg^{-1}] in chert concretions from southeastern FA

Table 4. Contents of major [wt.%] and trace elements [mg·kg^{-1}] in chert concretions from BW

Location	Sample	SiO_2	Al_2O_3	Fe_2O_3 (T)	MnO	MgO	CaO	Na_2O	K_2O	TiO_2	P_2O_5	LOI	Total	Ba	Rb	Sr	Pb	Th	U	Nb	Y	Zr	Ni	Co	Cu	Cr	Zn	Ga	Hf	V	Al/(Al+Fe+Mn)	Al_2O_3/TiO_2	MnO/TiO_2	Fe_2O_3/TiO_2
	Unit	%	%	%	%	%	%	%	%	%	%	%	%	mg·kg^{-1}	mg·kg^{-1}	mg·kg^{-1}	mg·kg^{-1}	mg·kg^{-1}	mg·kg^{-1}	mg·kg^{-1}	mg·kg^{-1}	mg·kg^{-1}	mg·kg^{-1}	mg·kg^{-1}	mg·kg^{-1}	mg·kg^{-1}	mg·kg^{-1}	mg·kg^{-1}	mg·kg^{-1}	mg·kg^{-1}				
	Detection Limit	0.01	0.01	0.01	0.001	0.01	0.01	0.01	0.01	0.001	0.01		0.01	2	0.2	2	0.5	0.05	0.01	0.1	0.1	1	0.5	0.1	0.2	1	0.2	0.1	0.1	1				
	Analytical Method	FUS-ICP	FUS-ICP	FUS-ICP	FUS-ICP	FUS-ICP	FUS-ICP	FUS-ICP	FUS-ICP	FUS-ICP	FUS-ICP	GRAV	FUS-ICP	FUS-ICP	TD-MS	FUS-ICP	TD-MS	FUS-MS	FUS-MS	TD-MS	TD-MS	FUS-ICP	TD-MS	TD-MS	TD-MS	TD-MS	TD-MS	TD-MS	FUS-MS	TD-MS				
FLINTSBACH	FL1	98.42	0.27	0.98	0.009	0.02	0.14	0.05	0.03	0.004	0.02	0.68	100.6	28	1.2	6	< 0.5	0.17	0.22	0.2	1.1	3	3.4	0.6	5.8	8	3	0.89	< 0.1	2	0.21	67.50	2.25	245
	F1	98.75	0.19	0.93	0.008	< 0.01	0.15	0.04	0.02	0.003	0.06	0.54	100.7	20	0.8	5	< 0.5	0.14	0.24	0.2	1.5	3	3.3	0.5	5.5	7	3	0.77	< 0.1	2	0.17	63.33	2.67	310
	F2	97.19	0.25	0.91	0.008	0.01	0.36	0.04	0.03	0.004	0.01	0.73	99.55	35	1	7	0.6	0.13	0.2	0.2	1.6	3	4.1	0.6	7	14	6	1	< 0.1	2	0.21	62.50	2.00	228
	F3"	95.35	0.23	1.12	0.008	0.02	0.59	0.05	0.04	0.004	0.02	0.88	98.31	32	0.9	6	1.5	0.22	0.29	0.2	1.6	3	6.7	1.1	6.1	5	31	0.92	< 0.1	4	0.17	57.50	2.00	280
MÜNSTER	M1sk	86.74	0.4	0.8	0.01	0.1	6.41	0.09	0.09	0.006	< 0.01	6.18	100.8	49	2.1	15	0.8	0.14	0.24	0.3	1.7	4	8.8	1.8	32.8	5	10	1.28	< 0.1	2	0.33	66.67	1.67	133
	M1	99.07	0.22	0.8	0.007	< 0.01	0.07	0.04	0.03	0.003	< 0.01	0.59	100.8	31	0.8	4	0.6	0.08	0.2	0.2	1.1	3	2.8	0.6	5.7	7	< 2	2.07	< 0.1	2	0.21	73.33	2.33	267
	M2	98.37	0.23	0.93	0.008	0.01	0.23	0.05	0.03	0.003	< 0.01	0.75	100.6	20	1	4	< 0.5	0.08	0.35	0.2	2.1	3	3.5	0.6	6.9	8	4	1.19	< 0.1	2	0.20	76.67	2.67	310
	M3	95.91	0.32	1.39	0.012	0.02	0.56	0.08	0.05	0.005	0.01	1.88	100.2	29	1.4	5	< 0.5	0.14	0.38	0.4	0.8	4	4.9	0.8	7.7	13	3	1.08	< 0.1	2	0.19	64.00	2.40	278
	M3s	92.09	0.36	1.13	0.011	0.06	2.85	0.07	0.08	0.007	< 0.01	3.53	100.2	47	1.7	13	0.9	0.13	0.12	0.3	1.3	5	7.4	1.3	5.5	9	5	1.2	< 0.1	2	0.24	51.43	1.57	161
	M4	96.62	0.22	1.03	0.01	< 0.01	0.17	0.04	0.03	0.003	0.02	0.52	98.67	28	0.9	3	1.2	0.14	0.26	0.2	2.4	3	5.5	1.5	7.1	7	25	1.84	< 0.1	2	0.17	73.33	3.33	343
	M5	98.81	0.23	1.24	0.013	< 0.01	0.15	0.06	0.03	0.003	< 0.01	0.42	100.9	27	0.9	4	1.4	0.09	0.23	0.2	1.4	5	4.6	0.9	10.9	8	13	1.22	< 0.1	2	0.16	76.67	4.33	413
	M7	99.08	0.22	0.87	0.008	< 0.01	0.07	0.04	0.03	0.003	< 0.01	0.4	100.7	36	0.7	3	0.9	0.06	0.06	0.2	1.3	3	3.2	0.6	4.9	6	3	1.72	< 0.1	1	0.20	73.33	2.67	290
	M8	98.97	0.16	0.96	0.009	< 0.01	0.14	0.03	0.02	0.003	< 0.01	0.24	100.5	17	0.7	3	0.7	0.08	0.29	0.2	1.9	3	3.3	0.7	16.1	4	8	1.24	< 0.1	1	0.14	53.33	3.00	320
	M10	99.15	0.2	1.1	0.01	< 0.01	0.08	0.05	0.03	0.002	< 0.01	0.37	101	20	0.8	3	< 0.5	0.06	0.06	0.2	2	3	3.9	0.7	6.9	11	5	0.72	< 0.1	1	0.15	100.00	5.00	550
	M11	98.98	0.2	1	0.011	< 0.01	0.08	0.05	0.02	0.003	0.02	0.32	100.7	30	0.7	4	0.9	0.12	0.23	0.2	12.4	6	3.2	0.6	5.4	50	3	1.79	< 0.1	2	0.17	66.67	3.67	333
	M12	96.49	0.16	1.45	0.012	< 0.01	0.08	0.04	0.03	0.003	0.01	0.26	98.54	21	0.7	3	0.6	0.09	0.26	0.2	6.2	3	4.7	1	7.4	9	4	0.81	< 0.1	2	0.10	53.33	4.00	483
	M13	99.14	0.21	0.84	0.008	< 0.01	0.1	0.04	0.02	0.003	< 0.01	0.49	100.8	27	0.8	3	0.5	0.06	0.26	0.2	1.7	4	3.1	0.6	4.9	5	2	1.62	< 0.1	2	0.20	70.00	2.67	280

Table 5. Contents of major [wt.%] and trace elements [mg·kg^{-1}] in bedded cherts from S-KCU

Location	Sample	SiO_2	Al_2O_3	Fe_2O_3 (T)	MnO	MgO	CaO	Na_2O	K_2O	TiO_2	P_2O_5	LOI	Total	Ba	Rb	Sr	Pb	Th	U	Nb	Y	Zr	Ni	Co	Cu	Cr	Zn	Ga	Hf	V	Al/(Al+Fe+Mn)	Al_2O_3/TiO_2	MnO/TiO_2	Fe_2O_3/TiO_2
	Unit	%	%	%	%	%	%	%	%	%	%	%	%	mg·kg^{-1}	mg·kg^{-1}	mg·kg^{-1}	mg·kg^{-1}	mg·kg^{-1}	mg·kg^{-1}	mg·kg^{-1}	mg·kg^{-1}	mg·kg^{-1}	mg·kg^{-1}	mg·kg^{-1}	mg·kg^{-1}	mg·kg^{-1}	mg·kg^{-1}	mg·kg^{-1}	mg·kg^{-1}	mg·kg^{-1}				
	Detection Limit	0.01	0.01	0.01	0.001	0.01	0.01	0.01	0.01	0.001	0.01		0.01	2	0.2	2	0.5	0.05	0.01	0.1	0.1	1	0.5	0.1	0.2	1	0.2	0.1	0.1	1				
	Analytical Method	FUS-ICP	FUS-ICP	FUS-ICP	FUS-ICP	FUS-ICP	FUS-ICP	FUS-ICP	FUS-ICP	FUS-ICP	FUS-ICP	GRAV	FUS-ICP	FUS-ICP	TD-MS	FUS-ICP	TD-MS	FUS-MS	FUS-MS	TD-MS	TD-MS	FUS-ICP	TD-MS	TD-MS	TD-MS	TD-MS	TD-MS	TD-MS	FUS-MS	TD-MS				
UJAZDD	SA-1	85.38	0.15	0.48	0.009	0.07	7.78	0.05	0.03	0.005	0.01	6.6	100.6	6	0.7	32	1	0.1	0.21	0.2	3	2	1.4	0.4	2.5	3	5	0.3	< 0.1	1	0.23	30.00	1.80	96
	SA-2A	98.44	0.13	0.92	0.01	0.01	0.08	0.04	0.03	0.004	< 0.01	0.39	100.1	6	0.4	3	0.5	0.08	0.14	0.2	0.7	1	2.7	0.7	5.5	3	2.1	0.6	< 0.1	1	0.12	32.50	2.50	230
	SA-2B	96.46	0.19	0.82	0.009	0.02	1.42	0.05	0.05	0.005	0.01	1.89	100.9	7	1.6	15	0.8	0.12	0.12	0.2	1.7	2	2.6	0.5	3.5	5	3.1	0.7	< 0.1	1	0.19	38.00	1.80	164
	SA-2C	91.55	0.18	0.48	0.008	0.04	4.24	0.04	0.04	0.005	0.01	3.99	100.6	6	1.2	31	0.7	0.12	0.17	0.1	2.2	1	1.7	0.3	2.3	3	3.6	0.4	< 0.1	2	0.27	36.00	1.60	96
	SA-2D	95.62	0.15	0.95	0.011	0.02	1.82	0.04	0.03	0.004	0.01	2	100.7	7	0.8	14	0.7	0.11	0.23	0.1	1.6	1	2.4	0.5	6	4	3.3	0.4	< 0.1	2	0.14	37.50	2.75	238
	SA-9A	69.65	0.12	0.21	0.009	0.14	16.94	0.03	0.03	0.004	0.02	13.43	100.6	7	0.8	60	1.6	0.1	0.2	0.1	4.6	< 1	< 0.5	0.2	1.8	2	4.6	0.2	< 0.1	1	0.35	30.00	2.25	53
	SA-9B	94.27	0.16	0.81	0.009	0.03	2.4	0.04	0.04	0.004	< 0.01	2.49	100.3	8	1.2	16	2.3	0.11	0.15	0.2	1.8	1	2.5	0.6	5.8	4	4	0.5	< 0.1	< 1	0.16	40.00	2.25	203
	SA-9'A	91.17	0.16	0.74	0.01	0.04	4.05	0.04	0.03	0.005	0.03	3.85	100.1	7	1.1	21	1.3	0.11	0.16	0.1	2	2	2.3	0.5	2.2	7	3.8	0.3	< 0.1	2	0.18	32.00	2.00	148
	SA-9'B	58.74	0.12	0.14	0.011	0.21	23.05	0.03	0.03	0.004	0.04	18.08	100.4	7	0.8	78	1.6	0.1	0.27	0.1	6	1	3.4	0.2	3.3	4	5.8	0.2	< 0.1	2	0.44	30.00	2.75	35
SIKORNIK	SB-1B	92.76	0.19	0.61	0.009	0.04	3.58	0.04	0.03	0.005	0.02	2.81	100.1	25	0.7	15	1.6	0.14	0.18	0.1	2.4	2	2.1	0.5	2.6	3	4.5	0.3	< 0.1	1	0.23	38.00	1.80	122
	SB-1C	92.8	0.19	0.73	0.01	0.04	3.62	0.06	0.03	< 0.001	0.02	3.39	100.9	9	0.6	13	5.9	0.12	0.21	0.2	2.4	4	2.2	0.5	4.7	3	2.5	0.4	< 0.1	1	0.20	n. c.	n. c.	n. c.
	SB-1D	86.15	0.15	0.38	0.01	0.06	7.61	0.04	0.03	0.005	0.03	6	100.4	29	0.6	25	3.1	0.12	0.22	0.1	3.1	2	2.1	0.5	1.8	2	4.6	0.1	< 0.1	1	0.28	30.00	2.00	76
	SB-2	84.84	0.16	0.4	0.014	0.08	7.7	0.03	0.02	0.005	0.05	6.01	99.31	34	0.6	27	2.2	0.12	0.23	0.1	3.1	2	1.8	0.5	2	3	3.8	< 0.1	< 0.1	2	0.28	32.00	2.80	80
WIELKANOC HILL	SC-1A	87.11	0.09	0.52	0.009	0.06	7.08	0.03	0.01	0.003	0.02	5.37	100.3	37	0.3	23	2.3	0.08	0.11	0.1	2.6	2	1.9	0.5	4.2	2	3.4	0.1	< 0.1	< 1	0.15	30.00	3.00	173
	SC-1B	98.19	0.1	0.85	0.01	< 0.01	0.14	0.04	0.02	0.004	< 0.01	0.46	99.84	11	0.2	3	2.3	0.06	0.19	0.1	0.9	2	3.6	0.6	5.7	3	2.1	0.4	< 0.1	1	0.10	25.00	2.50	213
	SC-1C	84.11	0.12	0.44	0.011	0.07	8.98	0.03	0.02	0.003	0.02	6.85	100.6	41	0.4	28	3.9	0.09	0.13	< 0.1	3	2	1.9	0.4	5.9	3	4.8	< 0.1	< 0.1	2	0.21	40.00	3.67	147
	SC-2	83.47	0.14	0.48	0.011	0.08	9.32	0.03	0.02	0.003	0.02	7.11	100.7	37	0.4	29	4.7	0.08	0.12	0.1	2.9	1	1.6	0.4	2.9	5	3	0.1	< 0.1	2	0.22	46.67	3.67	160
	SC-4	98.14	0.11	0.96	0.01	< 0.01	0.08	0.05	0.02	0.003	< 0.01	0.54	99.93	6	0.3	2	0.6	0.07	0.23	0.1	0.7	1	3.6	0.6	4.1	7	1.9	0.4	< 0.1	2	0.10	36.67	3.33	320

Table 6. Contents of major [wt.%] and trace elements [mg·kg^{-1}] in bedded cherts from N-KCU

Location	Sample	SiO_2	Al_2O_3	Fe_2O_3 (T)	MnO	MgO	CaO	Na_2O	K_2O	TiO_2	P_2O_5	LOI	Total	Ba	Rb	Sr	Pb	Th	U	Nb	Y	Zr	Ni	Co	Cu	Cr	Zn	Ga	Hf	V	Al/(Al+Fe+Mn)	Al_2O_3/TiO_2	MnO/TiO_2	Fe_2O_3/TiO_2
	Unit	%	%	%	%	%	%	%	%	%	%	%	%	mg·kg^{-1}	mg·kg^{-1}	mg·kg^{-1}	mg·kg^{-1}	mg·kg^{-1}	mg·kg^{-1}	mg·kg^{-1}	mg·kg^{-1}	mg·kg^{-1}	mg·kg^{-1}	mg·kg^{-1}	mg·kg^{-1}	mg·kg^{-1}	mg·kg^{-1}	mg·kg^{-1}	mg·kg^{-1}	mg·kg^{-1}				
	Detection Limit	0.01	0.01	0.01	0.001	0.01	0.01	0.01	0.01	0.001	0.01		0.01	2	0.2	2	0.5	0.05	0.01	0.1	0.1	1	0.5	0.1	0.2	1	0.2	0.1	0.1	1				
	Analytical Method	FUS-ICP	FUS-ICP	FUS-ICP	FUS-ICP	FUS-ICP	FUS-ICP	FUS-ICP	FUS-ICP	FUS-ICP	FUS-ICP	GRAV	FUS-ICP	FUS-ICP	TD-MS	FUS-ICP	TD-MS	FUS-MS	FUS-MS	TD-MS	TD-MS	FUS-ICP	TD-MS	TD-MS	TD-MS	TD-MS	TD-MS	TD-MS	FUS-MS	TD-MS				
SIEDLEC	PC-3A	96.47	0.19	0.76	0.009	0.01	1	0.05	0.03	0.005	0.01	1.47	99.99	5	0.5	6	< 0.5	0.1	0.13	0.2	0.8	2	4.5	0.7	6.9	6	5.3	0.5	< 0.1	1	0.20	38.00	1.80	152
	PC-4A	84.08	0.17	0.21	0.01	0.07	9.04	0.04	0.03	< 0.001	0.02	7.13	100.8	7	0.6	27	0.6	0.09	0.12	0.2	2.4	3	2.1	0.4	4	2	5.1	0.2	< 0.1	< 1	0.44	n. c.	n. c.	n. c.
	PC-4B	94.45	0.19	0.64	0.008	0.03	2.22	0.05	0.03	0.004	0.01	2.34	99.99	5	0.5	10	< 0.5	0.09	0.12	0.1	1.2	2	3.8	0.6	5.5	3	5.2	0.3	< 0.1	1	0.23	47.50	2.00	160
	PC-4	87.88	0.13	0.32	0.007	0.06	6.33	0.04	0.02	0.004	0.01	5.38	100.2	4	0.5	22	< 0.5	0.09	0.13	0.1	1.9	< 1	2.8	0.4	3.7	4	5.1	0.2	< 0.1	< 1	0.28	32.50	1.75	80
	PC-5	72.85	0.11	0.15	0.008	0.12	15.39	0.03	0.01	0.004	0.03	11.87	100.6	5	0.4	44	0.7	0.09	0.16	0.1	3.6	2	2.2	0.3	2.6	3	7	0.2	< 0.1	1	0.41	27.50	2.00	38

Table 7. Contents of major [wt.%] and trace elements [mg·kg^{-1}] in bedded cherts from southeastern FA

Location	Sample	SiO_2	Al_2O_3	Fe_2O_3 (T)	MnO	MgO	CaO	Na_2O	K_2O	TiO_2	P_2O_5	LOI	Total	Ba	Rb	Sr	Pb	Th	U	Nb	Y	Zr	Ni	Co	Cu	Cr	Zn	Ga	Hf	V	Al/(Al+Fe+Mn)	Al_2O_3/TiO_2	MnO/TiO_2	Fe_2O_3/TiO_2
	Unit	%	%	%	%	%	%	%	%	%	%	%	%	mg·kg^{-1}	mg·kg^{-1}	mg·kg^{-1}	mg·kg^{-1}	mg·kg^{-1}	mg·kg^{-1}	mg·kg^{-1}	mg·kg^{-1}	mg·kg^{-1}	mg·kg^{-1}	mg·kg^{-1}	mg·kg^{-1}	mg·kg^{-1}	mg·kg^{-1}	mg·kg^{-1}	mg·kg^{-1}	mg·kg^{-1}				
	Detection Limit	0.01	0.01	0.01	0.001	0.01	0.01	0.01	0.01	0.001	0.01		0.01	2	0.2	2	0.5	0.05	0.01	0.1	0.1	1	0.5	0.1	0.2	1	0.2	0.1	0.1	1				
	Analytical Method	FUS-ICP	FUS-ICP	FUS-ICP	FUS-ICP	FUS-ICP	FUS-ICP	FUS-ICP	FUS-ICP	FUS-ICP	FUS-ICP	GRAV	FUS-ICP	FUS-ICP	TD-MS	FUS-ICP	TD-MS	FUS-MS	FUS-MS	TD-MS	TD-MS	FUS-ICP	TD-MS	TD-MS	TD-MS	TD-MS	TD-MS	TD-MS	FUS-MS	TD-MS				
KELHEIM	KD1	96.18	0.1	1.51	0.012	0.02	0.14	0.04	0.02	0.002	0.02	0.52	98.55	34	0.4	5	0.5	< 0.05	0.68	0.2	0.1	3	8.8	1.4	25.4	8	6	0.98	< 0.1	6	0.06	50.00	6.00	755
	K3/3	94.77	0.2	0.95	0.009	0.07	1.84	0.08	0.03	0.001	< 0.01	2.79	100.7	43	0.7	17	< 0.5	< 0.05	0.34	0.1	0.2	3	2.8	0.5	7.5	6	3	0.84	< 0.1	2	0.17	200.00	9.00	950
HEMAU	H1	98.17	0.14	1.24	0.009	0.01	0.43	0.04	0.02	0.001	< 0.01	0.69	100.8	45	0.5	4	0.6	< 0.05	0.12	< 0.1	0.6	4	6.5	1.4	10.9	46	10	0.88	< 0.1	11	0.10	140.00	9.00	1240
	H5	97.29	0.24	0.88	0.008	0.02	0.13	0.05	0.02	0.008	< 0.01	0.85	99.49	429	0.7	14	9.2	0.18	0.1	0.3	0.5	5	3.5	1.7	28.9	8	4	6.46	0.2	3	0.21	30.00	1.00	110

Table 8. Contents of major [wt.%] and trace elements [mg·kg^{-1}] in chert concretions hosted within gravity flow from S-KCU

Location	Sample	SiO_2	Al_2O_3	Fe_2O_3 (T)	MnO	MgO	CaO	Na_2O	K_2O	TiO_2	P_2O_5	LOI	Total	Ba	Rb	Sr	Pb	Th	U	Nb	Y	Zr	Ni	Co	Cu	Cr	Zn	Ga	Hf	V	Al/(Al+Fe+Mn)	Al_2O_3/TiO_2	MnO/TiO_2	Fe_2O_3/TiO_2
	Unit	%	%	%	%	%	%	%	%	%	%	%	%	mg·kg^{-1}	mg·kg^{-1}	mg·kg^{-1}	mg·kg^{-1}	mg·kg^{-1}	mg·kg^{-1}	mg·kg^{-1}	mg·kg^{-1}	mg·kg^{-1}	mg·kg^{-1}	mg·kg^{-1}	mg·kg^{-1}	mg·kg^{-1}	mg·kg^{-1}	mg·kg^{-1}	mg·kg^{-1}	mg·kg^{-1}				
	Detection Limit	0.01	0.01	0.01	0.001	0.01	0.01	0.01	0.01	0.001	0.01		0.01	2	0.2	2	0.5	0.05	0.01	0.1	0.1	1	0.5	0.1	0.2	1	0.2	0.1	0.1	1				
	Analytical Method	FUS-ICP	FUS-ICP	FUS-ICP	FUS-ICP	FUS-ICP	FUS-ICP	FUS-ICP	FUS-ICP	FUS-ICP	FUS-ICP	GRAV	FUS-ICP	FUS-ICP	TD-MS	FUS-ICP	TD-MS	FUS-MS	FUS-MS	TD-MS	TD-MS	FUS-ICP	TD-MS	TD-MS	TD-MS	TD-MS	TD-MS	TD-MS	FUS-MS	TD-MS				
UJAZD	SA-3	99.02	0.12	1.03	0.01	0.01	0.1	0.05	0.03	0.003	< 0.01	0.38	100.8	8	0.4	3	< 0.5	0.08	0.17	0.2	0.6	< 1	3.1	0.7	3.6	4	1.7	0.5	< 0.1	< 5	0.10	40.00	3.33	343
	SA-4	98.96	0.1	0.85	0.009	0.01	0.11	0.04	0.02	0.004	< 0.01	0.53	100.6	6	0.3	3	0.6	0.07	0.17	0.1	0.8	< 1	2.8	0.6	3.2	4	1.2	0.4	< 0.1	< 5	0.10	25.00	2.25	213
	SA-5	98.82	0.12	0.91	0.01	0.01	0.11	0.04	0.03	0.004	< 0.01	0.54	100.6	8	0.4	3	< 0.5	0.06	0.17	0.3	0.7	2	3.1	0.6	3	5	1.5	0.4	< 0.1	< 5	0.12	30.00	2.50	228
	SA-6	98.59	0.17	0.97	0.01	0.02	0.38	0.06	0.03	0.005	< 0.01	0.58	100.8	6	0.5	4	0.7	0.1	0.14	0.2	0.9	2	3	0.6	5.1	5	3.4	0.6	< 0.1	< 5	0.15	34.00	2.00	194
	SA-7	98.26	0.16	1	0.01	< 0.01	0.05	0.06	0.04	0.004	< 0.01	0.74	100.3	5	0.5	3	0.6	0.1	0.18	0.2	0.8	1	3.4	0.6	7.1	3	3.4	0.6	< 0.1	< 5	0.14	40.00	2.50	250
	SA-8	97.94	0.16	0.96	0.01	0.01	0.05	0.06	0.04	0.005	< 0.01	0.75	99.98	4	0.5	3	< 0.5	0.09	0.21	0.2	0.7	2	3.3	0.5	4	58	2.3	0.7	< 0.1	< 5	0.14	32.00	2.00	192

Table 9. Contents of major [wt.%] and trace elements [mg·kg^{-1}] in chert concretions hosted within gravity flow from N-KCU

Location	Sample	SiO_2	Al_2O_3	Fe_2O_3 (T)	MnO	MgO	CaO	Na_2O	K_2O	TiO_2	P_2O_5	LOI	Total	Ba	Rb	Sr	Pb	Th	U	Nb	Y	Zr	Ni	Co	Cu	Cr	Zn	Ga	Hf	V	Al/(Al+Fe+Mn)	Al_2O_3/TiO_2	MnO/TiO_2	Fe_2O_3/TiO_2
	Unit	%	%	%	%	%	%	%	%	%	%	%	%	mg·kg^{-1}	mg·kg^{-1}	mg·kg^{-1}	mg·kg^{-1}	mg·kg^{-1}	mg·kg^{-1}	mg·kg^{-1}	mg·kg^{-1}	mg·kg^{-1}	mg·kg^{-1}	mg·kg^{-1}	mg·kg^{-1}	mg·kg^{-1}	mg·kg^{-1}	mg·kg^{-1}	mg·kg^{-1}	mg·kg^{-1}				
	Detection Limit	0.01	0.01	0.01	0.001	0.01	0.01	0.01	0.01	0.001	0.01		0.01	2	0.2	2	0.5	0.05	0.01	0.1	0.1	1	0.5	0.1	0.2	1	0.2	0.1	0.1	1				
	Analytical Method	FUS-ICP	FUS-ICP	FUS-ICP	FUS-ICP	FUS-ICP	FUS-ICP	FUS-ICP	FUS-ICP	FUS-ICP	FUS-ICP	GRAV	FUS-ICP	FUS-ICP	TD-MS	FUS-ICP	TD-MS	FUS-MS	FUS-MS	FUS-MS	TD-MS	TD-MS	FUS-ICP	TD-MS	TD-MS	TD-MS	TD-MS	TD-MS	TD-MS	FUS-MS	TD-MS				
SIEDLEC	PC-1C	97.03	0.18	0.72	0.008	0.01	0.18	0.04	0.02	0.003	< 0.01	1.34	99.53	6	0.8	3	< 0.5	0.08	0.23	0.1	0.2	2	2.9	0.5	4.2	8	5.5	0.4	< 0.1	< 5	0.20	60.00	2.67	240
	PC-2A	97.96	0.17	0.39	0.006	< 0.01	0.1	0.04	0.02	0.005	0.01	2.16	100.9	4	0.3	2	< 0.5	0.09	0.19	0.2	0.2	2	2.2	0.3	7.3	4	5.7	0.2	< 0.1	< 5	0.30	34.00	1.20	78
	PC-2C	97.81	0.19	0.42	0.006	0.01	0.23	0.04	0.02	0.003	< 0.01	1.37	100.1	7	0.4	3	< 0.5	0.07	0.53	0.2	0.2	9	2.3	0.5	4.2	7	2.6	0.3	0.2	< 5	0.31	63.33	2.00	140
	PC-6	98.36	0.16	0.68	0.008	0.01	0.15	0.04	0.02	0.004	< 0.01	0.66	100.1	6	0.3	3	< 0.5	0.08	0.09	0.1	0.4	2	2.6	0.4	3.6	3	3.7	0.3	< 0.1	< 5	0.19	40.00	2.00	170

Table 10. Contents of major [wt.%] and trace elements [mg·kg^{-1}] in chert concretions hosted within gravity flow from southeastern FA

Location	Sample	SiO_2	Al_2O_3	Fe_2O_3 (T)	MnO	MgO	CaO	Na_2O	K_2O	TiO_2	P_2O_5	LOI	Total	Ba	Rb	Sr	Pb	Th	U	Nb	Y	Zr	Ni	Co	Cu	Cr	Zn	Ga	Hf	V	Al/(Al+Fe+Mn)	Al_2O_3/TiO_2	MnO/TiO_2	Fe_2O_3/TiO_2
	Unit	%	%	%	%	%	%	%	%	%	%	%	%	mg·kg^{-1}	mg·kg^{-1}	mg·kg^{-1}	mg·kg^{-1}	mg·kg^{-1}	mg·kg^{-1}	mg·kg^{-1}	mg·kg^{-1}	mg·kg^{-1}	mg·kg^{-1}	mg·kg^{-1}	mg·kg^{-1}	mg·kg^{-1}	mg·kg^{-1}	mg·kg^{-1}	mg·kg^{-1}	mg·kg^{-1}				
	Detection Limit	0.01	0.01	0.01	0.001	0.01	0.01	0.01	0.01	0.001	0.01		0.01	2	0.2	2	0.5	0.05	0.01	0.1	0.1	1	0.5	0.1	0.2	1	0.2	0.1	0.1	1				
	Analytical Method	FUS-ICP	FUS-ICP	FUS-ICP	FUS-ICP	FUS-ICP	FUS-ICP	FUS-ICP	FUS-ICP	FUS-ICP	FUS-ICP	GRAV	FUS-ICP	FUS-ICP	TD-MS	FUS-ICP	TD-MS	FUS-MS	FUS-MS	TD-MS	TD-MS	FUS-ICP	TD-MS	TD-MS	TD-MS	TD-MS	TD-MS	TD-MS	FUS-MS	TD-MS				
KELHEIM	K1/1	90.69	0.07	1.11	0.01	0.06	4.26	0.04	0.01	0.001	0.01	2.93	99.19	69	0.3	13	0.5	< 0.05	0.2	0.2	0.3	3	5.9	1	10.7	7	7	1.02	< 0.1	< 5	0.06	70.00	10.00	1110
	K1/2	83.7	0.09	0.81	0.008	0.08	8.56	0.04	0.01	< 0.001	< 0.01	6.44	99.73	59	0.3	27	< 0.5	< 0.05	0.23	0.1	0.4	2	4.5	0.6	10.1	6	4	0.99	< 0.1	< 5	0.10	n. c..	n. c.	n. c.
	K1/3	97.17	0.2	1.48	0.012	0.02	0.49	0.06	0.03	0.004	< 0.01	0.89	100.3	30	0.7	8	0.6	< 0.05	0.3	0.2	0.2	3	6.9	0.8	15.3	6	9	0.86	< 0.1	7	0.12	50.00	3.00	370
	K2/1	97.25	0.38	1.05	0.009	0.02	0.16	0.06	0.06	0.009	< 0.01	1.43	100.4	33	1.3	8	< 0.5	0.08	0.19	0.3	0.2	4	4	0.6	11.2	6	4	0.88	< 0.1	< 5	0.26	42.22	1.00	117
	K2/2	97.38	0.24	0.85	0.008	0.03	0.14	0.04	0.03	0.003	< 0.01	1.13	99.84	25	0.8	5	< 0.5	< 0.05	0.75	0.2	0.4	3	3.5	0.5	7.8	5	3	0.66	< 0.1	< 5	0.22	80.00	2.67	283
	K2/2j	95.42	0.35	1.4	0.01	0.02	0.1	0.06	0.05	0.009	< 0.01	1.32	98.75	18	1.2	5	0.7	0.05	0.24	0.3	0.2	4	8.4	0.8	14.5	16	12	1.16	< 0.1	11	0.20	38.89	1.11	156
	K2/1L	98.56	0.11	1.21	0.01	0.01	0.28	0.04	0.02	0.001	0.01	0.66	100.9	35	0.4	5	< 0.5	< 0.05	0.58	0.2	< 0.1	3	4.6	0.7	10.5	10	7	0.87	< 0.1	< 5	0.08	110.00	10.00	1210
	K2/3	97.84	0.32	1.02	0.009	0.02	0.11	0.06	0.05	0.007	< 0.01	1.31	100.7	24	1.1	5	< 0.5	0.07	0.26	0.3	0.1	4	3.8	0.7	14.1	39	4	0.73	< 0.1	< 5	0.24	45.71	1.29	146
	K3/1	98.81	0.09	1.02	0.008	0.02	0.35	0.04	0.01	0.002	< 0.01	0.31	100.7	37	0.3	7	< 0.5	< 0.05	0.15	0.1	0.2	3	6.7	0.9	8.7	6	7	0.86	< 0.1	12	0.08	45.00	4.00	510
HEMAU	H2	98.62	0.07	1.05	0.009	0.01	0.08	0.03	0.01	0.001	< 0.01	0.49	100.4	19	0.3	< 2	< 0.5	< 0.05	0.47	0.2	0.5	3	3.8	0.6	6.5	8	3	0.69	< 0.1	< 5	0.06	70.00	9.00	1050
	H3	97.16	0.25	0.97	0.009	0.02	0.28	0.06	0.02	0.009	0.01	0.79	99.57	334	0.7	12	8.2	0.18	0.1	0.4	0.6	5	3.6	1.3	10.2	16	2	4.35	0.2	< 5	0.20	27.78	1.00	108
	H4	98.41	0.08	1.49	0.011	0.02	0.19	0.03	< 0.01	0.001	< 0.01	0.41	100.6	34	0.3	3	< 0.5	< 0.05	0.2	0.2	0.4	3	7.1	1	8.2	8	8	0.76	< 0.1	8	0.05	80.00	11.00	1490
	H6	98.93	0.14	0.76	0.007	< 0.01	0.22	0.03	0.02	0.135	< 0.01	0.32	100.6	95	0.5	9	2.2	0.48	0.29	3.2	0.8	18	3.4	0.6	7.3	9	4	1.95	0.4	6	0.15	1.04	0.05	6

Table 11. Contents of REE [mg·kg^{-1}] in chert concretions from S-KCU

Location	Sample	La	Ce	Pr	Nd	Sm	Eu	Gd	Tb	Dy	Ho	Er	Tm	Yb	Lu	Total	$LREE_{measured}/HREE_{measured}$	$LREE_{SN}/HREE_{SN}$	La_{SN}/Yb_{SN}	La_{SN}/Sm_{SN}	Sm_{SN}/Yb_{SN}	Eu/Eu*	Ce/Ce*	Pr/Pr*	Gd/Gd*
	Unit	mg·kg^{-1}	mg·kg^{-1}	mg·kg^{-1}	mg·kg^{-1}	mg·kg^{-1}	mg·kg^{-1}	mg·kg^{-1}	mg·kg^{-1}	mg·kg^{-1}	mg·kg^{-1}	mg·kg^{-1}	mg·kg^{-1}	mg·kg^{-1}	mg·kg^{-1}										
	Detection Limit	0.05	0.05	0.01	0.05	0.01	0.005	0.01	0.01	0.01	0.01	0.01	0.005	0.01	0.002										
	Analytical Method	FUS-MS	FUS-MS	FUS-MS	FUS-MS	FUS-MS	FUS-MS	FUS-MS	FUS-MS	FUS-MS	FUS-MS	FUS-MS	FUS-MS	FUS-MS	FUS-MS										
PIEKARY	KA-1	1.14	1.95	0.25	1.05	0.19	0.02	0.16	0.02	0.11	0.02	0.05	0.008	0.05	0.009	5.027	10.77	0.93	1.69	0.88	1.93	0.54	0.84	1.02	1.55
	KA-2	1.64	3.44	0.44	1.78	0.35	0.046	0.27	0.04	0.26	0.05	0.14	0.019	0.13	0.024	8.629	8.25	0.71	0.94	0.68	1.37	0.70	0.93	1.04	1.23
	KA-3	1.05	1.22	0.22	0.84	0.2	0.033	0.2	0.03	0.13	0.03	0.08	0.01	0.06	0.009	4.112	6.49	0.68	1.30	0.77	1.69	0.77	0.58	1.24	1.24
	KA-3’	0.93	1.05	0.18	0.76	0.13	0.03	0.18	0.02	0.14	0.03	0.07	0.008	0.05	0.008	3.586	6.09	0.64	1.38	1.04	1.32	0.90	0.59	1.14	1.44
	KA-3”	1.24	1.58	0.25	1	0.2	0.034	0.21	0.03	0.19	0.04	0.11	0.015	0.09	0.015	5.004	6.15	0.58	1.02	0.91	1.13	0.78	0.65	1.15	1.28

Location	KA-4	1.34	1.3	0.25	1.04	0.22	0.046	0.24	0.04	0.21	0.04	0.12	0.016	0.1	0.017	4.979	5.36	0.56	0.99	0.89	1.12	0.93	0.51	1.20	1.09
	KA-5	0.95	0.8	0.17	0.73	0.14	0.031	0.17	0.02	0.13	0.03	0.07	0.009	0.05	0.009	3.309	5.78	0.63	1.41	0.99	1.42	0.93	0.45	1.22	1.34
	KA-6	0.61	0.79	0.13	0.44	0.08	0.02	0.1	0.02	0.1	0.02	0.06	0.007	0.05	0.007	2.434	5.69	0.54	0.91	1.11	0.81	1.03	0.64	1.29	0.97
	KA-6’	0.79	0.87	0.16	0.67	0.12	0.029	0.15	0.02	0.12	0.02	0.06	0.008	0.05	0.008	3.075	6.05	0.65	1.17	0.96	1.22	1.00	0.56	1.18	1.22
DĄBROWA SZLACHECKA	KB-1	0.36	0.44	0.07	0.29	0.04	0.008	0.08	0.01	0.07	0.01	0.05	0.007	0.05	0.007	1.492	4.25	0.37	0.53	1.31	0.41	0.61	0.64	1.13	1.69
	KB-3	1.87	1.01	0.28	1.15	0.2	0.048	0.26	0.04	0.23	0.05	0.14	0.019	0.11	0.014	5.421	5.28	0.56	1.26	1.37	0.92	0.97	0.31	1.36	1.16
	KB-5	0.67	0.66	0.13	0.51	0.09	0.022	0.12	0.02	0.09	0.02	0.06	0.008	0.05	0.008	2.458	5.54	0.55	0.99	1.09	0.91	0.97	0.51	1.26	1.11
	KB-7B	1.46	0.97	0.26	1.04	0.21	0.046	0.26	0.03	0.23	0.04	0.13	0.016	0.09	0.012	4.794	4.93	0.58	1.20	1.02	1.19	0.91	0.36	1.37	1.37
	KB-8	0.73	0.54	0.14	0.56	0.1	0.022	0.14	0.02	0.12	0.03	0.08	0.011	0.08	0.012	2.585	4.24	0.43	0.68	1.07	0.64	0.85	0.39	1.36	1.30
	KB-9	2.82	1.26	0.35	1.42	0.23	0.06	0.39	0.05	0.35	0.08	0.23	0.027	0.16	0.026	7.453	4.68	0.47	1.31	1.79	0.73	0.89	0.28	1.37	1.39
	KB-10	0.52	0.5	0.11	0.43	0.08	0.017	0.12	0.01	0.08	0.02	0.05	0.006	0.04	0.005	1.988	5.01	0.56	0.96	0.95	1.02	0.78	0.48	1.31	1.80
	KB-11	0.92	0.59	0.17	0.79	0.15	0.039	0.18	0.03	0.15	0.03	0.1	0.012	0.07	0.01	3.241	4.57	0.54	0.98	0.90	1.09	1.10	0.34	1.25	1.03
GUMINEK HILL	KC-1	0.49	0.48	0.11	0.37	0.08	0.015	0.09	0.01	0.08	0.01	0.03	0.005	0.03	0.004	1.804	5.97	0.69	1.21	0.89	1.35	0.82	0.48	1.47	1.44
	KC-2	0.4	0.33	0.09	0.32	0.07	0.015	0.08	0.01	0.09	0.02	0.05	0.006	0.04	0.005	1.526	4.07	0.48	0.74	0.83	0.89	0.93	0.40	1.50	1.28
	KC-3	0.29	0.31	0.07	0.25	0.04	0.008	0.07	0.01	0.05	0.01	0.03	< 0.005	0.02	0.003	1.161	5.02	0.57	1.08	1.06	1.02	0.67	0.50	1.41	1.48
	KC-5	0.34	0.43	0.07	0.27	0.04	0.012	0.06	0.01	0.05	0.01	0.04	0.006	0.04	0.004	1.382	5.28	0.49	0.63	1.24	0.51	1.11	0.64	1.19	1.07
LIBAN QUARRY	KD-1	0.57	0.45	0.11	0.39	0.08	0.012	0.1	0.02	0.09	0.02	0.05	0.008	0.04	0.005	1.945	4.84	0.47	1.06	1.04	1.02	0.62	0.41	1.45	1.16
	KD-2	0.91	0.59	0.16	0.69	0.11	0.028	0.16	0.03	0.15	0.03	0.08	0.011	0.07	0.009	3.028	4.61	0.49	0.96	1.21	0.80	0.96	0.35	1.31	1.06
BONARKA QUARRY	B-1	0.51	0.41	0.11	0.44	0.05	0.023	0.09	0.01	0.08	0.02	0.04	0.005	0.04	0.005	1.833	5.32	0.61	0.95	1.49	0.64	1.50	0.40	1.37	1.13
	B-2	0.65	0.61	0.13	0.55	0.09	0.024	0.09	0.01	0.07	0.02	0.05	0.009	0.05	< 0.002	2.353	6.87	0.75	0.96	1.05	0.91	1.25	0.48	1.23	1.10
	B-4	0.32	0.45	0.07	0.26	0.05	0.013	0.06	0.01	0.03	< 0.01	0.01	< 0.005	0.01	< 0.002	1.283	9.69	1.29	2.37	0.93	2.54	1.10	0.69	1.19	1.03
	B-5	0.68	0.48	0.12	0.57	0.12	0.03	0.13	0.02	0.1	0.02	0.05	0.008	0.06	0.002	2.390	5.13	0.65	0.84	0.83	1.02	1.12	0.38	1.19	1.04
	B-6	0.46	0.39	0.09	0.36	0.06	0.021	0.06	0.01	0.06	0.01	0.03	< 0.005	0.02	< 0.002	1.571	7.27	1.03	1.71	1.12	1.52	1.64	0.44	1.31	0.80
	B-7	0.65	0.46	0.13	0.6	0.11	0.032	0.13	0.02	0.09	0.02	0.04	0.007	0.04	0.006	2.335	5.61	0.69	1.21	0.86	1.40	1.24	0.36	1.25	1.01
	B-8	0.56	0.52	0.12	0.49	0.05	0.015	0.09	0.01	0.06	0.02	0.02	0.005	0.05	0.005	2.015	6.75	0.63	0.83	1.64	0.51	0.98	0.46	1.30	1.44
	B-9	0.46	0.35	0.09	0.37	0.08	0.018	0.09	0.01	0.06	0.01	0.03	< 0.005	0.02	0.002	1.590	6.16	0.89	1.71	0.84	2.03	0.99	0.39	1.33	1.31
	B-10	0.49	0.44	0.1	0.41	0.06	0.014	0.09	0.01	0.07	0.01	0.04	0.006	0.03	0.005	1.775	5.80	0.61	1.21	1.19	1.02	0.86	0.46	1.29	1.49
	B-11	0.66	0.4	0.11	0.51	0.12	0.024	0.09	0.02	0.11	0.02	0.05	0.006	0.03	0.002	2.152	5.56	0.69	1.63	0.80	2.03	1.09	0.34	1.24	0.80
	B-12	0.49	0.39	0.09	0.4	0.06	0.026	0.1	0.01	0.06	0.01	0.03	< 0.005	0.02	0.002	1.688	6.28	0.94	1.82	1.19	1.52	1.49	0.42	1.22	1.16
	B-13	0.31	0.29	0.05	0.27	0.05	0.018	0.05	0.01	0.05	0.01	0.02	< 0.005	0.02	0.003	1.151	6.06	0.78	1.15	0.91	1.27	1.69	0.53	0.98	0.73
	B-14	0.49	0.41	0.1	0.42	0.09	0.017	0.08	0.01	0.07	0.01	0.04	0.006	0.03	< 0.002	1.773	6.21	0.78	1.21	0.80	1.52	0.94	0.43	1.29	1.20
	B-15	0.31	0.32	0.05	0.26	0.04	0.017	0.07	0.01	0.03	0.01	0.02	< 0.005	0.02	< 0.002	1.157	6.23	0.83	1.15	1.13	1.02	1.42	0.58	0.97	1.05

Table 12. Contents of REE [mg·kg^{-1}] in chert concretions from N-KCU

Location	Sample	La	Ce	Pr	Nd	Sm	Eu	Gd	Tb	Dy	Ho	Er	Tm	Yb	Lu	Total	$LREE_{measured}$ / $HREE_{measure}$	$LREE_{SN}$/ $HREE_{SN}$	La_{SN}/Yb_{SN}	La_{SN}/Sm_{SN}	Sm_{SN}/Yb_{SN}	Eu/Eu*	Ce/Ce*	Pr/Pr*	Gd/Gd*
	Unit	mg·kg^{-1}	mg·kg^{-1}	mg·kg^{-1}	mg·kg^{-1}	mg·kg^{-1}	mg·kg^{-1}	mg·kg^{-1}	mg·kg^{-1}	mg·kg^{-1}	mg·kg^{-1}	mg·kg^{-1}	mg·kg^{-1}	mg·kg^{-1}	mg·kg^{-1}										
	Detection Limit	0.05	0.05	0.01	0.05	0.01	0.005	0.01	0.01	0.01	0.01	0.01	0.005	0.01	0.002										
	Analytical Method	FUS-MS	FUS-MS	FUS-MS	FUS-MS	FUS-MS	FUS-MS	FUS-MS	FUS-MS	FUS-MS	FUS-MS	FUS-MS	FUS-MS	FUS-MS	FUS-MS										
OLSZTYN	PA-2’	0.73	0.43	0.14	0.56	0.11	0.029	0.14	0.02	0.14	0.03	0.07	0.009	0.05	0.007	2.465	4.29	0.53	1.08	0.97	1.12	1.08	0.31	1.45	1.14
	PA-3	0.2	0.21	0.03	0.14	0.01	0.007	0.03	0.01	0.03	0.01	0.02	< 0.005	0.02	0.003	0.720	4.85	0.42	0.74	2.92	0.25	1.57	0.61	1.00	0.66
	PA-3’	0.45	0.93	0.09	0.35	0.07	0.018	0.1	0.02	0.11	0.02	0.07	0.011	0.07	0.01	2.319	4.64	0.38	0.48	0.94	0.51	0.98	1.06	0.93	1.01
	PA-4	0.41	0.33	0.07	0.26	0.03	0.013	0.08	0.01	0.05	0.01	0.03	< 0.005	0.03	0.005	1.328	5.18	0.57	1.01	2.00	0.51	1.07	0.44	1.34	1.38
JULIANKA	PB-1	0.32	0.26	0.06	0.22	0.05	0.009	0.06	0.01	0.04	0.01	0.03	< 0.005	0.03	0.004	1.103	4.99	0.57	0.79	0.93	0.85	0.76	0.43	1.39	1.21
	PB-2	0.75	0.44	0.13	0.61	0.11	0.025	0.16	0.02	0.13	0.03	0.07	0.007	0.04	0.006	2.528	4.46	0.54	1.39	1.00	1.40	0.85	0.32	1.25	1.40
	PB-3	0.39	0.23	0.07	0.28	0.06	0.011	0.07	0.01	0.06	0.01	0.04	0.005	0.03	0.003	1.269	4.57	0.53	0.96	0.95	1.02	0.79	0.32	1.42	1.30
	PB-4	0.6	0.47	0.1	0.44	0.09	0.021	0.12	0.02	0.08	0.02	0.05	0.006	0.04	0.006	2.063	5.03	0.55	1.11	0.97	1.14	0.93	0.44	1.20	1.14
	PB-5	0.23	0.21	0.05	0.21	0.02	0.006	0.06	0.01	0.05	0.01	0.02	< 0.005	0.03	< 0.002	0.906	4.03	0.46	0.57	1.68	0.34	0.67	0.45	1.28	1.39
	PB-6	0.88	0.31	0.11	0.44	0.08	0.018	0.12	0.02	0.11	0.02	0.08	0.011	0.07	< 0.002	2.269	4.26	0.48	0.93	1.61	0.58	0.83	0.22	1.48	1.21
	PB-7B	0.34	0.14	0.07	0.21	0.06	0.008	0.07	0.01	0.06	0.01	0.04	< 0.005	0.02	0.003	1.041	3.89	0.55	1.26	0.83	1.52	0.57	0.21	1.99	1.48
	PB-8	0.26	0.13	0.04	0.17	0.04	0.009	0.03	< 0.01	0.03	0.01	0.02	< 0.005	0.02	0.003	0.762	5.74	0.76	0.96	0.95	1.02	1.22	0.29	1.36	1.55
	PB-9	0.22	0.12	0.04	0.21	0.04	0.005	0.03	0.01	0.04	0.01	0.02	< 0.005	0.02	0.002	0.767	4.81	0.53	0.82	0.80	1.02	0.68	0.29	1.18	0.73
	PB-10	0.29	0.14	0.04	0.17	0.04	0.006	0.04	0.01	0.04	0.01	0.02	< 0.005	0.02	0.004	0.830	4.76	0.50	1.08	1.06	1.02	0.70	0.29	1.34	0.93
	PB-11B	2.14	0.49	0.26	1.07	0.19	0.052	0.26	0.03	0.24	0.06	0.16	0.02	0.12	0.019	5.111	4.62	0.52	1.32	1.65	0.80	1.07	0.14	1.56	1.28
	PB-12	0.92	0.26	0.11	0.5	0.09	0.016	0.11	0.02	0.1	0.02	0.06	0.009	0.06	0.009	2.284	4.89	0.49	1.14	1.49	0.76	0.74	0.18	1.38	1.16
	PB-13	0.29	0.14	0.04	0.21	0.04	0.006	0.04	0.01	0.04	0.01	0.03	< 0.005	0.02	0.003	0.879	4.75	0.51	1.08	1.06	1.02	0.70	0.29	1.14	0.93
	PB-14	0.35	0.18	0.04	0.18	0.06	0.006	0.05	0.01	0.04	0.01	0.03	< 0.005	0.02	0.003	0.979	5.01	0.56	1.30	0.85	1.52	0.52	0.33	1.20	1.16
	PB-15	0.2	0.16	0.02	0.12	0.02	0.008	0.02	< 0.01	0.02	< 0.01	0.01	< 0.005	0.02	0.003	0.601	7.23	0.92	0.74	1.46	0.51	1.88	0.53	0.82	1.16
	PB-16	0.16	0.11	0.02	0.13	0.01	< 0.005	0.02	< 0.01	0.02	0.01	0.02	< 0.005	0.02	0.003	0.523	4.62	0.34	0.59	2.34	0.25	n. c.	0.43	0.87	n. c.
	PB-17A	1.9	0.48	0.22	0.9	0.18	0.04	0.24	0.04	0.22	0.05	0.14	0.017	0.11	0.017	4.554	4.46	0.48	1.28	1.54	0.83	0.88	0.16	1.53	1.16
	PB-17B	0.64	0.23	0.08	0.36	0.09	0.02	0.08	0.01	0.07	0.02	0.05	0.007	0.04	0.005	1.702	5.04	0.59	1.19	1.04	1.14	1.11	0.22	1.34	1.09

RUDNIKI	R1	0.2	0.35	0.04	0.13	0.04	0.008	0.03	< 0.01	0.02	< 0.01	0.01	< 0.005	0.02	< 0.002	0.848	9.60	1.53	0.74	0.73	1.02	1.09	0.90	1.10	1.74
	R2A	0.38	0.74	0.09	0.31	0.06	0.008	0.04	< 0.01	0.02	< 0.01	0.01	< 0.005	0.01	0.002	1.670	19.37	2.32	2.82	0.93	3.05	0.76	0.92	1.11	2.32
	R2B	0.58	0.79	0.13	0.53	0.1	0.018	0.07	0.01	0.06	0.01	0.04	0.005	0.02	0.003	2.366	9.85	0.99	2.15	0.85	2.54	1.01	0.66	1.15	1.02
	R3/1	0.23	0.3	0.04	0.11	0.02	< 0.005	< 0.01	< 0.01	0.02	< 0.01	0.01	< 0.005	0.01	< 0.002	0.740	17.50	1.87	1.71	1.68	1.02	n. c.	0.71	1.29	n. c.
	R3/2	0.61	0.34	0.09	0.37	0.05	0.021	0.08	0.01	0.09	0.02	0.04	< 0.005	0.01	< 0.002	1.731	5.92	1.29	4.53	1.78	2.54	1.49	0.33	1.34	1.77
	R3/3	2.07	0.6	0.23	0.94	0.19	0.047	0.25	0.04	0.29	0.06	0.17	0.023	0.13	0.017	5.057	4.16	0.45	1.18	1.59	0.74	0.99	0.19	1.48	1.13
	R3/4	0.47	0.38	0.09	0.35	0.08	0.016	0.06	0.01	0.05	0.01	0.03	< 0.005	0.02	< 0.002	1.566	7.70	1.04	1.74	0.86	2.03	1.09	0.42	1.35	0.93
	R4	0.62	0.52	0.11	0.47	0.11	0.022	0.11	0.01	0.08	0.01	0.04	0.006	0.03	< 0.002	2.138	6.48	0.87	1.53	0.82	1.86	0.94	0.45	1.22	1.42

Table 13. Contents of REE [mg·kg^{-1}] in chert concretions from southeastern FA

Location	Sample	La	Ce	Pr	Nd	Sm	Eu	Gd	Tb	Dy	Ho	Er	Tm	Yb	Lu	Total	$LREE_{measured}/HREE_{measured}$	$LREE_{SN}/HREE_{SN}$	La_{SN}/Yb_{SN}	La_{SN}/Sm_{SN}	Sm_{SN}/Yb_{SN}	Eu/Eu*	Ce/Ce*	Pr/Pr*	Gd/Gd*
	Unit	mg·kg^{-1}	mg·kg^{-1}	mg·kg^{-1}	mg·kg^{-1}	mg·kg^{-1}	mg·kg^{-1}	mg·kg^{-1}	mg·kg^{-1}	mg·kg^{-1}	mg·kg^{-1}	mg·kg^{-1}	mg·kg^{-1}	mg·kg^{-1}	mg·kg^{-1}										
	Detection Limit	0.05	0.05	0.01	0.05	0.01	0.005	0.01	0.01	0.01	0.01	0.01	0.005	0.01	0.002										
	Analytical Method	FUS-MS	FUS-MS	FUS-MS	FUS-MS	FUS-MS	FUS-MS	FUS-MS	FUS-MS	FUS-MS	FUS-MS	FUS-MS	FUS-MS	FUS-MS	FUS-MS										
EMMERTHAL	E2	0.45	0.73	0.04	0.21	0.09	< 0.005	0.05	0.01	0.05	0.01	0.02	< 0.005	0.02	0.007	1.687	9.10	0.64	1.67	0.73	2.29	n. c.	1.12	0.59	1.66
	E2A	0.29	0.52	0.07	0.28	< 0.01	< 0.005	0.04	0.01	0.03	0.01	0.02	< 0.005	0.02	< 0.002	1.290	8.92	0.58	1.08	n. c.	0.00	n. c.	0.84	1.07	1.33
	E3	0.09	0.05	0.02	0.06	0.02	< 0.005	0.03	< 0.01	0.02	0.01	0.02	0.005	0.01	< 0.002	0.335	2.53	0.24	0.67	0.66	1.02	n. c.	0.27	1.89	n. c.

Table 14. Contents of REE [mg·kg^{-1}] in chert concretions from BW

Location	Sample	La	Ce	Pr	Nd	Sm	Eu	Gd	Tb	Dy	Ho	Er	Tm	Yb	Lu	Total	$LREE_{measured}/HREE_{measured}$	$LREE_{SN}/HREE_{SN}$	La_{SN}/Yb_{SN}	La_{SN}/Sm_{SN}	Sm_{SN}/Yb_{SN}	Eu/Eu*	Ce/Ce*	Pr/Pr*	Gd/Gd*
	Unit	mg·kg^{-1}	mg·kg^{-1}	mg·kg^{-1}	mg·kg^{-1}	mg·kg^{-1}	mg·kg^{-1}	mg·kg^{-1}	mg·kg^{-1}	mg·kg^{-1}	mg·kg^{-1}	mg·kg^{-1}	mg·kg^{-1}	mg·kg^{-1}	mg·kg^{-1}										
	Detection Limit	0.05	0.05	0.01	0.05	0.01	0.005	0.01	0.01	0.01	0.01	0.01	0.005	0.01	0.002										
	Analytical Method	FUS-MS	FUS-MS	FUS-MS	FUS-MS	FUS-MS	FUS-MS	FUS-MS	FUS-MS	FUS-MS	FUS-MS	FUS-MS	FUS-MS	FUS-MS	FUS-MS										
FLINTSBACH	FL1	0.38	0.44	0.12	0.64	0.12	0.022	0.14	0.02	0.14	0.02	0.07	0.009	0.05	0.007	2.178	3.78	0.48	0.56	0.46	1.22	0.79	0.47	1.11	1.30
	F1	0.73	0.45	0.14	0.58	0.12	0.015	0.15	0.02	0.12	0.02	0.07	< 0.005	0.04	< 0.002	2.455	4.85	0.65	1.35	0.89	1.52	0.52	0.32	1.39	1.62
	F2	0.8	0.46	0.14	0.7	0.15	0.035	0.19	0.02	0.15	0.04	0.09	0.012	0.05	< 0.002	2.837	4.14	0.56	1.19	0.78	1.52	0.96	0.31	1.20	1.40
	F3"	0.62	0.59	0.14	0.76	0.13	0.032	0.17	0.03	0.18	0.03	0.09	0.012	0.06	0.009	2.853	3.91	0.47	0.77	0.70	1.10	0.99	0.46	1.06	1.07
MÜNSTER	M1sk	1.03	0.91	0.18	0.49	0.07	0.047	0.17	0.02	0.17	0.03	0.1	< 0.005	0.01	< 0.002	3.227	5.45	0.77	7.64	2.15	3.56	1.77	0.48	1.57	1.05
	M1	0.65	0.4	0.1	0.32	0.04	0.058	0.09	< 0.01	0.16	0.03	0.08	0.009	0.02	< 0.002	1.957	4.03	0.74	2.41	2.37	1.02	4.05	0.35	1.57	0.72
	M2	1.23	0.52	0.15	0.66	0.09	0.043	0.2	0.03	0.14	0.03	0.12	0.011	0.07	< 0.002	3.294	4.48	0.56	1.30	2.00	0.65	1.35	0.26	1.31	1.09
	M3	0.27	0.47	0.08	0.38	0.11	0.016	0.1	0.02	0.09	0.01	0.04	< 0.005	0.03	0.005	1.621	4.49	0.60	0.67	0.36	1.86	0.72	0.73	1.06	1.06
	M3s	0.84	0.69	0.11	0.25	0.02	< 0.005	< 0.01	< 0.01	0.11	0.02	0.01	< 0.005	< 0.01	< 0.002	2.050	13.64	1.15	n. c.	6.13	n. c.	n. c.	0.50	1.55	n. c.
	M4	0.85	0.5	0.17	0.81	0.14	0.044	0.22	0.04	0.2	0.04	0.11	0.016	0.09	0.011	3.241	3.46	0.43	0.70	0.89	0.79	1.12	0.30	1.28	1.02
	M5	1.2	0.45	0.15	0.68	0.21	0.047	0.15	0.02	0.13	0.03	0.07	0.008	0.04	0.006	3.191	6.03	0.83	2.23	0.83	2.67	1.24	0.23	1.32	0.93
	M7	0.49	0.3	0.08	0.36	0.06	0.039	0.12	0.02	0.12	0.02	0.07	0.009	0.05	0.009	1.747	3.18	0.46	0.73	1.19	0.61	1.98	0.34	1.26	0.83
	M8	0.95	0.48	0.15	0.3	< 0.01	0.007	0.05	< 0.01	0.11	0.01	0.03	< 0.005	< 0.01	< 0.002	2.087	9.44	1.15	n. c.	n. c.	n. c.	n. c.	0.29	2.28	3.31
	M10	0.78	0.35	0.1	0.24	< 0.01	0.008	0.08	< 0.01	0.07	0.02	0.05	< 0.005	< 0.01	< 0.002	1.698	6.72	0.73	n. c.	n. c.	n. c.	n. c.	0.28	1.97	4.64
	M11	0.72	0.49	0.15	0.8	0.27	0.087	0.46	0.09	0.68	0.15	0.55	0.086	0.57	0.092	5.195	0.94	0.15	0.09	0.39	0.24	1.09	0.34	1.14	1.00
	M12	0.76	0.4	0.15	0.68	0.14	0.06	0.28	0.05	0.41	0.09	0.35	0.045	0.24	0.018	3.673	1.48	0.22	0.24	0.79	0.30	1.30	0.27	1.35	1.00
	M13	0.74	0.44	0.1	0.18	< 0.01	< 0.005	0.05	< 0.01	0.09	0.02	0.02	< 0.005	< 0.01	< 0.002	1.640	8.11	0.73	n. c.	n. c.	n. c.	n. c.	0.36	2.09	n. c.

Table 15. Contents of REE [mg·kg^{-1}] in bedded cherts from S-KCU

Location	Sample	La	Ce	Pr	Nd	Sm	Eu	Gd	Tb	Dy	Ho	Er	Tm	Yb	Lu	Total	$LREE_{measured}/HREE_{measured}$	$LREE_{SN}/HREE_{SN}$	La_{SN}/Yb_{SN}	La_{SN}/Sm_{SN}	Sm_{SN}/Yb_{SN}	Eu/Eu*	Ce/Ce*	Pr/Pr*	Gd/Gd*
	Unit	mg·kg^{-1}	mg·kg^{-1}	mg·kg^{-1}	mg·kg^{-1}	mg·kg^{-1}	mg·kg^{-1}	mg·kg^{-1}	mg·kg^{-1}	mg·kg^{-1}	mg·kg^{-1}	mg·kg^{-1}	mg·kg^{-1}	mg·kg^{-1}	mg·kg^{-1}										
	Detection Limit	0.05	0.05	0.01	0.05	0.01	0.005	0.01	0.01	0.01	0.01	0.01	0.005	0.01	0.002										
	Analytical Method	FUS-MS	FUS-MS	FUS-MS	FUS-MS	FUS-MS	FUS-MS	FUS-MS	FUS-MS	FUS-MS	FUS-MS	FUS-MS	FUS-MS	FUS-MS	FUS-MS										
UJAZD	SA-1	2.01	0.89	0.34	1.44	0.31	0.066	0.31	0.04	0.25	0.05	0.15	0.019	0.1	0.015	5.990	5.41	0.67	1.49	0.95	1.58	1.00	0.24	1.44	1.18
	SA-2A	0.43	0.3	0.08	0.39	0.07	0.015	0.07	0.01	0.07	0.01	0.04	0.005	0.02	0.003	1.513	5.64	0.67	1.60	0.90	1.78	1.01	0.37	1.19	1.12
	SA-2B	1.19	0.62	0.21	1.06	0.19	0.05	0.22	0.03	0.18	0.04	0.09	0.011	0.06	0.009	3.960	5.19	0.66	1.47	0.91	1.61	1.14	0.28	1.22	1.11
	SA-2C	1.49	0.72	0.27	1.19	0.25	0.054	0.26	0.04	0.23	0.05	0.12	0.014	0.08	0.013	4.781	4.92	0.61	1.38	0.87	1.59	0.99	0.26	1.39	1.10
	SA-2D	1.09	0.59	0.21	0.99	0.19	0.048	0.24	0.03	0.17	0.03	0.08	0.01	0.07	0.01	3.758	4.87	0.65	1.16	0.84	1.38	1.04	0.28	1.30	1.24
	SA-9A	3.56	1.21	0.48	2.16	0.41	0.092	0.45	0.07	0.42	0.09	0.25	0.032	0.18	0.028	9.432	5.21	0.58	1.47	1.27	1.16	1.00	0.21	1.38	1.10
	SA-9B	1.23	0.59	0.21	0.86	0.19	0.044	0.24	0.03	0.18	0.04	0.1	0.012	0.06	0.008	3.794	4.66	0.60	1.52	0.95	1.61	0.95	0.26	1.45	1.30
	SA-9'A	1.45	0.73	0.28	1.22	0.23	0.059	0.27	0.04	0.22	0.04	0.13	0.018	0.09	0.012	4.789	4.84	0.61	1.20	0.92	1.30	1.10	0.26	1.40	1.09
	SA-9'B	4.52	1.51	0.66	2.65	0.48	0.113	0.56	0.09	0.53	0.12	0.34	0.05	0.3	0.04	11.963	4.89	0.53	1.12	1.38	0.81	1.01	0.20	1.54	1.09

SIKORNIK	SB-1B	1.23	0.65	0.21	1.01	0.18	0.044	0.26	0.04	0.21	0.05	0.13	0.015	0.08	0.009	4.118	4.19	0.50	1.14	1.00	1.14	0.92	0.29	1.25	1.21
	SB-1C	1.26	0.57	0.2	0.91	0.18	0.039	0.24	0.04	0.2	0.04	0.11	0.014	0.07	0.008	3.881	4.38	0.52	1.34	1.02	1.31	0.86	0.26	1.33	1.17
	SB-1D	1.75	0.7	0.25	1.04	0.22	0.043	0.26	0.05	0.26	0.06	0.17	0.023	0.13	0.017	4.973	4.13	0.44	1.00	1.16	0.86	0.83	0.24	1.43	1.07
	SB-2	1.84	0.73	0.29	1.16	0.23	0.054	0.34	0.05	0.3	0.06	0.17	0.022	0.12	< 0.002	5.366	4.05	0.52	1.14	1.17	0.97	0.87	0.23	1.51	1.27
WIELKANOC HILL	SC-1A	1.53	0.58	0.24	0.99	0.2	0.051	0.24	0.04	0.23	0.05	0.14	0.018	0.1	0.014	4.423	4.32	0.51	1.14	1.12	1.02	1.08	0.22	1.49	1.04
	SC-1B	0.53	0.31	0.11	0.57	0.09	0.018	0.11	0.02	0.08	0.02	0.06	0.008	0.04	0.006	1.972	4.73	0.51	0.98	0.86	1.14	0.84	0.29	1.20	1.11
	SC-1C	1.86	0.68	0.29	1.14	0.23	0.052	0.29	0.04	0.25	0.06	0.17	0.024	0.15	0.021	5.257	4.23	0.48	0.92	1.18	0.78	0.93	0.21	1.56	1.25
	SC-2	1.78	0.61	0.24	1.06	0.22	0.052	0.3	0.04	0.25	0.05	0.14	0.02	0.13	0.019	4.911	4.17	0.49	1.02	1.18	0.86	0.93	0.21	1.40	1.29
	SC-4	0.34	0.25	0.08	0.32	0.09	0.018	0.08	0.01	0.05	0.01	0.04	0.005	0.03	0.005	1.328	4.77	0.64	0.84	0.55	1.52	1.00	0.35	1.44	1.16

Table 16. Contents of REE [mg·kg^{-1}] in bedded cherts from N-KCU

Location	Sample	La	Ce	Pr	Nd	Sm	Eu	Gd	Tb	Dy	Ho	Er	Tm	Yb	Lu	Total	$LREE_{measured}/HREE_{measured}$	$LREE_{SN}/HREE_{SN}$	La_{SN}/Yb_{SN}	La_{SN}/Sm_{SN}	Sm_{SN}/Yb_{SN}	Eu/Eu*	Ce/Ce*	Pr/Pr*	Gd/Gd*
	Unit	mg·kg^{-1}	mg·kg^{-1}	mg·kg^{-1}	mg·kg^{-1}	mg·kg^{-1}	mg·kg^{-1}	mg·kg^{-1}	mg·kg^{-1}	mg·kg^{-1}	mg·kg^{-1}	mg·kg^{-1}	mg·kg^{-1}	mg·kg^{-1}	mg·kg^{-1}										
	Detection Limit	0.05	0.05	0.01	0.05	0.01	0.005	0.01	0.01	0.01	0.01	0.01	0.005	0.01	0.002										
	Analytical Method	FUS-MS	FUS-MS	FUS-MS	FUS-MS	FUS-MS	FUS-MS	FUS-MS	FUS-MS	FUS-MS	FUS-MS	FUS-MS	FUS-MS	FUS-MS	FUS-MS										
SIEDLEC	PC-3A	0.49	0.38	0.08	0.38	0.06	0.014	0.09	0.01	0.07	0.01	0.04	< 0.005	0.03	0.004	1.658	5.53	0.68	1.21	1.19	1.02	0.86	0.43	1.13	1.49
	PC-4A	1.39	0.65	0.21	0.85	0.13	0.042	0.2	0.03	0.18	0.04	0.11	0.015	0.09	0.01	3.947	4.85	0.54	1.15	1.56	0.73	1.17	0.27	1.43	1.11
	PC-4B	0.71	0.41	0.11	0.5	0.12	0.029	0.11	0.02	0.12	0.02	0.06	0.008	0.04	0.005	2.262	4.91	0.62	1.32	0.86	1.52	1.19	0.33	1.25	0.90
	PC-4	1.19	0.54	0.18	0.73	0.16	0.043	0.19	0.03	0.16	0.04	0.1	0.013	0.07	0.011	3.457	4.63	0.55	1.26	1.09	1.16	1.14	0.26	1.44	1.04
	PC-5	2.48	0.93	0.33	1.38	0.26	0.067	0.35	0.05	0.3	0.07	0.2	0.028	0.16	0.023	6.628	4.61	0.50	1.15	1.39	0.83	1.02	0.23	1.43	1.19

Table 17. Contents of REE [mg·kg^{-1}] in bedded cherts from southeastern FA

Location	Sample	La	Ce	Pr	Nd	Sm	Eu	Gd	Tb	Dy	Ho	Er	Tm	Yb	Lu	Total	$LREE_{measured}/HREE_{measured}$	$LREE_{SN}/HREE_{SN}$	La_{SN}/Yb_{SN}	La_{SN}/Sm_{SN}	Sm_{SN}/Yb_{SN}	Eu/Eu*	Ce/Ce*	Pr/Pr*	Gd/Gd*
	Unit	mg·kg^{-1}	mg·kg^{-1}	mg·kg^{-1}	mg·kg^{-1}	mg·kg^{-1}	mg·kg^{-1}	mg·kg^{-1}	mg·kg^{-1}	mg·kg^{-1}	mg·kg^{-1}	mg·kg^{-1}	mg·kg^{-1}	mg·kg^{-1}	mg·kg^{-1}										
	Detection Limit	0.05	0.05	0.01	0.05	0.01	0.005	0.01	0.01	0.01	0.01	0.01	0.005	0.01	0.002										
	Analytical Method	FUS-MS	FUS-MS	FUS-MS	FUS-MS	FUS-MS	FUS-MS	FUS-MS	FUS-MS	FUS-MS	FUS-MS	FUS-MS	FUS-MS	FUS-MS	FUS-MS										
KELHEIM	KD1	0.74	1.03	< 0.01	0.08	0.03	0.011	0.02	< 0.01	0.03	< 0.01	0.01	< 0.005	0.03	0.008	1.989	19.30	1.16	1.83	3.60	0.51	2.10	n. c.	n. c.	n. c.
	K3/3	0.14	0.27	0.02	< 0.05	< 0.01	0.008	< 0.01	< 0.01	0.04	< 0.01	< 0.01	0.005	< 0.01	< 0.002	0.483	9.73	0.80	n. c.	n. c.	n. c.	n. c.	1.14	n. c.	n. c.
HEMAU	H1	0.5	0.51	0.13	0.49	0.13	0.025	0.08	0.02	0.1	0.02	0.05	0.009	0.05	< 0.002	2.114	5.43	0.67	0.74	0.56	1.32	1.14	0.46	1.41	0.70
	H5	0.87	0.99	0.16	0.52	0.12	0.008	0.09	0.01	0.08	0.01	0.04	< 0.005	0.03	< 0.002	2.928	10.26	1.16	2.15	1.06	2.03	0.36	0.61	1.30	1.90

Table 18. Contents of REE [mg·kg^{-1}] in chert concretions hosted within gravity flow from S-KCU

Location	Sample	La	Ce	Pr	Nd	Sm	Eu	Gd	Tb	Dy	Ho	Er	Tm	Yb	Lu	Total	$LREE_{measured}/HREE_{measured}$	$LREE_{SN}/HREE_{SN}$	La_{SN}/Yb_{SN}	La_{SN}/Sm_{SN}	Sm_{SN}/Yb_{SN}	Eu/Eu*	Ce/Ce*	Pr/Pr*	Gd/Gd*
	Unit	mg·kg^{-1}	mg·kg^{-1}	mg·kg^{-1}	mg·kg^{-1}	mg·kg^{-1}	mg·kg^{-1}	mg·kg^{-1}	mg·kg^{-1}	mg·kg^{-1}	mg·kg^{-1}	mg·kg^{-1}	mg·kg^{-1}	mg·kg^{-1}	mg·kg^{-1}										
	Detection Limit	0.05	0.05	0.01	0.05	0.01	0.005	0.01	0.01	0.01	0.01	0.01	0.005	0.01	0.002										
	Analytical Method	FUS-MS	FUS-MS	FUS-MS	FUS-MS	FUS-MS	FUS-MS	FUS-MS	FUS-MS	FUS-MS	FUS-MS	FUS-MS	FUS-MS	FUS-MS	FUS-MS										
UJAZD	SA-3	0.48	0.3	0.1	0.49	0.09	0.023	0.09	0.02	0.09	0.02	0.04	0.005	0.03	0.005	1.783	4.94	0.60	1.19	0.78	1.52	1.20	0.31	1.24	0.82
	SA-4	0.49	0.29	0.11	0.47	0.1	0.025	0.1	0.02	0.09	0.02	0.05	0.008	0.05	0.006	1.829	4.32	0.54	0.73	0.72	1.02	1.17	0.29	1.42	0.88
	SA-5	0.53	0.33	0.1	0.48	0.09	0.021	0.09	0.01	0.08	0.02	0.05	0.006	0.04	0.005	1.852	5.15	0.62	0.98	0.86	1.14	1.09	0.33	1.24	1.19
	SA-6	0.58	0.39	0.1	0.46	0.11	0.022	0.1	0.02	0.09	0.02	0.05	0.007	0.05	0.006	2.005	4.85	0.56	0.86	0.77	1.12	0.99	0.37	1.23	0.93
	SA-7	0.45	0.3	0.08	0.34	0.06	0.011	0.08	0.01	0.07	0.01	0.04	0.005	0.03	0.004	1.490	4.98	0.55	1.11	1.10	1.02	0.73	0.36	1.31	1.49
	SA-8	0.49	0.35	0.08	0.37	0.07	0.014	0.08	0.01	0.07	0.02	0.05	0.006	0.03	0.004	1.644	5.09	0.54	1.21	1.02	1.19	0.87	0.40	1.18	1.33

Table 19. Contents of REE [mg·kg^{-1}] in chert concretions hosted within gravity flow from N-KCU

Location	Sample	La	Ce	Pr	Nd	Sm	Eu	Gd	Tb	Dy	Ho	Er	Tm	Yb	Lu	Total	$LREE_{measured}/HREE_{measured}$	$LREE_{SN}/HREE_{SN}$	La_{SN}/Yb_{SN}	La_{SN}/Sm_{SN}	Sm_{SN}/Yb_{SN}	Eu/Eu*	Ce/Ce*	Pr/Pr*	Gd/Gd*
	Unit	mg·kg^{-1}	mg·kg^{-1}	mg·kg^{-1}	mg·kg^{-1}	mg·kg^{-1}	mg·kg^{-1}	mg·kg^{-1}	mg·kg^{-1}	mg·kg^{-1}	mg·kg^{-1}	mg·kg^{-1}	mg·kg^{-1}	mg·kg^{-1}	mg·kg^{-1}										
	Detection Limit	0.05	0.05	0.01	0.05	0.01	0.005	0.01	0.01	0.01	0.01	0.01	0.005	0.01	0.002										
	Analytical Method	FUS-MS	FUS-MS	FUS-MS	FUS-MS	FUS-MS	FUS-MS	FUS-MS	FUS-MS	FUS-MS	FUS-MS	FUS-MS	FUS-MS	FUS-MS	FUS-MS										

SIEDLEC	PC-1C	0.2	0.2	0.04	0.16	0.03	0.005	0.03	< 0.01	0.02	0.01	0.02	< 0.005	0.01	0.002	0.727	6.90	0.75	1.48	0.97	1.52	0.78	0.51	1.25	2.78
	PC-2A	0.24	0.24	0.04	0.15	0.03	0.007	0.03	< 0.01	0.03	0.01	0.01	< 0.005	0.01	0.002	0.799	7.68	0.87	1.78	1.17	1.52	1.09	0.56	1.22	1.99
	PC-2C	0.21	0.17	0.03	0.13	0.02	< 0.005	0.03	< 0.01	0.02	< 0.01	0.01	< 0.005	0.02	0.003	0.643	6.75	0.66	0.78	1.53	0.51	n. c.	0.48	1.14	n. c.
	PC-6	0.39	0.26	0.05	0.23	0.05	0.006	0.05	0.01	0.05	0.01	0.03	< 0.005	0.02	0.003	1.159	5.70	0.59	1.45	1.14	1.27	0.56	0.41	1.13	1.16

Table 20. Contents of REE [mg·kg^{-1}] in chert concretions hosted within gravity flow from southeastern FA

Location	**Sample**	**La**	**Ce**	**Pr**	**Nd**	**Sm**	**Eu**	**Gd**	**Tb**	**Dy**	**Ho**	**Er**	**Tm**	**Yb**	**Lu**	**Total**	**$LREE_{measured}$/ $HREE_{measured}$**	**$LREE_{SN}$/ $HREE_{SN}$**	**La_{SN}/Yb_{SN}**	**La_{SN}/Sm_{SN}**	**Sm_{SN}/Yb_{SN}**	**Eu/Eu***	**Ce/Ce***	**Pr/Pr***	**Gd/Gd***
	Unit	mg·kg^{-1}	mg·kg^{-1}	mg·kg^{-1}	mg·kg^{-1}	mg·kg^{-1}	mg·kg^{-1}	mg·kg^{-1}	mg·kg^{-1}	mg·kg^{-1}	mg·kg^{-1}	mg·kg^{-1}	mg·kg^{-1}	mg·kg^{-1}	mg·kg^{-1}										
	Detection Limit	0.05	0.05	0.01	0.05	0.01	0.005	0.01	0.01	0.01	0.01	0.01	0.005	0.01	0.002										
	Analytical Method	FUS-MS	FUS-MS	FUS-MS	FUS-MS	FUS-MS	FUS-MS	FUS-MS	FUS-MS	FUS-MS	FUS-MS	FUS-MS	FUS-MS	FUS-MS	FUS-MS										
KELHEIM	K1/1	< 0.05	0.07	0.01	0.08	0.03	0.01	0.02	< 0.01	0.03	< 0.01	0.02	< 0.005	0.01	< 0.002	0.280	2.50	0.90	n. c.	n. c.	1.52	1.91	1.55	0.70	0.93
	K1/2	0.19	0.06	0.02	0.09	< 0.01	< 0.005	0.06	< 0.01	0.03	0.01	0.02	0.007	0.02	< 0.002	0.507	2.45	0.18	0.71	n. c.	n. c.	n. c.	0.21	1.33	n. c.
	K1/3	0.15	0.21	0.01	< 0.05	< 0.01	< 0.005	< 0.01	< 0.01	< 0.01	< 0.01	< 0.01	< 0.005	< 0.01	< 0.002	0.370	n. c.	n. c.	n. c.	n. c.	n. c.	n. c.	1.04	n. c.	n. c.
	K2/1	0.21	0.36	0.03	0.16	< 0.01	0.01	0.04	0.01	0.02	0.01	0.02	< 0.005	< 0.01	< 0.002	0.870	7.70	0.64	n. c.	n. c.	n. c.	n. c.	1.01	0.74	0.77
	K2/2	0.18	0.28	< 0.01	< 0.05	< 0.01	< 0.005	< 0.01	< 0.01	< 0.01	< 0.01	< 0.01	< 0.005	< 0.01	< 0.002	0.460	n. c.	n. c.	n. c.	n. c.	n. c.	n. c.	1.49	n. c.	n. c.
	K2/2j	0.35	0.6	0.04	< 0.05	< 0.01	< 0.005	< 0.01	< 0.01	< 0.01	< 0.01	< 0.01	< 0.005	< 0.01	< 0.002	0.990	n. c.	n. c.	n. c.	n. c.	n. c.	n. c.	1.10	1.20	n. c.
	K2/1L	< 0.05	0.14	< 0.01	< 0.05	0.01	< 0.005	0.02	< 0.01	0.01	< 0.01	0.01	< 0.005	0.02	0.004	0.214	2.34	0.09	n. c.	n. c.	n. c.	n. c.	n. c.	n. c.	n. c.
	K2/3	0.18	0.34	0.03	< 0.05	< 0.01	< 0.005	< 0.01	< 0.01	0.05	< 0.01	0.01	< 0.005	< 0.01	< 0.002	0.610	9.17	0.87	n. c.	n. c.	n. c.	n. c.	1.05	1.59	n. c.
	K3/1	0.11	0.16	0.01	< 0.05	< 0.01	< 0.005	< 0.01	< 0.01	< 0.01	< 0.01	< 0.01	< 0.005	< 0.01	< 0.002	0.280	n. c.	n. c.	n. c.	n. c.	n. c.	n. c.	1.00	1.13	n. c.
HEMAU	H2	0.32	0.48	0.13	0.67	0.21	0.023	0.11	0.03	0.11	0.01	0.03	< 0.005	0.01	< 0.002	2.133	6.11	0.98	2.37	0.22	10.67	0.69	0.52	1.14	0.79
	H3	0.73	1.18	0.14	0.51	0.13	0.017	0.1	0.02	0.1	0.02	0.05	0.008	0.05	0.009	3.064	7.58	0.63	1.08	0.82	1.32	0.70	0.85	1.06	1.03
	H4	0.37	0.36	0.07	0.31	0.05	0.023	0.03	0.01	0.11	0.02	0.05	0.007	< 0.01	< 0.002	1.410	5.21	0.63	n. c.	1.08	n. c.	2.76	0.51	1.16	0.38
	H6	0.8	1.26	0.13	0.44	0.11	< 0.005	0.07	0.02	0.17	0.03	0.11	0.021	0.17	< 0.002	3.331	4.64	0.33	0.35	1.06	0.33	n. c.	0.88	1.02	1.16

Al/(Al+Fe+Mn) – Al_2O_3/(Al_2O_3+Fe_2O_3+MnO); n. c. - not calculated